A-Kinase anchoring protein GSKIP regulates tumorigenic pathways in lung cancer cells

DISSERTATION

Inaugural-Dissertation
to obtain the academic degree
Doctor rerum naturalium (Dr. rer. nat.)

submitted to the Department of Biology, Chemistry and Pharmacy
of Freie Universität Berlin

by

EKATERINA PERETS

from Moscow, Russia

Berlin, 2015

This work was conducted from July 2012 until August 2015 at Max-Delbrück Institute for Molecular Medicine in Berlin under the supervision of Priv.-Doz. Dr. Enno Klußmann.

Dissertation submitted on: 13/10/2015

Date of Disputation: 09/02/2016

1. Reviewer: PD Dr. Enno Klußmann
2. Reviewer: Prof. Dr. Udo Heinemann

Freie Universität Berlin, 2015

I hereby declare that the following work was performed by me alone, only with the use of literature and materials listed. I further declare that to the best of my knowledge this work is novel and does not conflict with any earlier published dissertations.

Berlin, 13.10.2015

Ekaterina Perets

Acknowledgments

I would like to thank PD Dr. Enno Klussmann and Prof. Dr. Walter Rosenthal for welcoming me into this group and also, for the supervision during the length of my PhD project. To Enno, I would like to thank for the valuable advice, the constructive criticism and attentiveness.
Thank you Gregor Beuster and Prof. Clemens Schmitt for the valuable help with the Seahorse XF24 experiments. I would also like to thank Nadine Mikuda and Dr. Michael Hinz from AG Scheiderheit for all the help and advice with NF-kB assays.
A special thank you goes to Nadia Batello, Sylvie Delcambre, Dr. Karsten Hiller and all the other members of the group, for the wonderful working atmosphere and invaluable assistance with metabolomics analysis.
Thank you also, Amit Kumar and Dr. Stephan Kempa for proteomics analysis.
A very warm thank you goes to all the amazing team members of AG Klussmann. You've made these 3 years fly by. To Alessandro, to Micha, Dörte and Tanja, for all your help with the experiments, the advice and above all your friendship, thank you from the bottom of my heart.
A special thanks to Alessandro for providing the GSKIP plasmids. To Andrea, Bärbel and Beate, thank you so very much for the daily technical assistance. Thank you, dear Kerstin and Caro for all the help with experiments and for the translation of the summary into German.
To Russ Hodge, for the motivation, mentoring and support, thank you so much! If it wasn't for you I never would have finished my PhD.
Lastly (but not leastly), I would like to thank my family and friends. To my parents, who never gave up on motivating and inspiring me with optimism and to my brother, for believing in me more than I did, thank you so much. I never would have made it without you.
To all my wonderful friends thank you for listening, supporting and just plain being there.

Table of Contents

I. Abbreviations

AKAP A-kinase anchoring protein
AMP adenosine-5'-monophosphate
AKT protein kinase B
APC adenomatosis polyposis coli
ATP adenosine-5'-triphosphate
AMF autocrine motility factor
AMFR autocrine motility factor receptor
AC adenylate cyclase
BMP Bone Morphogenetic Protein
BAX Bcl2-Associated X Protein
BAG Bcl2-associated athanogene
BSA bovine serum albumin
CAM cell adhesion molecule
cAMP cyclic adenosine-3',5'-monophosphate
CREB cAMP response element-binding protein
CDC42 Cell division control protein 42
CRF Corticotropin-releasing Factor
DMEM Dulbecco's modified eagle medium
DMSO dimethyl sulphoxide
DNA deoxyribonucleic acid
DTT dithiothreitol
DR death receptor
DCC deleted in colorectal carcinoma
dsRNA double stranded RNA
EMT epithelial-mesenchymal transition
ECM extra-cellular matrix
EDTA ethylenediaminetetraacetic acid
EGTA ethyleneglycoltetraacetic acid
ERM ezrin-radixin-moesin
ER endoplasmatic reticulum
ERK extracellular signal-related kinase
ET1 endothelin1
EXT2 Exostosin Glycosyltransferase 2
ECAR extracellular acidification rate
FCCP Trifluorocarbonylcyanide Phenylhydrazone
FGF fibroblast growth factor
FBS fetal bovine serum
FMP Leibniz-Institut für Molekulare Pharmakologie
FAK focal adhesion kinase
GAPDH glyceraldehyde-3-phosphate dehydrogenase protein
GTP guanosine-5'-triphosphate
GID GSK3 interaction domain
GSK3β glycogen synthase kinase 3beta
GSKIP GSK3β interaction protein
GLP glucagon-like peptide
GDF5OS growth and differentiation factor 5 opposite strand
g gauge
HGF hepatocyte growth factor
HIF-α hypoxia inducible factor alpha

HA hyaluronic acid
hrs hours
IQGAP IQ domain GTPase-activating protein
Ig immunoglobulin
IP immunoprecipitation
IF immunofluorescence
IGF insulin growth factor
KO knockout
Kd knockdown
LDL low density lipoproteins
LSM laser scanning microscope
LASP LIM and SH3 domain *protein*
miR microRNA
MAPK mitogen-activated protein kinase
mTORC mammalian target of rapamycin complex
MDC Max Delbrück Center for Molceular Medicine
MID mass isotopomer distribution
min minute(s)
MET Mesenchymal-Epithelial transition
MMP matrix metalloproteinase
NT non-targeting siRNA
NADPH nicotine adenine dinucleotide phosphate
NF-κB nuclear factor 'kappa-light-chain-enhancer' of activated B-cells
OXPHOS oxidative phosphorylation
OCR oxygen consumption rate
PAGE polyacrylamide gel electrophoresis
PBS phosphate buffered saline
PFA paraformaldehyde
PI3K phosphoinositide-3-kinase
PPP penthose phosphate pathway
PKA protein kinase A
PKB protein kinase B
PKC protein kinase
PDH pyruvate dehydrogenase
PDK pyruvate dehydrogenase kinase
PMSF phenylmethylsulphonyl fluoride
PVDF polyvinylidene fluoride
PTH Parathyroid hormone
PEX19 Peroxisomal Biogenesis Factor 19
RhoA Ras homolog family member A
RAC Ras-related C3 botulinum toxin substrate
RNA ribonucleic acid
RNAi RNA interference
ROS reactive oxygen species
R regulatory PKA subunit
RIIBD RII-binding domain
RNA ribonucleic acid
RT room temperature
RTK receptor tyrosine kinase
Rb retinoblastoma protein

RCR respiratory control ratio
RISC RNA-induced silencing complex
SDS sodium dodecylsulfate
STAT3 Signal transducer and activator of transcription 3
SMYD2 SET domain dependent methyltransferase 2
SEM standard error of mean
shRNA short hairpin RNA
siRNA short interfering RNA
Ser serine
TBS Tris buffered saline
TBS-T TBS with Tween 20
TOX toxic siRNA
TNFR tumor necrosis factor receptor
TCA cycle tricarboxylic acid cycle
TGFβ transforming growth factor beta
TGFβ1I1 transforming growth factor beta inducing factor 1
TβR TGFβ receptor
UV ultraviolet
VIS visible
VASP Vasodilator-stimulated phosphoprotein
VDAC voltage dependent anion channel
WT wild-type
ZO-1 Zonula occludens protein 1

II. List of figures

III. List of tables

1. Introduction

Cancer is the second leading cause of death in the developing countries and one in seven deaths worldwide is attributed to cancer. By the year 2030 an estimate of 1.7 million new cancer cases and 13 million cancer deaths is expected (American Cancer Society, 2015). Cancer is a group of more than 100 diseases characterized by abnormal cells that have the ability to rapidly proliferate and invade adjacent tissues (Hanahan and Weinberg, 2000). The *in-vitro* homogeneous cancer cell population shares the phenotypic traits of rapid and unlimited proliferation, loss of differentiation, invasion to neighboring tissues and metastasis, and evading immune surveillance and apoptosis. In addition, these cells enhance growth factor signals and downregulate antigrowth signals, have sustained angiogenesis and undergo metabolic reprogramming (Floor et al., 2012; Hanahan and Weinberg, 2000, 2011). Furthermore, tumor cell population is heterogeneous which results in variable traits in cancer cells depending on cell type, tumor location in the body, tumors microenvironment as well as genetic and environmental factors (Floor et al., 2012; Tomasetti and Vogelstein, 2015).
This difficulty in simplifying the complex nature of cancer poses a major therapeutic challenge, supporting the notion that future cancer treatments must be personalized. As a prerequisite, a greater understanding of the different intracellular signaling pathways that become deregulated in cancer is imperative as well as elucidation of the crosstalk between these pathways.
The following passages will describe several of the hallmark tumorigenic signaling pathways and their master regulators and effectors.

1.1 Epithelial-Mesenchymal transition (EMT)

The ability of cancer cells to detach from the initial tumor site, migrate and invade adjacent tissues is one of the hallmarks of tumorigenesis (Hanahan and Weinberg, 2000). This involves a complex organization of multiple intracellular signaling pathways and extracellular cross talk. This process is termed EMT (Epithelial-Mesenchymal Transition) and its activation in cancer cells signifies a first step in generation of usually fatal distant metastasis. Upon reaching distant tissues and invading them, cells undergo a reverse process termed MET (Mesenchymal-Epithelial Transition) and begin to proliferate at the new site. The EMT is an important developmental process by which epithelial cells lose cell-cell interactions and apico-basal polarity while at the same time acquiring mesenchymal and migratory properties. During EMT, cells initiate reorganization of the actin cytoskeleton characterized by disassembly of the cell-

cell junction complexes and formation of actin stress fibers that are anchored to focal adhesion complexes (Figure1).

In addition, cells undergoing EMT, undergo extensive reprogramming of gene expression and acquisition of resistance to senescence and apoptosis (Thiery, 2002). The EMT process in various cells and tissues follows a common program with shared hallmarks, however several features remain flexible and are locus-dependent (Lamouille et al., 2014; Thiery, 2002; Xu et al., 2009a).

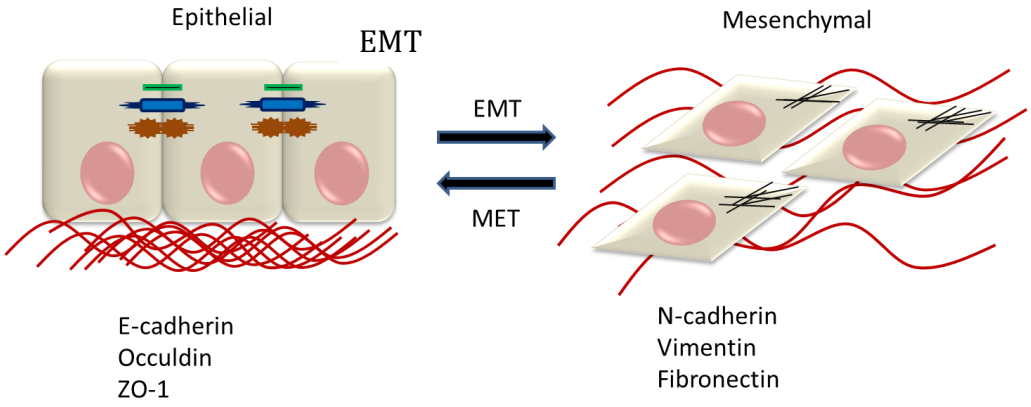

Figure 1: **Schematic representation of Epithelial-mesenchymal transition.** During EMT dissolution of cell-cell contacts occurs, affecting tight junctions (green), adherent junctions (blue) and desmosomes (brown). Formation of stress fibers (black) and reorganization of actin result in increased migration and invasion. The epithelial state is characterized by upregulation of epithelial markers such as E-cadherin, Occuldin and ZO-1 while the in the mesenchymal state markers such as N-cadherin, Vimentin and Fibronectin become upregulated.

1.1.1 Reprograming of gene expression during EMT

One of the hallmarks of EMT initiation in cancer is downregulation of E-Cadherin (Figure 1), an epithelial marker (Peinado, 2007; Xu et al., 2009a) that is part of the type I cadherin superfamily. E-cadherin is a Ca^{2+}-dependent, single-pass transmembrane glycoprotein that mediates the formation of adhesive bonds between actin microfilaments and one or more immunoglobulin (Ig) domains, thus characterizing adherent junctions in epithelial cells. These bonds are formed indirectly *via* E-cadherin binding to β-catenin in the cytoplasm, which interacts with α-catenin in the cytoskeleton either directly or *via* actin-binding proteins α-actinin and vinculin (Gooding et al., 2004; Xu et al., 2009a). In parallel to E-cadherin downregulation, the expression of mesenchymal proteins, such as N-cadherin and vimentin increases as well as the increased deposition of extracellular matrix (ECM) proteins, like collagens and fibronectin. These proteins stimulate integrin signaling, which is responsible for ECM modification and cellular communication with ECM (Lamouille et al., 2014; Xu et al., 2009a).

At the onset of EMT certain epithelial integrins are downregulated while others become overexpressed, for example α3β1 integrin promotes EMT through association with E-cadherin and integration of Transforming growth factor β (TGFβ) and Wnt signaling (Figure 2). In parallel, matrix metalloproteinases like MMP2 and MMP9 become over expressed, contributing to EMT *via* ECM protein degradation, loss of adherent junctions and increased TGFβ signaling (Lamouille et al., 2014; Mu et al., 2012).

In addition to cadherins and integrins, CD44 family members act as cell adhesion molecules (CAMs) and are prominently involved in the EMT process. CD44 transmembrane glycoproteins all have a hyaluronic acid (HA) binding domain in the N-terminal part while the cytoplasmic tail of CD44 binds to Ezrin-Radixin-Moesin (ERM) proteins, which crosslink the cytoskeleton and ECM (Orian-Rousseau, 2010). Protein kinase C (PKC) phosphorylation on Ser291of CD44 was shown to prevent Ezrin binding to CD44 resulting in attenuation of directional cell motility (Legg et al., 2002).

In general, high CD44 expression levels, CD44v6 isoform in particular, shows a positive correlation with cancer aggressiveness and poor prognosis in cancer patients. This correlation is most likely related to CD44's role in EMT and angiogenesis (Orian-Rousseau, 2010). This role was demonstrated in a study showing that binding of HA to CD44 is required for CD44 association with MMP9 at the cell surface in TA3 cells. This binding ultimately resulted in Collagen IV degradation and increased invasion. In addition, MMP9 anchored to the cell surface induced maturation and activation of the latent form of TGFβ, triggering angiogenesis (Yu and Stamenkovic, 1999). A recent study demonstrated the requirement of CD44 for EMT induction of hepatocellular carcinoma cells both *in vitro* and *in vivo*. Upon CD44 knockdown E-cadherin levels increased in parallel with a marked decrease in levels of N-cadherin and vimentin and attenuation of migration (Gao, 2015).

1.1.2 Master regulators of EMT

The changes in gene expression levels of EMT proteins as well as the types of genes affected are regulated by SNAIL, TWIST and ZEB transcription factor families. These proteins are collectively termed master regulators of EMT since they govern the EMT-MET transition processes in tumorigenesis, embryogenesis, wound healing and fibrosis. Their expression and mode of transcriptional regulation varies between different cells and tissues and they often cooperate with each other and regulate each other's expression (Lamouille et al., 2014).

The Snail superfamily of zinc finger transcriptional repressors includes SNAIL (SNAIL1) and SLUG (SNAIL2) and they repress epithelial genes by binding to E-box DNA sequences

through their carboxy-terminal zinc-finger domains (Xu et al., 2009b). Upregulation of SNAIL and SLUG is associated with distant metastasis and tumor recurrence as well as with poor prognosis and survival, in a wide variety of tumors and cancer cells including, breast, ovarian, colon, lung and melanoma (reviewed in (Peinado, 2007). Snail family proteins repress epithelial genes, such as E-cadherin and induce overexpression of mesenchymal genes such as N-cadherin as well as other master EMT regulators, ZEB1, ZEB2 and TWIST (Figure 2) (Lamouille et al., 2014).

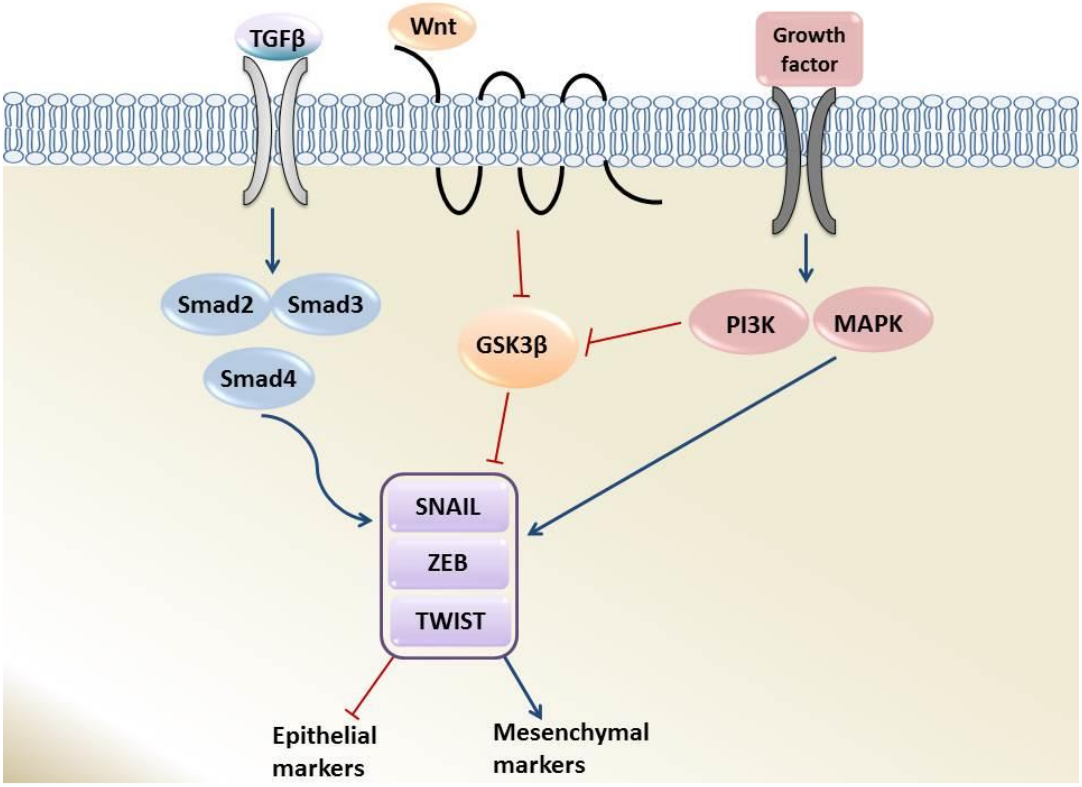

Figure 2: **Schematic representation of EMT regulation.** Protein families SNAIL, ZEB and TWIST induce EMT *via* inhibition of epithelial markers' expression and upregulation of mesenchymal markers. Their expression is positively regulated by TGFβ, Wnt and growth factor signaling. TGFβ induces SNAIL, ZEB and TWIST *via* Smad signaling cascade while growth factors induce PI3K/AKT and MAPK signaling. Active AKT and Wnt signaling inhibit GSK3β thus preventing SNAIL phosphorylation and degradation and MAPK signaling induces SNAIL, ZEB and TWIST expression, thus promoting EMT.

In addition to being regulated transcriptionally by EMT-inducers like TGFβ (see section 1.1.3.1), Snail proteins are subjected to strenuous post-translational regulation (Peinado, 2007). For example, GSK3β phosphorylates SNAIL six times at two Serine rich motifs. Phosphorylation of Ser97 and Ser101 in the first motif facilitates the nuclear export of SNAIL, and the subsequent phosphorylation of Ser108, Ser112, Ser116 and Ser120 targets SNAIL for ubiquitin-mediated degradation (Schlessinger and Hall, 2004; Zhou et al., 2004a). GSK3β-mediated phosphorylation of SNAIL is negatively regulated by Wnt (see section

1.1.3.2), PI3K/AKT, MAP Kinase (Figure 2), Notch and NF-κB signaling pathways, thus increasing SNAIL stability and promoting EMT progression (Sahlgren et al., 2008; Wu et al., 2009; Yook et al., 2006). On the other hand, P53 targets SLUG for degradation, thus reducing EMT activity (Wang et al., 2009).

Similarly to SNAIL and TWIST, ZEB1 and ZEB2 expression is induced in response to TGFβ and Wnt signaling (Xu et al., 2009b) as well as by cytokines such as GPI/AMF (see section 1.1.3.3). ZEB transcription factors bind E-boxes and function as transcriptional repressors of epithelial genes including E-cadherin and activators of mesenchymal genes, thus promoting EMT (Peinado, 2007). ZEB1 gene is directly targeted by SNAIL and SNAIL cooperates with TWIST to induce ZEB1 activation during EMT (Dave et al., 2011).

1.1.3 EMT induction

Many different growth factors as well as cytokines are required for EMT induction and/or regulation. These include TGFβ, which acts *via* serine/threonine kinase receptors, Wnt proteins, which act *via* Frizzled receptor, Fibroblast growth factor (FGF) and hepatocyte growth factor (HGF), which act *via* receptor tyrosine kinases (RTKs), as well as Hedgehog, Notch, PGI/AMF and integrin signaling pathways (Derynck et al., 2014; Lamouille et al., 2014; Xu et al., 2009a). The next sections will focus on several most potent EMT inducers in cancer cells.

1.1.3.1 TGFβ

TGFβ is the most potent and well characterized EMT inducer and regulator (Derynck et al., 2014). *In vitro* studies have shown that epithelial cells treated with TGFβ change their morphology to spindle shape, show decreased expression of epithelial markers in parallel to enhanced expression of mesenchymal markers and have enhanced motility. The three known isoforms TGFβ1, TGFβ2 and TGFβ3 possess equal capability to induce EMT in epithelial cells (Xu et al., 2009a). *In vivo* studies have shown that both TGFβ1 and TGFβ2 null mouse embryos have severe cardiac abnormalities, including defective atrioventricular junction and atrioventricular and outflow tract defects while TGFβ3 null mice present a lack of fusion of the two palatal shelves resulting in a cleft palate (Azhar et al., 2003; Mercado-Pimentel and Runyan, 2007; Nawshad et al., 2004). The TGFβ family of growth factors have three modes of EMT regulation: *via* Smad signaling, *via* Non-Smad signaling and *via* crosstalk with other signaling pathways like Wnt (see section 1..1.3.2 and Figure 2), Notch and RTK signaling (Derynck et al., 2014; Lamouille et al., 2014).

The transduction of TGFβ signaling is enabled by two transmembrane serine/threonine kinase receptors, TGFβ type I (TβRI) and TGFβ type II (TβRII). Stimulation with TGFβ leads to phosphorylation of TβRI receptors by TβRII receptors, resulting in activation of the receptor TβRI complex. TβRI then directly phosphorylates and activates Smad2 and Smad3, enabling them to form trimers with Smad4 (Figure 2). These trimers then translocate into the nucleus, where they associate with transcription factors to activate or repress EMT target genes.
The TGFβ-dependent activation of Smads is negatively regulated by Smad6 and Smad7; Smad6 expression is induced by BMP signaling and Smad7 expression is induced by TGFβ signaling, both resulting in a negative feedback loop inhibiting TGFβ signaling (Feng and Derynck, 2005; Wang et al., 2008; Xu et al., 2009a).
Smad7 directly binds to focal adhesion protein Hic-5 (also known as TGFβ1I1), which is induced by TGFβ. This binding results in Smad7 protein loss thus promoting TGFβ signaling in prostate cancer cells (Wang et al., 2008). Hic-5 expression results in matrix degradation and enhanced motility in TGFβ-treated breast carcinoma cells (Pignatelli et al., 2012) and induces cytoskeletal organization leading to the formation of actin stress fibers (Tumbarello and Turner, 2007) thus promoting EMT. In addition, high expression of TGFβ1I1 was shown to be associated with EMT activation and poor survival in patients with astrocytomas (Liu et al., 2014).
In addition to Smad signaling, TGFβ induces, to a lower extent non-Smad signaling pathways, which also regulate EMT. These pathways include small GTPases, MAP Kinase (MAPK) signaling pathways and the PI3 kinase/AKT signaling (Lamouille et al., 2014; Mu et al., 2012; Xu et al., 2009a). The small GTPases RhoA, CDC42 and RAC are important components of the tight junctions and their signaling drives the actin remodeling required for cellular migration and invasion (Ridley, 2011) and TGFβ was shown to regulate both their expression levels and activity (Lamouille et al., 2014; Moustakas, 2005). AKT is activated by PI3K in response to TGFβ thus initiating a downstream signaling cascade resulting in EMT. The downstream targets of AKT include GSK3β (see section 1.3), mTORC1 and mTORC2. While mTORC1 is mainly responsible for regulation of cell size, protein synthesis and motility, mTORC2 is required for metastatic potential of cancer cells (Lamouille et al., 2014).

1.1.3.2 Wnt signaling and EMT

The canonical Wnt signaling pathway has a major role in regulating EMT in mammalian cells and it is often deregulated in cancer (Reya and Clevers, 2005). The canonical Wnt signaling pathway is initiated by Wnt ligands binding to Frizzled receptor complexed to LDL receptor

related proteins (LRPs), LRP5 /LRP6. This binding recruits Axin1 away from the β-catenin destruction complex enabling β-catenin to translocate to the nucleus and interact with TCF family transcription factors. The β-catenin destruction complex contains Adenomatosis polyposis coli (APC) and GSK3β (see section 1.3). In the absence of Wnt ligands, Axin1 and APC interact with β-catenin which allows for GSK3β to phosphorylate β-catenin at Ser33. This phosphorylation leads to β-catenin ubiquitination and subsequently degradation by the proteasome (Figure 3). The active Wnt signaling pathway concludes when the nuclear β-catenin–LEF/TCF complex activates expression of a group of target genes such as C-myc, SNAIL, Axin2 and others, that affect EMT as well as other tumorigenic and developmental signaling pathways (He et al., 1996; Yook et al., 2006).

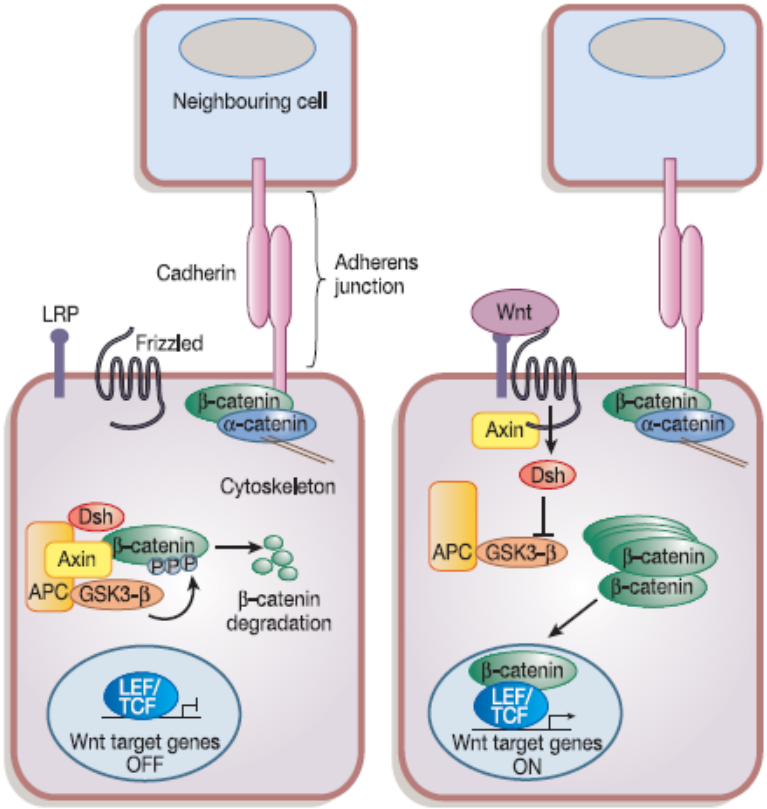

Figure 3: **The canonical Wnt signaling pathway**. In the absence of Wnt signal (left panel), β-catenin is in a complex with Axin1, APC and GSK3β, and phosphorylated and targeted for degradation. β-catenin also exists in a cadherin-bound form and regulates cell–cell adhesion. In the presence of Wnt signal (right panel), β catenin is uncoupled from the degradation complex and translocates to the nucleus, where its binds LEF/TCF transcription factors, thus activating target genes (Reya and Clevers, 2005).

1.1.3.3 GPI/AMF signaling in tumorigenesis

GPI/AMF (glucose-6-phosphate isomerase/autocrine motility factor) is a multifunctional cytokine, growth factor, neuroleukin and autocrine motility factor. In addition GPI/AMF catalyzes the isomerization of glucose-6-phosphate to fructose-6-phosphate in glycolysis (Sun,

1999). GPI/AMF is secreted from the tumor cells and promotes EMT *via* its receptor AMFR, and both GPI/AMF and AMFR are overexpressed in highly metastatic tumors and correlate with a poor prognosis (Hirono et al., 1996; Jiang et al., 2006; Tsutsumi et al., 2004).
Even though, the exact mechanism of EMT induction and regulation by GPI/AMF is not completely clear, several studies demonstrated increased motility and metastasis following GPI/AMF overexpression. For example, in pancreatic cancer GPI/AMF overexpression results in upregulation of SNAIL, downregulation of E-cadherin and increased invasion (Tsutsumi et al., 2004). Also, an induction of MET was demonstrated after knockdown of AMF/PGI in osteosarcoma cells, characterized by upregulation of E-cadherin and downregulation of TGF-β and SNAIL (Niinaka et al., 2010; Tsutsumi et al., 2004).
Furthermore, Funasaka et al. have demonstrated an induction of MET in lung fibrosarcoma and breast carcinoma cells upon GPI/AMF knockdown as well as a reduction in tumor growth *in vivo*. Interestingly, they concluded that only the endogenous GPI/AMF was required for EMT while the exogenous/secreted was mainly necessary for cell growth and proliferation. They also concluded that endogenous GPI/AMF activates SNAIL resulting in down-regulation of E-cadherin and upregulation of mesenchymal marker proteins, leading to EMT. On the other hand, exogenous GPI/AMF signaling inactivates GSK3β, resulting in up-regulation of nuclear β-catenin expression *via* Wnt signaling, which increases cell growth (Funasaka et al., 2007, 2009). Furthermore, GPI/AMF was shown to activate ZEB1 *via* the NF-κB and miR200, leading to increased cell motility and invasion of breast cancer cells (Ahmad et al., 2011).
Taken together, GPI/AMF signaling affects not only EMT/MET markers and downstream targets but also other EMT-inducers such as TGFβ, Wnt/ β-catenin/GSK3b signaling and NF-kB. Moreover, GPI/AMF provides a connection between EMT and another hallmark of tumorigenesis; metabolic reprogramming.

1.2 Metabolic reprogramming of cancer cells

During malignant transformation cells undergo extensive metabolic reprogramming in order to support increased rates of cell growth, proliferation, migration and invasion as well as survival (Hanahan and Weinberg, 2011).

1.2.1 The Warburg effect

The first evidence of altered metabolism in cancer is known as the ‘Warburg effect’ which states that, highly proliferative cells or cancer cells upregulate glycolysis rates regardless of the presence or absence of oxygen (Figure 4). In contrast, non-proliferating normal cells only use

glycolysis under anaerobic conditions and prefer the more efficient energy producing oxidative phosphorylation (OXPHOS) in aerobic conditions. However, Warburg and his colleagues erroneously assumed that the upregulation of glycolysis coincided with downregulation of OXPHOS, due to defective mitochondria, while in reality many cancer cells retain active OXPHOS and functionally healthy mitochondria (Koppenol et al., 2011).

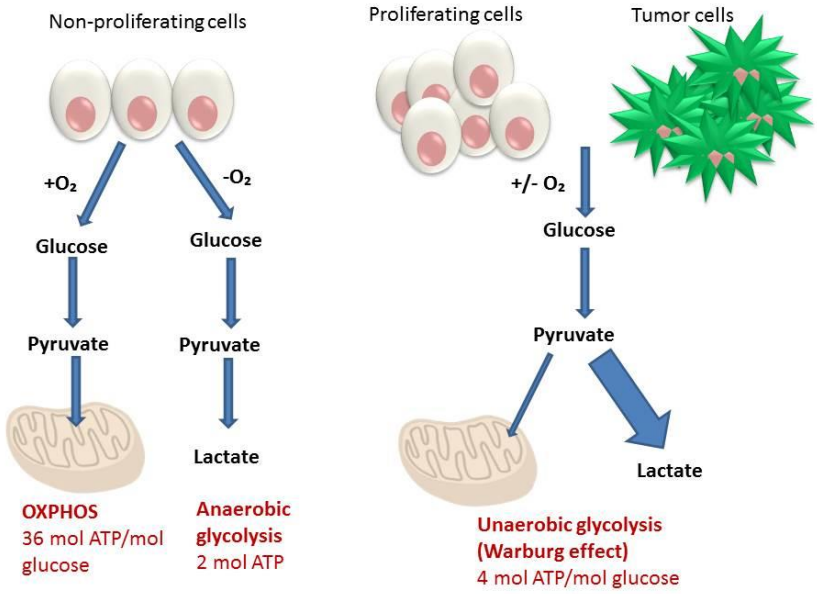

Figure 4: **The Warburg effect**. Non-proliferating cells (left panel) in the presence of oxygen convert glucose to pyruvate which enters the TCA cycle in the mitochondria and fuels oxidative phosphorylation to produce 36mol of ATP per mol of glucose. In the absence of oxygen, glucose is being converted to pyruvate and subsequently yields 2mol ATP per mol of glucose as well as lactate (anaerobic glycolysis). Proliferating cells and tumor cells produce almost all their energy *via* glycolysis regardless of oxygen presence (Warburg effect), yielding approximately 4mol ATP per mol of glucose and an excess of lactate.

1.2.2 Metabolic reprograming depends on the proliferation status

The current model of metabolic reprogramming of cancer cells differentiates between rapidly proliferating cells and quiescent cells (Ward and Thompson, 2012). According to this model, proliferating cells are anabolic (Figure 5), utilizing glucose *via* glycolysis (the Warburg effect) and glutamine to produce energy and building blocks required for mitosis, while quiescent cells are catabolic and utilize OXPHOS to maximize the energy production under metabolic stress caused by insufficient supply of nutrients (Figure 5) (Cha, 2015; Ward and Thompson, 2012).

For example, anabolic cells upregulate fatty acids synthesis required for construction of lipid bilayers of daughter cells' membranes (Cha, 2015; Jiang et al., 2015). Fatty acid synthesis is highly dependent on citrate and on reduced nicotinamide adenine dinucleotide phosphate (NADPH) which are supplied in high amount from the TCA cycle after upregulation of

reductive glutamine metabolism (DeBerardinis et al., 2007) and from the upregulated Penthose Phosphate Pathway (PPP), respectively (Cha, 2015).

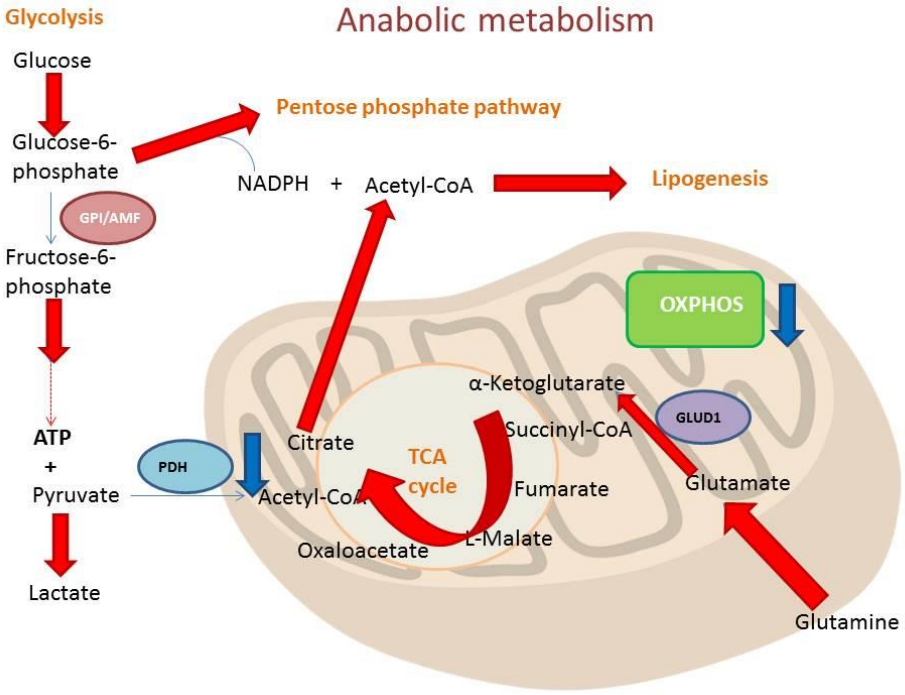

Figure 5: **Schematic representation of anabolic metabolism**. Highly proliferating cells require high amounts of ATP, nucleotides, amino acids and lipids compared to quiescent cells. Therefore, glucose and reductive glutamine metabolism increase and subsequently, pentose phosphate pathway and lipogenesis increase as well. Pyruvate uptake into the TCA cycle is reduced and instead lactate secretion increases. Since citrate is being diverted to fuel lipogenesis instead of NADH production, OXPHOS is reduced as well.

In contrast, catabolic cells maximize the efficacy of ATP production by upregulating the TCA cycle and thus OXPHOS (figure 6), reduce lipogenesis and activate survival pathways to protect themselves against starvation and oxidative stress due to reactive oxygen species (ROS) accumulation caused by upregulated OXPHOS (Jerby et al., 2012). NADPH deriving from the PPP is directed to quench the excessive ROS instead of lipogenesis in catabolic cells (Cha, 2015).

1.2.3 Metabolic reprograming during EMT

Cancer cells undergoing EMT switch to catabolism in order to survive Anoikis (Cha, 2015). Anoikis is a programmed cell death induced upon cell detachment from extracellular matrix and metastasizing tumor cells must develop resistance to Anoikis in order to survive (Paoli et al., 2013). Recently, it has been observed that upon EMT induction by TGFβ, A549 lung carcinoma cells downregulate pyruvate dehydrogenase kinase 4 (PDK4) an inhibitor of pyruvate dehydrogenase (PDH), thus increasing mitochondrial respiration. In addition, low expression of PDK4 was shown to correlate with poor prognosis in lung cancer (Sun et al.,

2014). In addition, highly invasive ovarian cancer cells were shown to upregulate pyruvate uptake into the TCA cycle as well as OXPHOS (Caneba et al., 2012). Another recent report has demonstrated a dramatic increase in OXPHOS only during EMT and this increase had no effect on anabolic pathway and proliferation (LeBleu et al., 2014). Lastly, induction of EMT by TGFβ in A549 cells was recently shown to decrease the fatty acid synthesis in addition to elevation of oxygen consumption required for upregulation of mitochondrial OXPHOS (Jiang et al., 2015). In summary, tumor cells undergoing EMT undergo extensive metabolic reprogramming which closely resembles catabolic metabolism under nutrient depletion. These similarities include upregulation of PDH resulting in increased pyruvate uptake into the TCA cycle, subsequent OXPHOS upregulation and downregulation of lipogenesis (Figure 6). In order to get further insight into the crosstalk between EMT and metabolic reprogramming, the proteins and transcription factors integrating both pathways require further research. One of these potential integrators is the multifunctional kinase GSK3β, known to be involved in many tumorigenic pathways including EMT and metabolism.

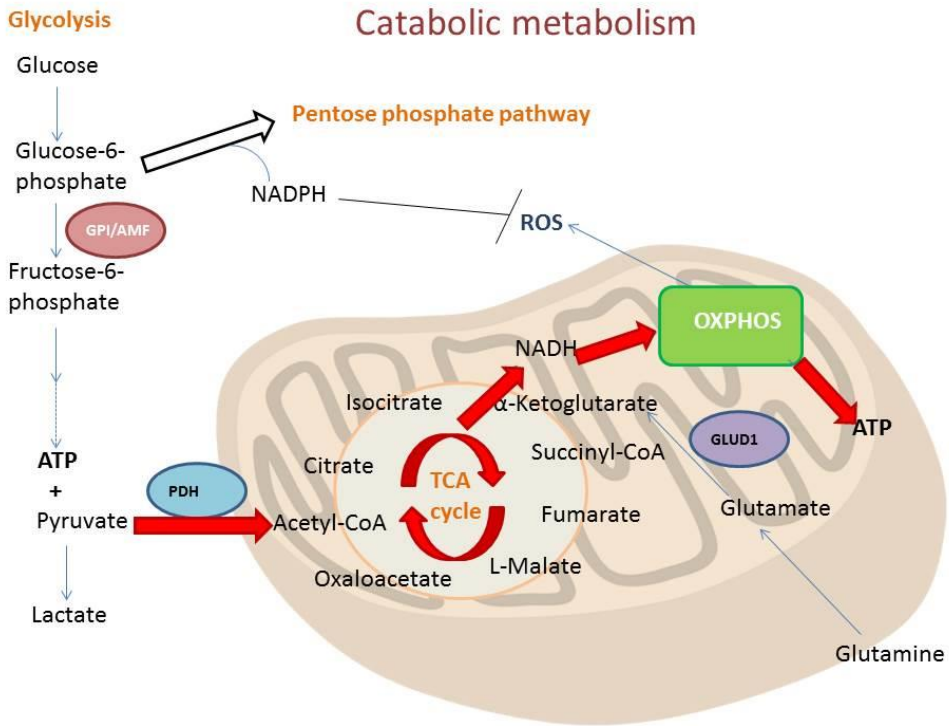

Figure 6: **Schematic representation of catabolic metabolism**. Non-proliferating or metastasizing cells as well as cells under stress such as low nutrient supply require ATP conservation and increased efficiency of energy production. Therefore, the energy-costly lipogenesis is downregulated via downregulation of reductive glutamine metabolism. Pyruvate uptake into the TCA cycle increases which enhances OXPHOS resulting in higher amount of ATP compared to glycolysis. NADPH from the PPP is redirected to quench increased ROS production from OXPHOS and less lactate is produced which increases survival.

1.3 Glycogen synthase kinase 3 (GSK3) and its role in cancer progression

1.3.1 General features and regulation

Glycogen synthase kinase 3 (GSK3) is a Ser/Thr protein kinase that has a very high basal enzymatic activity in resting cells (Medina et al., 2011) and can be inhibited by direct phosphorylation by various kinases, including PKA (Fang et al., 2000), PKB/AKT (Cross, 1995), PKC (Goode, 1992) and others (Figure 7). Three isoforms of GSK3 exist: GSK3α, GSK3β and GSK3β2 (Mukai et al., 2002). Isoforms GSK3α and GSK3β share 97% homology (Woodgett, 1990) and have similar functions (Rayasam et al., 2009), however despite these similarities GSK3α is unable to compensate for GSK3β after its knockout in mice, resulting in embryonic lethality due to liver degeneration (Hoeflich, 2000).

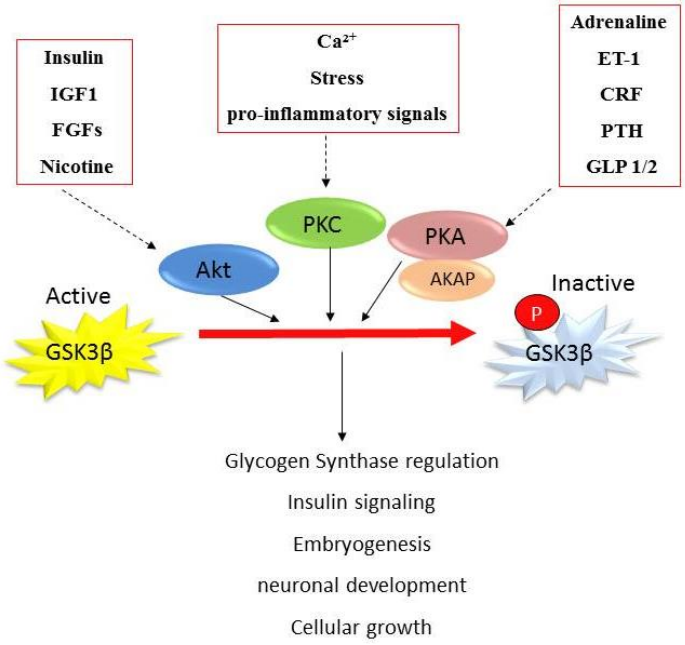

Figure 7: Schematic representation of GSK3β signaling. GSK3β is constitutively active in its basal state and is regulated by inhibitory phosphorylation by Akt (in response to insulin, nicotine, insulin growth factor1, fibroblast growth factor), PKC (in response Ca^{2+}, stress, pro-inflammatory signals) and PKA which requires an AKAP in order to phosphorylate GSK3β (in response to adrenaline, endothelin1, corticotropin-releasing factor, parathyroid hormone, glucagon-like peptide). In addition to regulating glycogen synthase, GSK3β is involved in regulation of multiple processes such as insulin signaling, embryogenesis, neuronal development and cell growth. Deregulation of GSK3β is implicated in various diseases such as Type 2 diabetes, cancer, Alzheimer's and others.

GSK3β regulates many signaling pathways including glucose/glycogen metabolism, insulin signaling, embryogenesis and oncogenesis (Eldar-Finkelman; Medina et al., 2011; Rayasam et al., 2009). Deregulation of GSK3β is implicated in cancer progression as well as in many other diseases such as Type 2 Diabetes, Alzheimer's and Parkinson's disease, bipolar disorder,

osteoporosis and others (Bhat and Budd, 2002; Eldar-Finkelman; Jope, 2007; Nikoulina, 2000; Polakis, 2007; Ralston, 2006).

1.3.2 GSK3β in cancer

GSK3β's roles in cancer are both extensive and controversial. Several studies have suggested that GSK3β suppresses tumor growth, for example by negatively regulating SNAIL in the EMT while others demonstrate that GSK3β promotes tumor growth (Kulikov, 2005; Maccario, 2007; McCubrey et al., 2014; Zhou et al., 2004a)(Figure 8). In addition, GSK3β was shown to be present in the cytoplasm, nucleus and mitochondria (Chiara and Rasola, 2013), and the protein's function can differ from one organelle to the other. For example, in the Wnt signaling, while the cytoplasmic GSK3β directly phosphorylates β–catenin and targets it for degradation, the nuclear GSK3β forms a complex with β-catenin and lowers the levels of β-catenin/TCF-dependent transcription (Caspi, 2008).

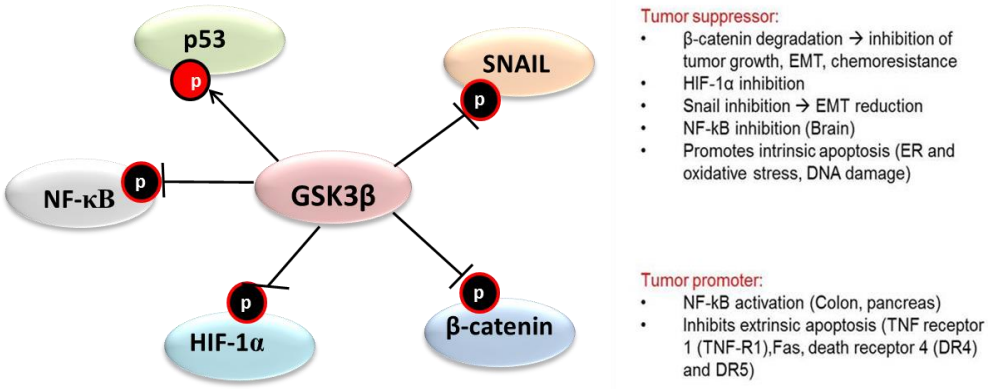

Figure 8: GSK3β's roles in cancer. GSK3β acts as a tumor suppressor by phosphorylating β–catenin thus targeting it for degradation, by inhibiting SNAIL, hypoxia inducible factor or NF-kB signaling pathway (brain cancer), or by promoting intrinsic apoptosis in response to stress or DNA damage *via* p53 and BAX activation. GSK3β acts as a tumor promoter by participating in activation of the NF-kB pathway in colon and pancreatic cancer or inhibiting extrinsic apoptosis via tumor necrosis factor receptor, Fas and death receptors). Adapted from McCubrey et al. 2014

In the mitochondria GSK3β contributes to the pro-apoptotic phenotype of cancer cells by controlling the mitochondrial localization and the activation status of a number of proteins of the cell death machinery (Beurel, 2006; Chiara and Rasola, 2013; Linseman, 2004), including p53, Mcl-1, Bcl-2, BAX, voltage-dependent anion channel (VDAC), and adenine nucleotide transporter (ANT). Apoptotis in mitochondria is termed intrinsic apoptosis and activated by stress conditions such as ER and oxidative stress, chemotherapeutics and growth factors depletion (Chiara and Rasola, 2013) or anoikis (section 1.2.3), activated by ECM detachment

upon EMT (Paoli et al., 2013). Since GSK3β lacks canonical protein-lipid interaction domains, the localization of GSK3β needs to be regulated through protein-protein interactions, e.g. by adaptor or scaffolding proteins such as Axin (Medina & Wandosell, 2011), or AKAPs like AKAP220 (Tanji, 2002) and GSKIP (see section 1.6) which also facilitate GSK3β's inhibition by PKA (Hundsrucker, 2010; Skroblin, 2011).

1.4 cAMP/PKA signaling and its role in cancer progression

1.4.1 cAMP signaling

Adenosine 3'5'-cyclic monophosphate (cyclic AMP, cAMP) is a second messenger that mediates signal transduction from various extracellular stimuli, such as hormones and neurotransmitters, to intracellular targets (Figure 9). The signals are transmitted *via* guanine-nucleotide-binding (G)-protein-coupled receptors (GPCRs), which bind stimuli in the form of agonists. This binding induces conformational change in the attached Gs protein complex, which results in the activation and release of Gs alpha subunit from the complex. The Gs alpha subunit, in turn, activates adenylyl cyclase (AC), which quickly converts ATP into second messenger cAMP (Hanoune and Defer, 2001) and ultimately activates cAMP-dependent protein kinase A (see section 1.4.2) by binding to PKA's regulatory subunits. cAMP also activates Epac proteins and cyclic-nucleotide-activated-ion channels (Gancedo, 2013; Montminy, 1997). Intracellular levels of cAMP are negatively regulated by PDEs which degrade cAMP into adenosine 5'-monophosphate (Omori and Kotera, 2007) and this regulation is achieved *via* feedback loop mechanisms influencing PDE expression levels (Gancedo, 2013).

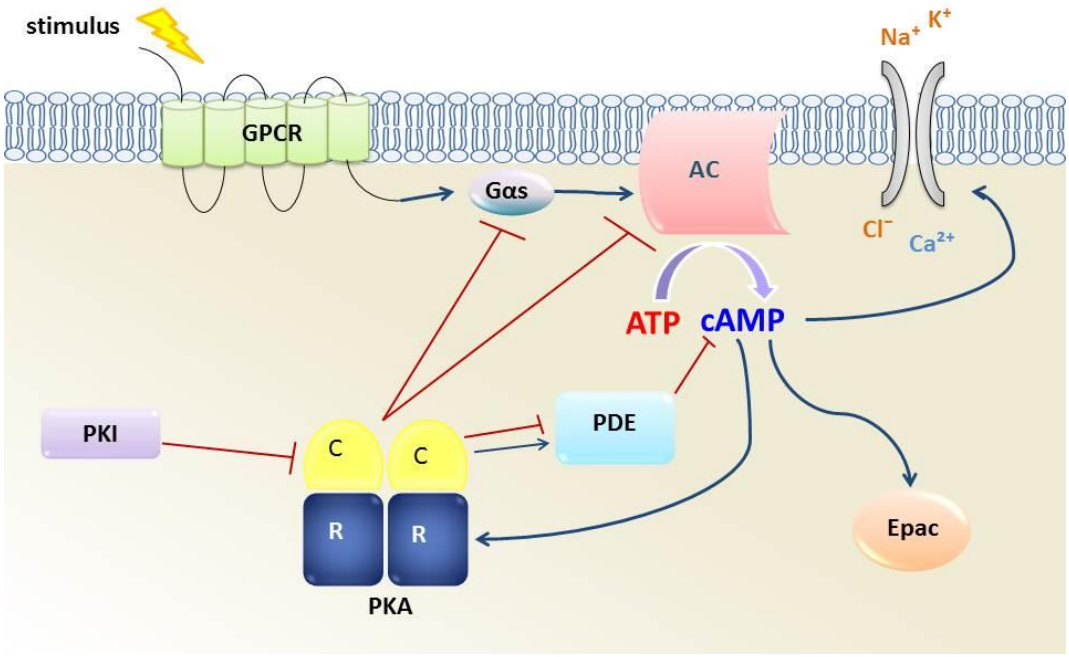

Figure 9: **Schematic representation of the cAMP signaling pathway**. Extracellular stimuli in the form of agonists bind to guanine nucleotide binding (G)-protein-coupled receptors and activate Gs alpha subunit which then activates adenylyl cyclase (AC). ACs converts ATP into second messenger cAMP and cAMP proceeds to activate cAMP-dependent protein kinase A (PKA) regulatory subunits resulting in the release of catalytic subunits which activate nearby substrates. cAMP also activates Epac proteins and cyclic-nucleotide-activated-ion channels. cAMP is negatively regulated by Phosphodiesterases (PDEs). PKA negatively regulates PDEs as well as AC and GPCR. PKA is negatively regulated by PKI.

The cAMP signaling cascade has significant roles in a wide variety of cellular processes many of which are deregulated in cancer, including metabolism, differentiation, proliferation, apoptosis and EMT. These roles are accomplished in a PKA-dependent or independent manner, as well as *via* crosstalk with other signaling pathways (Cho et al., 2014; Dong et al., 2015).

1.4.2 PKA

In its inactive state, PKA consists of two homodimeric regulatory subunits each bound to one catalytic (C) subunit (Figures 9 and 10). Two molecules of cAMP bind to each of the regulatory subunits of PKA causing the release of the catalytic subunits, which are then free to phosphorylate their substrates. The regulatory subunits can interact with a wide variety of proteins due to their multi-domain highly dynamic structure (Bruystens et al., 2014; Kim et al., 2007; Taylor et al., 2013; Wu et al., 2007).

There are four isoforms of PKA regulatory subunits (RIα, RIβ, RIα, RIβ) which all share common structural properties. In addition to having two cAMP binding domains at the C-terminus, all isoforms possess a dimerization/docking (D/D) domain at the N-terminus and an

inhibitor domain (Das et al., 2006; Gold et al., 2006). The isoforms RIα and RIβ are collectively termed PKA type I holoenzyme (PKAI) and isoforms RIα, RIβ are termed PKA type II holoenzyme (PKAII). PKAI has higher affinity for cAMP than PKAII and thus can be activated by lower concentrations of cAMP.

In addition, subcellular location differs between the two holoenzymes, with PKAI being primarily cytoplasmic while PKAII is targeted to various subcellular compartments via A-kinase anchoring proteins (see section 1.4).

There are four isoforms of catalytic (C) subunits (Cα, Cβ, Cγ and PrKX). Moreover, several splice variants were reported for C subunit isoforms adding diversity to PKA signaling (Caretta and Mucignat-Caretta, 2011; Skalhegg and Tasken, 2000).

PKA regulates, by direct phosphorylation, the activity of various proteins involved in cardiac muscles contractility, glucose and lipid metabolism, gene transcription, sperm motility, cell growth and differentiation, and a plethora of other processes (Lefkimmiatis and Zaccolo, 2014; Sapio et al., 2014; Walsh, 1994). Due to the multifunctional nature of cAMP/PKA axis, its deregulation has been implicated in many pathologies including cancer progression.

1.4.3 cAMP/PKA signaling in cancer

cAMP/PKA signaling is involved in a variety of malignacies thus targeting this pathway may be therapeutically beneficial (Naviglio et al., 2009; Sapio et al., 2014).

cAMP/PKA signaling is crucial to cell growth and differential cAMP levels were shown to be present during cell cycle progression. In addition, PKA phosphorylates macromolecular complexes responsible for the destruction of mitotic cyclins and separation of the sister chromatids at anaphase-metaphase transition (Ferrari, 2006). Moreover, colorectal cancer cells exhibit an anti-proliferative phenotype upon reduction in cAMP levels (Löffler et al., 2008) and PKA was suggested to induce mitogenesis in endocrine cells by acting synergistically with Epac (Hochbaum et al., 2008).

The involvement of cAMP/PKA in apoptosis regulation was demonstrated in highly metastatic MDA-MB-231 breast cancer cells, where elevation in cAMP levels resulted in increase of leptin-mediated apoptosis *via* ERK1/2 and STAT3 phosphorylation and down-regulation of PKA (Naviglio et al., 2010). The same group later showed that cAMP elevation inhibits leptin-induced migration of MDA-MB-231 breast cancer cells *via* β3 integrin and focal adhesion kinase (FAK) downregulation (Spina et al., 2012).

Malignant transformation and rapid proliferation were shown to be highly dependent on the ratio between PKAI and PKAII expression levels as well as on RIα expression. Generally,

overexpression of RIα is observed in many tumor cells and is associated with poor prognosis, whereas increased expression of RIIα is associated with healthy non-proliferating and terminally differentiated cells. Downregulation of RIα using antisense oligonucleotides designed against the N terminus of RIα subunit specifically inhibit PKA-I expression (not PKA-II) and induce differentiation, cell growth arrest, and/or apoptosis. Similar inhibition of malignant transformation was observed after overexpression of RIIα and mutant RIα (Bossis and Stratakis, 2004; Neary et al., 2004).

In addition to regulating tumorigenic pathways *via* cAMP signaling, PKA can affect malignant transformation in a cAMP independent manner. For example, PKA modulates TGFβ signaling (see section1.1.3.1) through a direct interaction with Smad3 and Smad4 resulting in TGFβ-mediated increases in PKA activity, induction of the cell cycle regulatory protein p21 and CREB phosphorylation, growth inhibition, induction of EMT and invasion of pancreatic cancer cells as well as *in vivo* tumor growth (Yang et al., 2013; Zhang et al., 2004). Moreover, PKA activation was shown to be required for TGFβ-mediated EMT and apoptosis *via* STAT3 signaling (Yang, 2006). In addition, the involvement of PKA in EMT induction and regulation has been demonstrated in breast carcinoma (Jiang et al., 2009), ovarian carcinoma (McKenzie et al., 2011), colorectal carcinoma (Chowdhury et al., 2011) and lung carcinoma (Shaikh et al., 2012). Other than PKA's interaction with TGFβ signaling proteins, PKA is a major player in regulating actin-cytoskeleton remodeling of the ECM which is a crucial step in EMT. PKA regulates actin dynamics, either in a cAMP-dependent or independent manner by targeting actin, integrins, VASP, LASP, myosin light chain, Rho GTPases, Src kinases, p21 activated kinases, phosphatases and proteases. PKA's mode of targeting is accomplished either interacting directly with the proteins or indirectly *via* AKAP-PKA binding (Howe, 2004). Furthermore, recent study demonstrated that PKA can phosphorylate SNAIL (see section 1.1.2) resulting in SNAIL stabilization thus promoting EMT (MacPherson et al., 2010).

In summary, targeting cAMP/PKA signaling in cancer metastasis has become very attractive and holds high promise for future therapeutic strategies (Sapio et al., 2014).

1.5 A-Kinase anchoring proteins (AKAPs)

1.5.1 General features of AKAPs

A-kinase anchoring proteins (AKAPs) are a family of approximately 50 scaffolding proteins, which anchor various proteins, such as protein kinases, and localize them to specific

intracellular locations, thus limiting their activities to substrates in close proximity (Hedrick et al., 2013; Skroblin et al., 2010; Tröger et al., 2012). All AKAPs have in common the ability to bind PKA (Langeberg and Scott, 2015; Troeger, 2012), as well as other ligands (Figure 10) and a few AKAPs have their own catalytic activity.

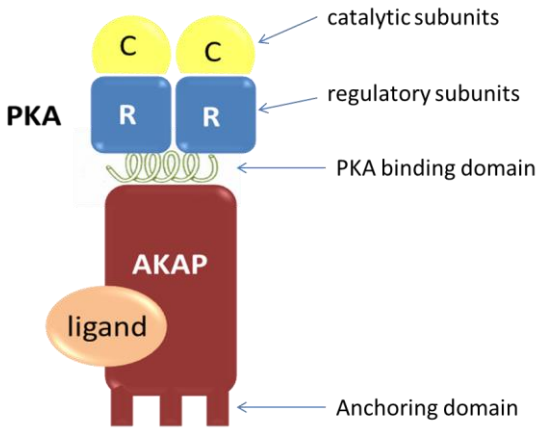

Figure 10: Schematic representation of AKAPs' structure and AKAP-PKA binding. AKAPs share three common properties: 1) AKAPs bind to the regulatory subunit of PKA through a conserved PKA binding domain; 2) a unique subcellular anchoring domain directs AKAP-signaling complexes to discrete locations inside a cell; 3) additional binding sites for other ligands such as kinases, phosphatases, or substrates.

AKAPs regulate PKA signaling by compartmentalizing it in various cellular areas and organelles (Schächterle et al., 2015; Troeger, 2012; Wong and Scott, 2004). Many cells can express as many as 10 to 15 different AKAPs localized to different intracellular compartments. A few examples include, AKAP95 which acts in the nucleus, Ezrin and AKAP84 in the cytosol, and AKAP220 in peroxisomes (Skalhegg and Tasken, 2000; Skroblin et al., 2010).

1.5.2 AKAPs in cancer

Many AKAPs are reported to be differentially expressed in cancer cells and tissues (Uhlén et al., 2015) where they regulate proliferation, survival and metastasis (Diviani and Scott, 2001; Frank et al., 2008; Hedrick et al., 2013). These include AKAP-Lbc (AKAP13), which regulates cancer cell proliferation by enhancing ERK signaling and catalyzes the GDP-GTP exchange reaction required for RhoA activated tumor invasion and growth (Langeberg and Scott, 2015; Smith et al., 2010; Wirtenberger et al., 2006). Another important AKAP in tumorigenesis is gravin (AKAP12), which suppresses tumor growth and metastasis by removing Src kinase from both focal adhesion kinase (FAK) as well as PKC-mediated activation of ERK signaling (Su et al., 2013).

In addition, the AKAP function of Ezrin-Radixin-Moesin (ERM) family members is required for PKA-mediated regulation of Netrin-1/DCC (deleted in colorectal carcinoma) signaling (Deming et al., 2015), which has previously been shown to influence angiogenesis, epithelial migration and tumor pathogenesis (Mehlen and Furne, 2005).

Additional AKAPs that have recently emerged as regulators of EMT include AKAP79 (AKAP5) and AKAP220, which were found to directly interact with IQ domain GTPase-activating protein 1 (IQGAP1) and IQGAP2 respectively (Logue et al., 2011; Nauert et al., 2003). IQGAPs are scaffolding proteins regulating migration and invasion *via* the actin cytoskeleton and microtubule dynamics and are frequently deregulated in malignant transformation (Liu et al., 2010; White et al., 2009; Xie et al., 2012).

Due to the fact that PKA and AKAPs are intricately involved in cancer pathogenesis, elucidating their exact function may hold promise for development of novel cancer therapeutics targeting AKAPs and PKA-AKAP interactions (Sapio et al., 2014; Troeger, 2012).

1.6 GSK3β interacting protein (GSKIP)

1.6.1 General features and structure of GSKIP

GSKIP is a member of the AKAP family, also known as C14orf129, after its chromosomal localization, chromosome14, open reading frame 129 (Swiss-Prot ID, GSKIP_human).

GSKIP is ubiquitously expressed and anchors PKA RII subunits through an evolutionarily conserved domain (RIIBD in Figure 11). In addition, GSKIP binds GSK3β *via* a GSK3b interaction domain (GID) domain (Figure 11), which is also evolutionary conserved, and facilitates PKA inhibitory phosphorylation of GSK3β on Ser9 (Hundsrucker, 2010).

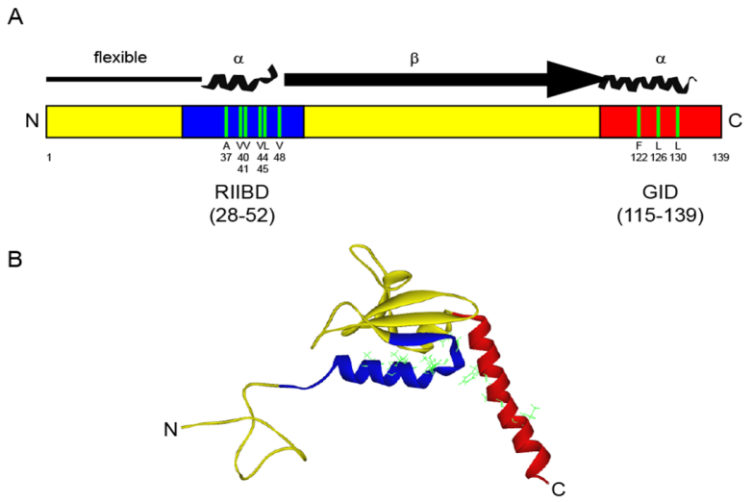

Figure 11: Schematic representation of GSKIP. A. GSKIP is divided into four fragment, a flexible N-terminus (line), two α-helices (α) and a β-strand region (β,arrow). The positions of functionally assigned domains are indicated, the RII-binding domain (RIIBD, blue) and the GSK3β interaction domain (GID, red). The positions of essential hydrophobic amino acids within these two interaction domains are indicated by green lines (Skroblin, 2011). B. Tertiary structure of GSKIP. The RIIBD, the GID and their important amino acids are highlighted in the same colors as in A (Ramelot et al., Unpublished work).

1.6.2 GSKIP is ubiquitously expressed in tumor tissues

The human protein atlas (Uhlén et al., 2015) shows GSKIP antibody staining in 20 different cancer types (Figure 12). GSKIP shows high expression in breast, liver, lung, head and neck, endometrial, testis, neuroendocrine, ovarian and cervical cancers, as well as in melanoma, lymphoma and glioma compared to healthy tissues. This evidence suggests GSKIP to function as a tumor promoter in the majority of cancer tissues tested. Several studies have demonstrated GSKIP to function as a tumor promoter and are detailed in the next section.

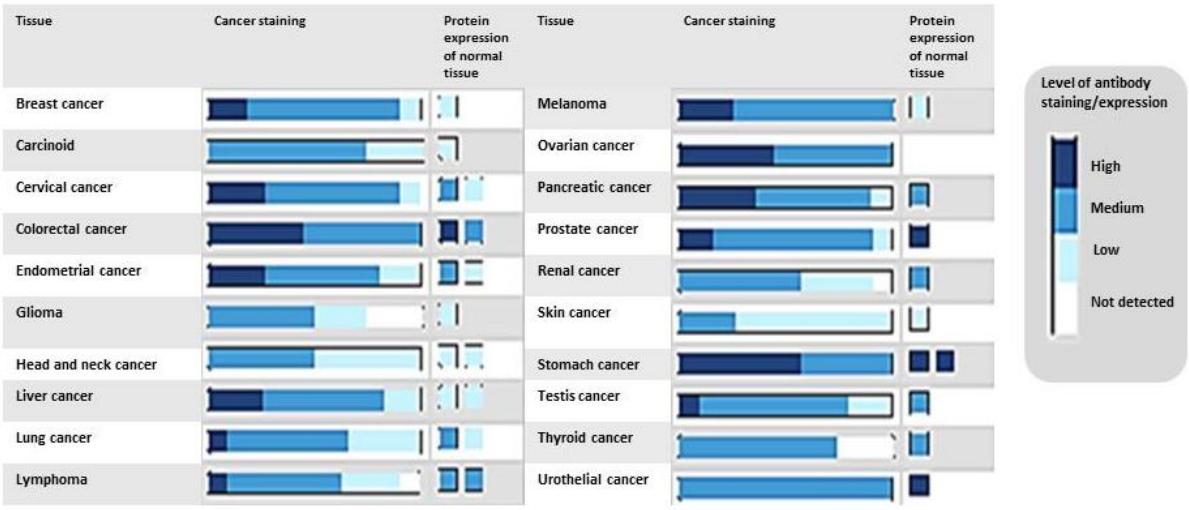

Figure 12: **GSKIP is ubiquitously expressed in tumor tissues**. The staining summary describes the total fraction of patient samples with GSKIP antibody staining/protein expression using all the available antibodies to the protein targets encoded by this gene. For each cancer, the fraction of samples with antibody staining/protein expression level high, medium, low or not detected are displayed (as described by the color-coding scale in the box to the right). The length of the bar represents the number of patient samples analyzed (≤ 12 patients). Adapted from Human Protein Atlas.

1.6.3 Functions of GSKIP

1.6.3.1 GSKIP promotes cell cycle progression in neuroblastoma cells

GSKIP binds to GSK3β via a binding domain homologous to that of Axin and is able to negatively regulate GSK3β in the Wnt signaling pathway (Chou et al., 2006). GSKIP establishes distinct pools of GSK3β/β-catenin, β-catenin/cyclin D1 and N-cadherin/β-catenin and it is important during neuron development and retanoic acid-induced neuronal differentiation. Namely, neurite extension following RA treatment in GSKIP-overexpressing cells was blocked. Furthermore, GSKIP expression promotes cell cycle progression by increasing the accumulation of β-catenin in the nucleus, resulting in higher transcription of cell cycle promoter protein Cyclin-D1. These results suggest that overexpression of GSKIP can affect the transcriptional state of the cell and promote tumor growth (Lin et al., 2009).

Another study by Chou et al. suggested GSKIP may be important for GSK3β-mediated phosphorylation of Dynamin related protein 1 (Drp1), an important regulator of mitochondrial morphology and biogenesis, in HEK293 cells (Chou et al., 2012). However the exact mechanism of GSKIP's involvement in Drp1 phosphorylation needs further research.

In addition to GSK3β, GSKIP interacts with five additional proteins, all of which have important roles in tumorigenesis. Wang et al. have shown that GSKIP interacts with PEX19, SMYD2, EXT2 and GSK3α by high-stringency Yeast-two-Hybrid (Y2H) protein interaction analysis (Wang et al., 2014).

Peroxisomal Biogenesis Factor 19 (PEX19) is one of the proteins required for the normal assembly of peroxisomes and mutations in PEX19 gene are associated with Zellweger syndrome, characterized by severe neurologic dysfunction, craniofacial abnormalities, and liver dysfunction. Peroxisomes are a single-membrane-bounded ubiquitous organelles containing enzymes that catalyze various metabolic pathways, such as β-oxidation of very long-chain fatty acids. In all types of cells, peroxisomes were defined to contain one or more enzymes that form hydrogen peroxide from organic substrates as well as catalase (CAT), a typical marker enzyme of the peroxisomal matrix that degrades hydrogen peroxide (Fujiki et al., 2012)

Another interaction partner of GSKIP is SET domain-dependent methyltransferase 2 (SMYD2). SMYD2 is a histone lysine methyltransferase that was identified to methylate tumor suppressors p53 and Rb, thus inhibiting their functions (Wang et al., 2011). SMYD2 was also

shown to regulate estrogen signaling by methylating Estrogen Receptor α (Jiang et al., 2014) possibly implicating SMYD2 in estrogen signaling related pathologies which include breast and cervical cancer. SMYD2 was also shown to interact with GSK3β (Skroblin, 2011).
Exostosin Glycosyltransferase 2 (EXT2) is another predicted interaction partner of GSKIP and it was shown to be mutated in in breast carcinoma patients (Yoneda et al., 2012).
EXT2 is required for post translational modification of Heparan sulfate proteoglycans, which are involved in cell growth, differentiation, angiogenesis and cellular response to the environment (Blackhall et al., 2001).
In addition, GSKIP interacts with GSK3α, an isoform of GSK3β. GSK3α has specific functions in tumorigenes, which differ from GSK3β functions. A recent report has shown that silencing of GSK3α, but not GSK3β expression inhibited proliferation, survival and colony formation in prostate cancer cells, and the growth of PC3 tumor xenografts in mice. On the other hand, silencing GSK3β resulted in the inhibition of cell scattering, establishment of cell-cell contacts, increased expression and membrane localization of β-catenin, and reduced expression of EMT markers such as SNAIL and MMP-9. This demonstrated the isoform specific role of GSK3α and GSK3β in prostate cancer cells *via* distinct molecular and cellular mechanisms (Gao et al., 2015).
Recently GSKIP was shown, *via* quantitative immunoprecipitation combined with knockdown (Kd) and human proteome microarray analysis, to interact with Bcl2-associated athanogene 3 (BAG3). BAG3 is a member of the BAG family of co-chaperones, which plays a critical role in regulating intrinsic apoptosis, development, cell motility, autophagy, and tumor metastasis (Wang et al., 2014).
All of these newly discovered GSKIP interacting proteins remain to be further validated. However, since they all have been implicated in tumorigenesis regulation, the role of GSKIP in cancer seems very likely.

1.7 Aims of this thesis

GSKIP binds GSK3β and PKA and facilitates PKA's inhibitory phosphorylation of GSK3β and both GSK3β and PKA have extensive roles in tumorigenesis. Thus GSKIP may have an important role in tumorigenesis as a regulator of GSK3β activity *via* PKA, and PKA activity *via* its AKAP function. Although several of GSKIP's functions have been previously suggested (1.6.3), its exact mechanism of action remains unknown. Therefore, this PhD project aims to elucidate GSKIP's role in tumorigenesis by studying its interactions with PKA and GSK3β in cultured cancer cells.

In addition, several potential interaction partners of GSKIP, such as SMYD2 and others (1.6.3) have possible regulatory roles in cancer signaling pathways. Evaluation of predicted as well as discovery of novel interaction partners of GSKIP, may provide further insight into GSKIP's roles in cancer progression. Therefore, this project aims to evaluate some of the predicted interaction partners as well as to discover novel interactors, and to elucidate GSKIP's role in their regulation. Prospectively, new insights into GSKIP's roles may lead to the development of novel targeted cancer therapies.

2. Materials and Methods

2.1 Materials

2.1.1 Mammalian cell lines and culture mediums

Cell lines	Description	Culture medium	Supplier
HEK293	Human embryonic kidney cell line	DMEM, low glucose, GlutaMAX™ Supplement, pyruvate, Life Technologies GmbH (Darmstadt, DE; # 10567-014); 10 % fetal bovine serum (FBS); 1 % penicillin/streptomycin (100 U/ml)	Deutsche Sammlung von Mikroorganismen und Zellkulturen GmbH (DSMZ) (Braunschweig DE)
A549	Human lung carcinoma cell line	DMEM, low glucose, GlutaMAX™ Supplement, pyruvate, Life Technologies GmbH (Darmstadt, DE; # 10567-014); 10 % fetal bovineserum (FBS); 1 % penicillin/streptomycin (100 U/ml)	American Type Culture Collection (ATCC) (Virginia, US) ATCC® CCL-185™
MCF-7	Human breast adenocarcinoma	DMEM, low glucose, GlutaMAX™ Supplement, pyruvate, Life Technologies GmbH (Darmstadt, DE; # 10567-014); 10 % fetal bovine serum (FBS); 1 % penicillin/streptomycin (100 U/ml)	DSMZ (Braunschweig DE)
SH-SY5Y	Human neuroblastoma	DMEM/F-12, GlutaMAX™ supplement, Life Technologies GmbH (Darmstadt, DE; # 10565-018); 10 % fetal bovine serum (FBS); 1 % penicillin/streptomycin (100 U/ml)	DSMZ (Braunschweig DE)
Hela S3	Human cervix carcinoma	RPMI 1640 Medium, GlutaMAX™ Supplement, Life Technologies GmbH (Darmstadt, DE; # 61870-010); 10 % fetal bovine serum (FBS); 1%penicillin/streptomycin (100 U/ml)	DSMZ (Braunschweig DE)
Jurkat	Human T cell leukemia	RPMI 1640 Medium, GlutaMAX™ Supplement, Life Technologies GmbH	Kindly provided by AG Izsvak, MDC (Berlin, DE)

		(Darmstadt, DE; # 61870-010); 10 % fetal bovine serum (FBS); 1%penicillin/streptomycin (100 U/ml)	
MiaPaca-2	Human pancreatic carcinoma	RPMI 1640 Medium, GlutaMAX™ Supplement, Life Technologies GmbH (Darmstadt, DE; # 61870-010); 10 % fetal bovine serum (FBS); 1%penicillin/streptomycin (100 U/ml)	Kindly provided by AG Poy, MDC (Berlin, DE)
MDAMB-231	Human mamary gland/breast adenocarcinoma	DMEM, low glucose, GlutaMAX™ Supplement, pyruvate, Life Technologies GmbH (Darmstadt, DE; # 10567-014); 10 % fetal bovine serum (FBS); 1 % penicillin/streptomycin (100 U/ml)	Kindly provided by AG W. Birchmeier, MDC (Berlin, DE)
HepG2	Human hepatocytes from tumor tissue	DMEM, low glucose, GlutaMAX™ Supplement, pyruvate, Life Technologies GmbH (Darmstadt, DE; # 10567-014); 10 % fetal bovine serum (FBS); 1 % penicillin/streptomycin (100 U/ml)	Kindly provided by AG Rocks, MDC (Berlin, DE)
SW480	Human colon adenocarcinoma	RPMI 1640 Medium, GlutaMAX™ Supplement, Life Technologies GmbH (Darmstadt, DE; # 61870-010); 10 % fetal bovine serum (FBS); 1%penicillin/streptomycin (100 U/ml)	DSMZ (Braunschweig DE)
HT-29	Human colon adenocarcinoma	DMEM, low glucose, GlutaMAX™ Supplement, pyruvate, Life Technologies GmbH (Darmstadt, DE; # 10567-014); 10 % fetal bovine serum (FBS); 1 % penicillin/streptomycin (100 U/ml)	Kindly provided by AG Jentsch, MDC (Berlin, DE)

Table 1: Mammalian cell lines and culture mediums

2.1.2 Equipment, disposable materials and Software

Equipment	Description	Supplier
Enspire® 2300	Microplate reader	PerkinElmer (Rodgau, DE)
BZ-8100E microscope	UV-VIS Microscope and camera	Keyence Deutschland GmbH (Neu-Isenburg, DE)
XF24 Extracellular flux analyzer	System to measure the rate of change of dissolved oxygen and pH in the media of living cells	Seahorse Bioscience (Massachusetts, US)
LSM780	Confocal microscope	Carl Zeiss MicroImaging GmbH (Jena, DE)
MiniProtean®	Polyacrylamide gel electrophoresis cell	Bio-Rad Laboratories GmbH (München, DE)
Odyssey Imager	Western Blot detection system	LI-COR Biosciences (Bad-Homburg, DE)
Scepter™ 2.0	Automated cell counter	Merck Millipore (Schwalbach, DE)
TransBlot	Semi-Dry Western Blot module	Bio-Rad Laboratories GmbH (München, DE)

Table 2: Equipment used for experimental procedures

Equipment	Description	Supplier/ catalogue number(#)
6-well plate	6-well cell culture plate	TPP (Trasadingen, CH) #92006
96-Well Microplate	96-well microplate	Greiner bio-one (Solingen, DE) #655101
Transwell® permeable support	24-well culture plate with 8.0µm Pore Polycarbonate Membrane Insert	Corning Inc. (NY, US) #3422
XF24 culture microplates	24 well culture plate V7-PS	Seahorse Bioscience (Massachusetts, US) #25213
XF24 extracellular flux assay kits	24 well XF assay cartridge	Seahorse Bioscience (Massachusetts, US) #Q25913
Cryo-vials	Cell conservation	Carl Roth GmbH & Co KG (Karlsruhe, DE) #E309.1
PVDF membranes	Western Blotting membranes	Carl Roth GmbH & Co KG (Karlsruhe, DE) #T830.1
ScepterTM Sensors 60 µM	Cell counting	Merck Millipore (Schwalbach, DE) #PHCC60050
T75 cell culture flask	Cell culture flask	TPP (Trasadingen, CH)

Table 3: Disposable materials used for experimental procedures

Software	Description	Supplier/URL
XF24 Extracellular Flux Analyzer	Analysis of extracellular flux to determine rates of OXPHOS and glycolysis	Seahorse Bioscience (Massachusetts, US)
Excel 2010	Spreadsheet, statistical analysis	Microsoft (Redmond, US)
Illustrator	Graphics, drawing	Adobe Systems, Inc. (San Jose, US)
Image J	Image processing	rsb.info.nih.gov/ij/
Image Studio Ver 2.0	Western Blot analysis	LI-COR Biosciences (Bad-Homburg, DE)
Photoshop	Image processing	Adobe Systems, Inc. (San Jose, US)
Power Point 2010	Presentations	Microsoft (Redmond, US)
Word 2010	Word processing	Microsoft (Redmond, US)
ZEN 2011	Confocal microscopy, image acquisition and analysis	Carl Zeiss MicroImaging GmbH (Jena, DE)

Table 4: Software

2.1.3 Antibodies, siRNAs and recombinant plasmids

Name	Origin	Supplier/catalogue number (#)
Primary antibody		
GSKIP	Rabbit	Custom-made by Biogenes (Berlin, DE) as described in (Hundsrucker, 2010)
E-Cadherin	Rabbit	Cell Signalling Technology (Danvers, US) #3195S
GPI	Mouse	Santa Cruz Biotechnologies (Heidelberg, DE) #sc-365066
PDH	Rabbit	Cell Signalling Technology (Danvers, US) #3205
N-Cadherin (D4R1H)	Rabbit	Cell Signalling Technology (Danvers, US) #13116P
ZEB1/TCF8	Rabbit	Cell Signalling Technology (Danvers, US) #3396
GAPDH	Rabbit	Cell Signalling Technology (Danvers, US) #2118S
SNAIL (C15D3)	Rabbit	Cell Signalling Technology (Danvers, US) #3879S
CD44	Rabbit	Cell Signalling Technology (Danvers, US) #3578S
TGFβ	Rabbit	Cell Signalling Technology (Danvers, US) #3711S
GDF5OS	Rabbit	Abcam (Cambridge, UK) #ab174617
SMYD2 (D14H7)	Rabbit	Cell Signalling Technology (Danvers, US) #9734S
α-Tubulin (DM1a)	Mouse	Calbiochem (Nottingham, UK) #CP06
IgG	Rabbit	Cell Signaling Technology (Danvers, USA) #2729
V-1 (Myotrophin)	Mouse	BD Biosciences (Heidelberg, D) #611830

AKAP 12 / Gravin	Sheep	Abcam (Cambridge, UK) #ab10346
Rab27	Mouse	BD Biosciences (Heidelberg, D) #558532
Secondary antibody		
POD-F(ab)2-anti-Rabbit-IgG	Donkey	Dianova (Hamburg, D)#711-036-152
POD-anti-Mouse IgG	Donkey	Dianova (Hamburg, D) #715-035-151
POD-anti-Sheep IgG	Donkey	Dianova (Hamburg, D) #713-035-147

Table 5: Antibodies used for this work

Name	**Target/sequence (5'-3')**	**Supplier/catalogue number(#)**
GSKIP (siGENOME-SMART pool)	CCAGGUAGAUGAUCAUUUA, CAACAUGUUUGUCUCGAAA, CGGAUGAUGUGGCCUAUAU, GCUCAAGGUGGUAGGCUAU	Thermo Fisher Scientific (Darmstadt, DE) # M-020252-01-0010
NT#2 (siGENOME Non-targeting siRNA Pool #2)	Firefly luciferase/ UAAGGCUAUGAAGAGAUAC, AUGUAUUGGCCUGUAUUAG, AUGAACGUGAAUUGCUCAA, UGGUUUACAUGUCGACUAA	Thermo Fisher Scientific (Darmstadt, DE) #D-001206-14-20
TOX (TOX Transfection Control)	Proprietary	Thermo Fisher Scientific (Darmstadt, DE) #D-001500-01-20

Table 6: siRNAs used for this work

All recombinant plasmids used for this work were generated by Alessandro Dema (AG Klussmann). GSKIP target sequences were cloned into pCMV vector with FLAG tag and transformed in TOP10 *E.coli* cells.

Name	**Target region**	**description**
pCMV6_Gskip_Hs_Wt_Flag _Non resistant	WT GSKIP	Wild type GSKIP
pCMV6_Gskip_Hs_L130P_Flag_Non resistant	GID of GSKIP	GSK3β binding deficient mutant
pCMV6_Gskip_Hs_N42I_Flag_Non resistant	RIIBD of GSKIP	PKA binding deficient mutant

Table 7: Recombinant plasmids used for this work

2.1.4 Chemicals and buffers

Chemical	Description	Supplier/ catalogue number (#)
Lipofectamine 2000	siRNA transfection reagent	Thermo Fisher Scientific (Darmstadt, DE) #1683448
Viafect	DNA transfection reagent	Promega, #E4983
Oligomycin	ATP-synthase inhibitor	Sigma-Aldrich, Inc. (Taufkirchen, DE) #O4876
FCCP	Mitochondrial uncoupler	Sigma-Aldrich, Inc. (Taufkirchen, DE) #C2920
Antimycin A	Mitochondrial Complex III inhibitor	Sigma-Aldrich, Inc. (Taufkirchen, DE)#A8674
Rotenone	Mitochondrial Complex I inhibitor	Sigma-Aldrich, Inc. (Taufkirchen, DE) #R8875
Tumor necrosis factor α	TNF-α	Generously donated by AG Scheiderheit, MDC (Berlin, DE)
Protease inhibitor cocktail tablets (complete EDTA free)	protease inhibitors added to lysis buffer	Roche Diagnostics GmbH (Berlin, DE) #4693159001
Alamar blue	Cell Viability indicator	Thermo Fisher Scientific (Darmstadt, DE) #DAL1025
DAPI	Cell nuclei dye	Roche Diagnostics GmbH (Berlin,DE) #10236276001
Phalloidin-Tetramethylrhodamine B isothiocyanate (TRITC-Phalloidin)	Actin cytoskeleton dye	Sigma-Aldrich, Inc. (Taufkirchen, DE) #P1951

Table 8: Chemicals

All chemicals used for preparing buffers and solutions in Table 9 were purchased from Sigma-Aldrich Inc. (Taufkirchen, DE) or Carl Roth GmbH & Co. KG. (Karlsruhe, DE) and prepared with *Aqua deion*, unless otherwise specified.

Water (referred to as *Aqua deion*) was purified by the Milli-Q Plus system (Millipore, Schwalbach, DE) to ≤10µS/cm at room temperature (RT) in the MDC institute.

Buffer/solution	Composition / Supplier
XF Calibrant (pH=7.4)	Seahorse Bioscience (Massachusetts, US) #100840-000
XF Assay medium modified DMEM	Seahorse Bioscience (Massachusetts, US) #102352-000
Blocking buffer (IF)	0.27 % fish skin gelatine in 1x PBS
Blocking buffer (Western Blot)	1% Albumin bovine serum BSA in 1xTBS-T
Blocking buffer (protein-peptide overlay)	3% Albumin bovine serum BSA in 1xTBS-T
RIPA Lysis buffer (Western Blot)	50 mM Tris-HCl, pH 7.4; 150 mM NaCl; 1 mM EDTA; 1mM DTT; 0.5% Triton-X 100;0.5% Na-deoxycholate; 0.1% SDS; 1 Protease Inhibitors tablet (Rosche) per 10mL
PBS lysis buffer (IP)	137 mM NaCl; 2.7 mM KCl; 1.5 mM KH_2PO_4; 8.1 mM Na_2HPO_4 (pH 7.4); 1 Protease Inhibitors tablet (Rosche) per 10mL; 0,2% Triton-X 100; 1mM EDTA; 1mM EGTA
Opti-MEM®	Life Technologies GmbH (Darmstadt, DE); #11058-021
Phosphate-buffered saline (PBS)	137mM NaCl; 2.7mM KCl; 1.5mM KH_2PO_4; 8.1mM Na_2HPO_4; pH 7.4
Sample buffer 3x	30 % glycerol; 3 % SDS; 200mM Tris-HCl; 30mM DTT; pH 6.8
Sample buffer 4x	25% glycerol; 2% SDS; 62.5 mM Tris-HCl; 0.01% Bromophenol Blue; pH 6.8
SDS-polyacrylamide gel electrophoresis (PAGE) running buffer	25 mM Tris; 192mM glycine; 0.1 % SDS
Semi-dry transfer buffer (Western Blot)	48 mM Tris; 39 mM glycine; 1.3 mM SDS; 20 % methanol
Separating gel buffer (SDS-PAGE)	0.625 M Tris-HCl; pH 6.8
Stacking gel buffer (SDS-PAGE)	0.75 M Tris-HCl; pH 8.8
TBS + Tween (TBS-T)	1x TBS; 0.05 % Tween-20
Tris-buffered saline (TBS)	10 mM Tris-HCl; 150 mM NaCl; pH 7.4
1% Trypsin-EDTA	Thermo Fisher Scientific (Darmstadt, DE) #25200-056
Glutaraldehyde-Crystal violet fixation-staining solution	6 % (v/v) Glutaraldehyde; 0.5% (w/v) Crystal Violet

Table 9: Buffers and solutions

2.2 Methods

2.2.1 Mammalian cell culture

2.2.1.1 Culturing of mammalian cells

Adherent A549, MCF-7, HEK293, SW480, SHSY-5Y, Hela S3, MiaPaca-2, MDAMB-231, HepG2 and HT-29 cells were grown in appropriate medium (Table 1) and subcultured twice a week. Confluent cells were washed with ice-cold PBS and incubated with 1x Trypsin-EDTA for 2-4 min at 37°C. After cell detachment, trypsinization was stopped by serum containing

medium. A defined volume of cell suspension was transferred into a new cell culture flask with fresh culture medium. Non-adherent Jurkat cells were grown in appropriate medium (Table 1) and sub-cultured twice a week. Cell suspension was transferred to a 15 ml falcon tube and centrifuged (2 min, 300xg, at 4 °C). The supernatant was removed and cell pellet re-suspended in 10 ml of fresh culture medium. A defined volume of cell suspension was transferred into a new cell culture flask with fresh culture medium.

2.2.1.2 Freezing and thawing of mammalian cell lines

After reaching confluency in a T75 cell culture flask cells were trypsinized and centrifuged (2 min, 300xg, at 4 °C). The pellet was resuspended in 1 ml medium without antibiotics containing 10 % FBS and 10% dimethyl sulfoxide (DMSO) and the cell suspension was transferred to 2 ml vials, which were stored overnight at -80 °C in a Cryo-container to achieve a cooling rate of 1 °C/min. The next day the cell-containing vials were transferred to a liquid nitrogen tank.

To reculture cells, frozen vials were quickly thawed in a water bath at 37 °C. Cells were transferred from the Cryo-vial to a T75 cell culture flask, containing 12 ml medium. After 24 hour incubation, the medium was replaced with fresh medium in order to prevent DMSO toxicity. After additional 1-2 days cells reached confluency and were subcultered.

2.2.1.3 Cell counting

Cells were detached from plastic surfaces of culture dishes by trypsinisation. The cell suspension was diluted 1:10 in a 1.5 ml reaction tube using PBS. Using the Scepter ^{TM} 2.0 pipette with 60 µM tips, cells of 9-21 µM size were counted.

2.2.1.4 Reverse siRNA transfection

siRNA (small interfering RNA) are double stranded RNAs (dsRNAs) used to silence expression of target genes in mammalian cells (Martinez et al., 2002). siRNAs range in size between 21-23 nucleotides and mediate the process of RNA interference (RNAi) (Elbashir et al., 2001). Mammalian cells are equipped with defense mechanisms against foreign genetic elements which are triggered by dsRNA (Fire, 1999). siRNAs escape these defenses due to their small size but are dissociated into its single strands and the guide strand is incorporated into the RNA-induced silencing complex (RISC). Activated RISC targets homologous sense as well as well antisense single-stranded RNAs for degradation resulting in inhibition of expression of the target gene (Elbashir et al., 2001).

Human GSKIP siRNA SMARTpool (Table 6) was resuspended in RNAse-free water and aliquoted. On the day of transfection siRNA was incubated with Lipofectamine® 2000 transfection reagent for 20 min at RT. A549 cells were trypsinized and reversely transfected by seeding cells onto the siRNA-lipid complex and incubation for 24 hrs at 37 °C. In a 6-well format, 4 µl of 20 µM siRNA were suspended in 250 µl Opti-MEM® and after 5 min incubation at RT mixed with 250 µl Opti-MEM®, containing 2 µl Lipofectamine® 2000. After 20 min incubation at RT, 200,000 cells/ml in 1500 µl medium were added to each well, resulting in 40 nM final siRNA concentration in 2000 µl transfection volume per well. Transfection efficiency was confirmed visually 24 hrs later using 40 nM toxic siRNA (TOX) and 40 nM Non-targeting siRNA (NT) was used a negative control. 24 hrs post transfection, medium was replaced with fresh medium and cells were harvested 48 hrs post transfection.

2.2.1.5 Rescue experiments: Forward DNA transfection

The rescue of GSKIP proteins' expression (wild type and mutants) after GSKIP Kd with siRNA, was achieved by lipid-mediated transfection of A549 cells with plasmid DNA containing the respective coding sequence.

Knockdown of GSKIP with siRNA was performed on A549 cells (section 2.2.1.4) and 24 hrs later, medium was changed to 2 ml fresh medium per well and forward DNA transfection was performed with FLAG-tagged expression vectors (Table 7) using ViaFect as a transfection reagent. In a 6-well format, 1 µg of DNA were dissolved in 99 µl Opti-MEM® and gently mixed by flicking the Eppendorf tube. Then 3 µl of ViaFect were added and incubated for 10 min at RT. 103 µl of DNA/lipid complex solution were added to each well. 24 hrs later transfection medium was replaced by 2 ml fresh medium per well and cells were harvested after additional 24 hrs.

2.2.1.6 Determination of cell viability

A549 Cells were seeded on 24-well plates and transfected with siRNA as described in section 2.2.1.4. 48 hrs post transfection the medium was replaced with a fresh medium and alamarBlue® was added to each well in a dilution of 1:10. Cells were incubated for 2 hrs at 37 °C, the absorbance of alamarBlue® was measured at 570 nm, with 600 nm as a reference wavelength, using the Enspire®2300 plate reader. The alamarBlue® absorbance at 570 nm is proportional to the amount of living cells. Viability was assessed according to the manufacturer's protocol (O'Brien et al., 2000).

2.2.1.7 Wound healing assays

A549 cells were seeded on a 24-well plate and transfected with siRNA/DNA as described in sections 2.2.1.4 and 2.2.1.5. The middle line of each well was marked with a dashed line using a marker on the bottom of each well. 24 hrs post transfection the cells have formed a confluent monolayer and the medium was aspirated and PBS was added to each well. This was performed, in order to prevent cell death on the edges of the scratch wound. Using a 10µl pippete tip a scratch wound was made with a single motion in each well parallel to the middle line marker. PBS was replaced with fresh medium and cells were incubated at 37 °C. Time point zero pictures were taken of scratch wounds using BZ-8100E microscope x20 magnification. Scratch wounds were monitored until closure of the wound (25-36 hrs) using the appropriate marker on the bottom of the well in order to ensure that the same field was monitored. The area of the scratch wound was measured using ImageJ. The protocol was adapted from (Justus et al., 2014).

2.2.1.8 Transwell migration assays

A549 cells were seeded on a 6-well plate and reversely transfected with siRNA (section 2.2.1.4). 48 hrs later cells were trypsinized and counted using Scepter^{TM} 2.0. 5,000 cells per well were seeded in 100 µl DMEM medium with 0% FBS on top of a plastic insert with polycarbonate membrane (Corning) in triplicates. The bottom of each well was filled with DMEM medium supplemented with 10% FBS. Cells were incubated at 37 °C for 24 hrs during which they migrated by chemotaxis from low FBS (0%) media to high FBS (10%), through the polycarbonate membrane. The membrane-containing inserts were gently washed with PBS and fixed and stained for 60 min with glutaraldehyde-crystal violet solution. The non-migrated cells were gently removed with a cotton swab from the inner side of the insert and pictures of an entire surface of the wells were taken using BZ-8100E microscope with x20 magnification. Individual cells were counted using ImageJ on 8 randomly selected pictures from each insert.

2.2.1.9 Analysis of mitochondrial functions

The Seahorse XF24 extracellular flux analyser allows for complete assessment of mitochondrial function in intact cells. The XF24 uses a piston (Fig. 13C) to reversibly enclose a small volume (7 µl) above the cells, monitoring oxygen uptake in that volume for 2–5 min, then raising the piston, allowing the bulk incubation medium to re-equilibrate followed by measurement of oxygen consumption rate (OCR) and extra-cellular acidification rate (ECAR). OCR and ECAR were validated as indicators of cellular respiration and glycolysis, respectively

(Wu et al., 2006). The cells were reversely transfected in a 6-well format 48 hrs before the XF measurements with GSKIP siRNA (section 2.2.1.4) and Non-targeting (NT) siRNA served as control. A549 cells were trypsinized and counted using Scepter^{TM} 2.0. 20,000cells per well were seeded on a 24-well XF24 culture microplate (Fig. 13A) in the culture medium and incubated for 24 hrs at 37 °C, 5% CO_2. Each condition had five wells and five additional wells containing media alone served as blanks. The 24-well XF assay cartridge was placed in calibrant solution and incubated at 37 °C, 0% CO_2 overnight to ensure proper piston calibration. After cells have reached 90% confluency, the culture medium was replaced by XF un-buffered medium, supplemented with 5.5 mM D-glucose, 1.0 mM sodium-pyruvate and 10% FBS. The cells were incubated at 37 °C, 0% CO_2 for 60 min. Appropriate volumes of injectable compounds (final concentration of 1 µM per well) were pippeted into each well of the XF assay cartridge and transferred from the calibrant solution to the cell culture microplate. Seahorse experimental setup allows up to four compounds to be added to each well during the experiment and different parameters of the mitochondrial function (Basal respiration, proton leak, etc.) can be quantified by measuring the area under the curve following each administration (Fig. 13B).

Four compounds were added to each well in this experiment:

1. Oligomycin inhibits ATP synthase resulting in a build-up of protons in the intermembrane space, resulting in the subsequent loss of electron flow through the electron transport chain and loss of oxygen consumption.
2. FCCP (Trifluorocarbonylcyanide Phenylhydrazone) uncouples mitochondrial respiration by carrying protons across the inner membrane, thus re-stimulating mitochondrial respiration by dissipating mitochondrial proton gradient allowing electrons to flow to complex IV and allowing the resumption of oxygen consumption. Failure of cells to respond to FCCP treatment is indicative of dysfunctional mitochondria (Brand, 2011).
3. Rotenone and Antimycin A are complex I and III inhibitors, respectively. The simultaneous addition of these compounds results in inhibition of electron flow through the respiration chain, diminishing all oxygen consumption through the mitochondria.

The Seahorse XF24 protocol (Supplementary table 3) was set up to run automatically for 3-4 hrs. Subsequently, the cells' viability was measured using Alamar blue (section 2.2.1.6) and protein concentration was measured using Bradford assay (section 2.2.2.2). The different mitochondrial parameters were assessed using Seahorse XF24 software according to manufacturer's protocol by measuring area under the curve (AUC) of OCR and ECAR plots and the values normalized to protein amount in each well.

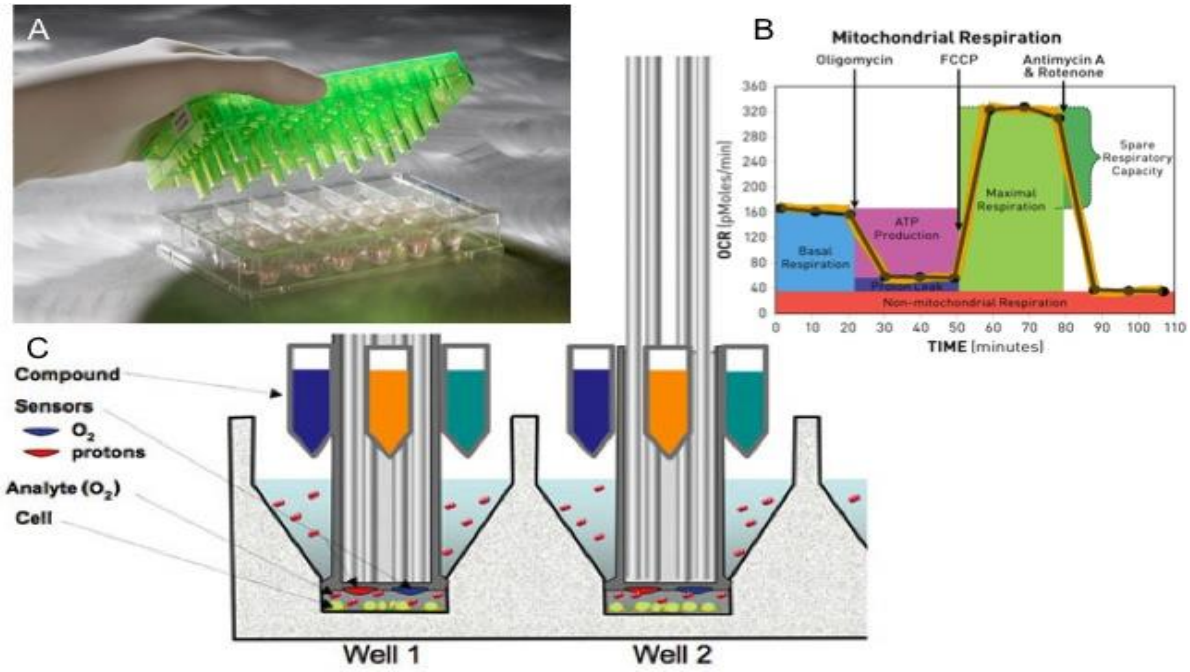

Figure 13: Seahorse XF24 mitochondrial function assay. A. Seahorse XF24 cell culture plate and cartridge for injectable compounds (green). B. Estimation of mitochondrial parameters from area under the curve of OCR vs. time. C-Schematic view of a test well showing the Seahorse XF24 pistons enclosing a volume above the cells and measuring oxygen and pH levels.

2.2.2 Biochemical methods

2.2.2.1 Cell lysis

Confluent mammalian cells were washed with ice-cold PBS and scraped into ice-cold lysis buffer (Table 4) and incubated on ice for 30 min. Cell debris was removed by centrifugation at 15,000x g, for 15 min, 4°C and the supernatant was used for Bradford assays followed by Western Blot analyses or for immunoprecipitation.

2.2.2.2 Bradford assay

Protein concentration of cell lysates was determined using the colorimetric Bradford assay (Bradford, 1976). 5µl of sample lysate or standard curve samples (fixed concentrations of 0.125-2 mg/ml BSA in *Aqua deion*) and 250µl Coomassie Plus™ Protein Assay Reagent were mixed per well of a 96-well microplate, and incubated for 10 min at RT, protected from light. Using the Enspire®2300 microplate reader, absorbance was measured at 595 nm. According to the extinction of standards, the protein concentration of samples was determined using a standard curve.

2.2.2.3 Western Blotting

Protein samples were heated in 4x sample buffer for 5 min at 95 °C and separated by SDS-PAGE. Polyvinylidene fluoride (PVDF) membranes were briefly activated with ethanol and proteins from the polyacrylamide gel were transferred to the membranes using the TransBlot Semi-dry Western Blot system (20 V for 90 min). Membranes were blocked for 60 min at RT (blocking buffer) and agitated with primary antibody, diluted in blocking buffer, at 4 °C over night. Membranes were washed 3x 10 min in TBS-T and incubated with POD-labelled secondary antibodies, diluted in blocking buffer, for 60 min at RT. Membranes were washed 3x 10 min in TBS-T and protein signals were visualized by Immobilon® Western Chemiluminescent HRP substrate using Odyssey Imager. Precision Plus Protein Standard Dual Color marker was used to determine protein molecular weight. Image Studio Ver. 2.0 and ImageJ were used for image processing and densitometry analysis, respectively.

2.2.2.5 Immunoprecipitation

Cells were lysed as described in section 2.2.2.1 with PBS lysis buffer (Table 8) and cell debris was removed by centrifugation at 15.000xg for 10 min. Protein concentration were determined by Bradford assay and specific proteins were precipitated from cell lysates (protein concentration 1 mg/ml) by overnight incubation at 4 °C with 5 µl of specific antibody. Precipitation of the antibody/antigen complex was performed using 30 µl IgG-binding Protein-A-sepharose beads (70 mg/ml). After the incubation the beads were gently centrifuged (700 × g, RT, 2 min) and washed x4 with 500 µl of lysis buffer. After the final washing step, the wash buffer was removed completely and protein were eluted from the beads by adding 32 µl Sample buffer 3x and heating at 95 °C for 5 min. The eluate was subjected to SDS-PAGE and subsequent Western Blot detection of proteins.

2.2.2.6 Peptide spotting

Peptide arrays were produced by Sylvia Niquet (FMP) by automatic SPOT-synthesis on cellulose membranes using an AutoSpot-Robot ASS 222 (Intavis Bioanalytical Instruments AG, Köln, D) as described previously (Frank, 2002).

The binding of GSKIP to potential interaction partners was determined using peptide spots of SMYD2 (Appendix A, supplementary Table 1) and GDF5OS (Appendix A, supplementary Table 2) which were incubated with recombinant HIS-tagged GSKIP protein. To determine the binding region of GSKIP to peptide spots, peptide arrays were briefly equilibrated in ethanol and blocked in 3% BSA in TBS-T blocking buffer, for 120 min at RT. The membranes were

incubated with 1 µg/ml HIS-GSKIP or blocking buffer (control) overnight at 4 °C. The membranes were washed three times with TBS-T and incubated with primary GSKIP antibody for 60min at RT. Membranes were washed again three times in TBS-T and protein-peptide spots were visualized by Immobilon® Western Chemiluminescent HRP substrate using Odyssey Imager. Image Studio Ver. 2.0 was used for image processing.

2.2.2.7 Immunofluorescence microscopy

Cells were grown to confluency on cover slides with 12 mm diameter. Medium was aspirated and the cells were fixed with 2.5 % PFA for 15 min at RT. Cells were washed three times with 1x PBS and permeabilised with 0.1 % Triton X-100 for 5 min at RT. Unspecific binding was prevented by blocking with 0.27 % fish skin gelatine for 60 min at 37 °C. Cells were incubated with 1x TRITC-Phalloidin and 1x DAPI for 45 min at 37 °C and then washed with 1x PBS. Using Immu-Mount™, cover slides with cells were fixed on microscope slides and stored at 4 °C overnight. Microscope slides were analyzed with LSM780 confocal laser scanning microscope, using 40x magnification. Two channels were acquired: DAPI, using a 405 nm laser and filter for 415-502 nm, and TRITC-Phalloidin, using a 561 nm laser and filter for 563-699 nm. Pinholes were set to 100-130 µM, digital gain was set to 1.00 and master gain to approximately 550 for both channels.

2.2.3 Proteomics analysis using SILAC labeling

A549 cells were transfected with GSKIP siRNA and NT siRNA (section 2.2.1.4). 48 hrs later cells were washed twice with ice-cold PBS, scraped and pelleted by centrifugation (2 min, 300xg, at 4 °C). Cell pellets were transferred to the lab of Dr. Stephan Kempa (Berlin Institute for Medical Systems Biology located in Berlin, Germany) where proteomics analysis using stable isotope labelling was performed by Amit Kumar.

Briefly, cells are grown in complete growth media lacking the standard amino acid leucine and instead supplemented with isotopically labelled leucine. After subculturing the cells five times every leucine-containing peptide incorporates the isotope-labelled leucine (Ong et al., 2002). The GSKIP Kd cells were grown in normal growth medium ("Light") while the NT siRNA transfected cells (control) were grown in isotope labelled growth medium ("Heavy") and after five doublings the cell populations were mixed with a 1:1 (Light:Heavy) ratio and subjected to LC-MS analysis. For each protein the "Light" and "Heavy" LC-MS peaks corresponded to the protein abundance in GSKIP Kd and control samples, respectively. The LC-MS raw data was

analysed using MaxQuant Software (Cox and Mann, 2008) and statistical analysis was performed using Microsoft Excel and Perseus Software (http://www.perseus-framework.org).

2.2.4 Metabolomics analysis using stable isotope labelling

Metabolomics analysis was performed in the lab of Dr. Karsten Hiller at the Luxembourg Centre for Systems Biomedicine, University of Luxembourg.

2.2.4.1 Stable isotope labelling

A549 cells were reversely transfected with either GSKIP SiRNA or with NT SiRNA as described in section 2.2.1.4 on three 6-well culture plates in triplicates and incubated overnight at 37 °C in 5 % CO_2. The next day cell culture medium was aspirated and replaced with either stable isotope labelling medium (plates No.1 and 2) or unlabelled DMEM medium (plate No.3). Cells in Plate No.1 (Glucose labelled) were cultured in DMEM supplemented with 10 % dialyzed FBS (Invitrogen), 25 mM [U-$^{13}C_6$]glucose (Cambridge Isotope Laboratories) and 4mM glutamine (Sigma Aldrich). Cells in Plate No.2 (Glutamine labelled) were cultured in DMEM supplemented with 10 % dialyzed FBS (Invitrogen), 25mM glucose (Sigma Aldrich) and 4mM [U-$^{13}C_5$] glutamine (Cambridge Isotope Laboratories). Cells in Plate No.3 were cultured in DMEM supplemented with 10 % dialyzed FBS (Invitrogen), 25mM glucose (Sigma Aldrich) and 4mM glutamine (Sigma Aldrich). All the plates were incubated over night at 37 °C, 5% CO_2 before metabolite extraction.

2.2.4.2 Extraction of intracellular metabolites

Medium samples from each well in plates No. 1 and 2 were collected and glucose, glutamine, glutamate and lactate uptake/secretion rates were measured by enzymatic assay with electrochemical detection on a YSI7200 instrument (YSI, Yellow Springs, US). The cells were washed with 0.9% NaCl and quenched with 400µL of ice-cold methanol. After adding an equal volume of 4°C cold water, cells were collected using a cell scraper and transferred into Eppendorf tubes containing 400µL of ice-cold chloroform. The extracts were shaken at 1,400 rpm for 20 min at 4 °C using Thermomixer Eppendorf and then centrifuged at 16,000xg for 5 min at 4°C. 300µL of the upper aqueous phase was collected in specific glass vials with micro-inserts and evaporated under vacuum at -4°C using a refrigerated CentriVap Concentrator (Labconco).

Next metabolites were analysed *via* GC-MS using an Agilent 7890A GC equipped with a 30m DB-35MS + 5m Duraguard capillary column. All GC-MS chromatograms were analysed using

MetaboliteDetector software (Hiller et al., 2009). Cells in plate No.3 were trypsinized and counted using automated cell counter. Metabolites' levels were normalized to cell number.

2.2.5 Statistics

Statistical analysis was performed using unpaired students t-test in Excell 2010. Mean ± standard error of mean (SEM) are plotted. Significant differences are indicated as $p \leq 0.05$ = *, $p \leq 0.01$ = **, $p \leq 0.001$ = ***.

3. Results

3.1 GSKIP is ubiquitously expressed in cancer cell lines

For the purpose of studying GSKIP's function in tumorigenesis, a cell model had to be chosen. To this end, 11 available cancer cell lines from various cancer types were screened for GSKIP's expression and GSKIP was expressed in all the tested cell lines (Figure 14). Due to an indication of GSKIP's involvement in lung and respiratory defects, which was observed in GSKIP knockout (KO) mouse pups (PhD thesis Veronika Deak), the A549 human lung carcinoma cell line was chosen for further research.

A549 cells are adherent alveolar epithelial cells used as *in vitro* model to study the physiology of the Alveolar type II (ATII) cells. ATII cells constitute approximately 60 % of alveolar epithelial cells and about 15 % of all lung parenchymal cells. ATII cells play major roles in alveolar homeostasis and are utilized for permeability screens for pulmonary administered therapeutics. However these studies have limited therapeutic impact due to the high permeability of the A549 cells caused by the cells' inability to form stable tight junctions (Forbes and Ehrhardt, 2005). This defect in tight junction formation is characterized by a more mesenchymal behavior of the cells and together with the ability of these cells to grow in a monolayer makes this cell line suited for studying EMT. In addition, the high permeability of A549 cells makes the cells easy to transfect with both DNA and siRNA for overexpression/ knockdown studies. Finally, in comparison to many other tumorigenic cell lines, A549 cells do not harbor multiple genetic mutations that may result in adverse effects in biochemical experiments. A549 cells only express mutated Kirsten rat sarcoma viral oncogene homolog (KRAS), which results in constitutive activation of Protein kinase B (PKB/AKT) allowing unrestricted proliferation (Yoon et al., 2010).

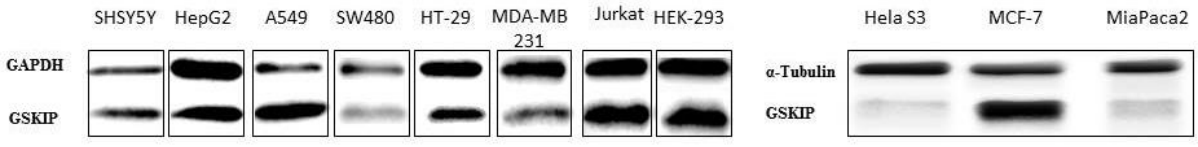

Figure 14: GSKIP is ubiquitously expressed in cancer cell lines. Western Blot protein expression signals of GSKIP and of loading control proteins, GAPDH or α-tubulin, in human immortalized cell lines.

3.2 GSKIP knockdown does not affect A549 cells' viability

In order to elucidate the role of GSKIP in A549 cells, GSKIP transient knockdown (Kd) using pooled siRNA was established as described in 2.2.1.4. The Kd was confirmed by Western Blot as described in 2.2.2.3 and Figure 16 shows 70-80 % downregulation of GSKIP protein expression relative to the NT (Non-targeting siRNA) control. The Kd is stable for 72 hrs post siRNA transfection.

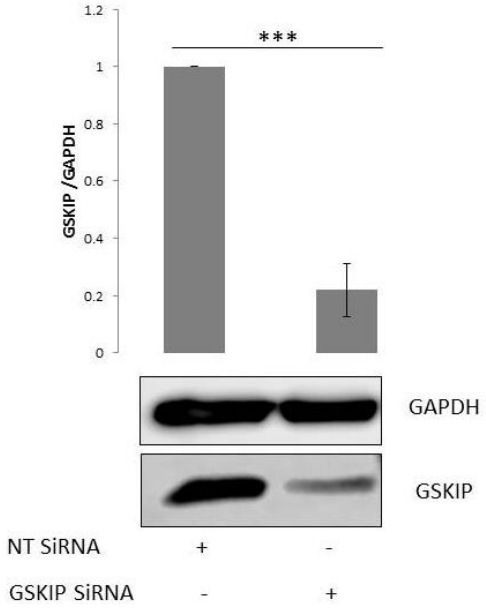

Figure 15: Knockdown of GSKIP in A549 cell line. Semi-quantitative analysis of protein expression levels was carried out using ImageJ (n=3). GSKIP protein levels were normalized to the loading control, GAPDH. Significant differences vs. NT control were determined using Students t-test (*= P <0.05 **= P <0.01 ***= P<0.001 ns=not significant)

Since GSK3β is involved in proliferation and survival signaling pathways in cancer cells (see section 1.3.2), the viability of A549 cells after GSKIP Kd was evaluated by Alamar Blue assay as described in 2.2.1.6 and confirmed by direct cell count as described in 2.2.1.3. The viability of cells was not affected by GSKIP Kd after 48 and 72 hours compared to the NT control (Figure 16B). Also, both the control and Kd cells appear to have the same confluency and morphology (Figure 16A). This indicates that GSKIP Kd does not affect survival or proliferation of A549 cells during the observed time interval.

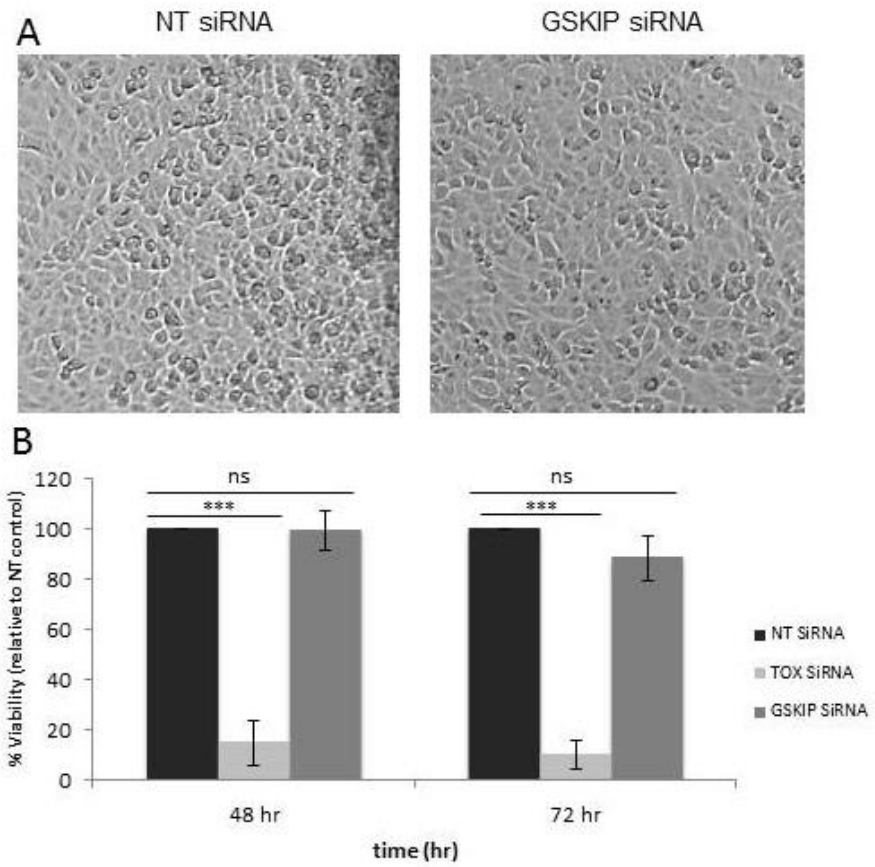

Figure 16: GSKIP Kd does not affect the viability of A549 cells. A. Microscopic images of A549 cells transfected with NT siRNA (left) and GSKIP siRNA (right) taken 72 hrs post transfection. B. Viability of A549 cells as examined using Alamar blue assay 48 and 72 hrs post transfection (% of viable cells relative to NT control plotted as means ±SEM, n=3). Viability of TOX siRNA transfected cells were used as positive control. Significant differences vs. NT control were determined using Students t-test (*= P <0.05 **= P <0.01 ***= P<0.001 ns=not significant)

3.3 GSKIP knockdown inhibits A549 cells' motility

In addition to regulating proliferation and survival, GSK3β has prominent roles in signaling pathways affecting motility of cancer cells (see sections 1.1.2 and 1.3.2). Hence, GSKIP's role in motility was evaluated in a wound healing assay as described in 2.2.1.7. The initial size of the scratch wound is similar in both the NT control and GSKIP Kd cells (350µm) (Figure 17, left panel, 0 hrs). However, after 25 hours the scratch wound appears closed in the control, while the GSKIP Kd cells failed to close the scratch wound during this period of time (Figure 17, right panel), indicating that GSKIP is involved in migration regulation in A549 cells.

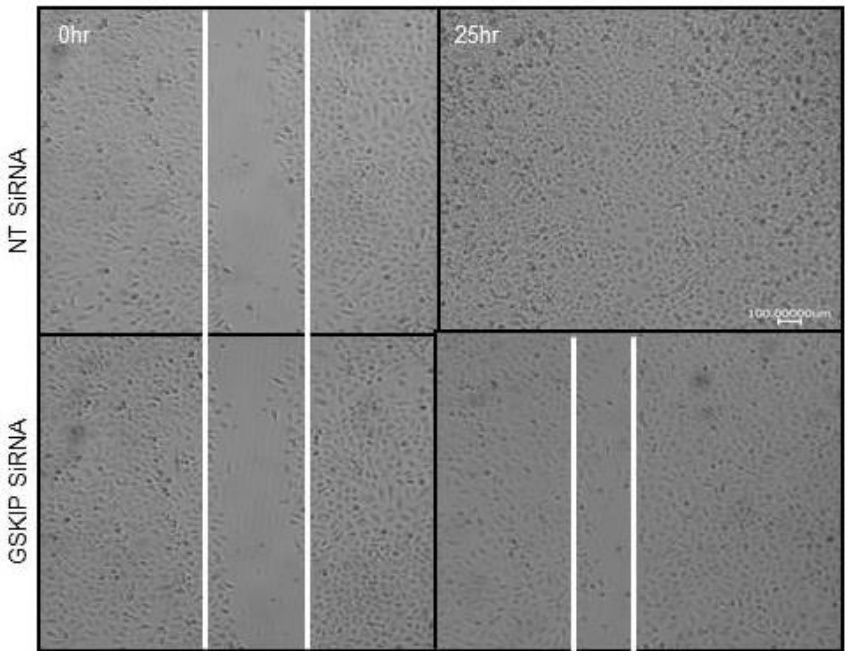

Figure 17: **GSKIP Kd attenuates motility of A549 cells**. Scratch wound assay of A549 cells after GSKIP Kd (bottom). NT siRNA-transfected cells (top) served as negative control. Scratch wounds were monitored for 25 hours. The images are representative of four independent experiments.

In order to confirm migration inhibition upon Kd of GSKIP, Transwell chemotaxis assays were performed. Figure 18 shows that the number of migrated cells after GSKIP Kd was reduced by more than 60% relative to NT control. This result confirms that A549 cells with low expression of GSKIP possess significantly impaired migration ability.

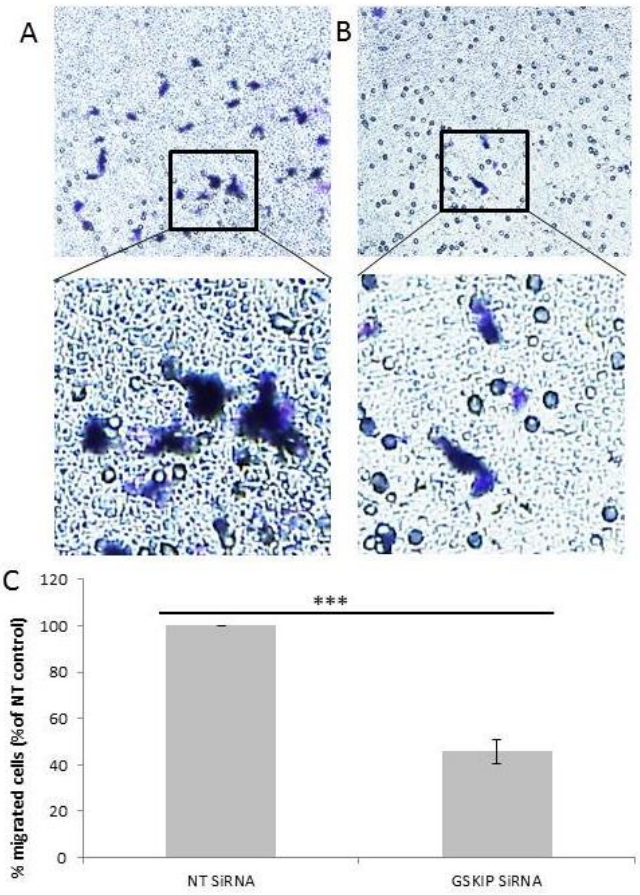

Figure 18: GSKIP Kd inhibits chemotaxis of A549 cells. Stained polycarbonate membranes showing migrated A549 cells (blue) transfected with either NT siRNA (A) or GSKIP siRNA (B). The membrane pictures are representative of 4 independent experiments. C. % of migrated cells after Kd relative to NT control as quantified by ImageJ (means ± SEM). Significant differences were determined using Student's t-test (*= P <0.05 **= P <0.01 ***= P<0.001 ns=not significant)

3.4 GSKIP knockdown induces MET in A549 cells

3.4.1 GSKIP knockdown results in E-cadherin upregulation

Since migratory defects in cancer cells can indicate a potential involvement of GSKIP in the EMT process, it was examined whether GSKIP knockdown is associated with loss of mesenchymal and/or with gain of epithelial markers.

Figure 19A and 19B show that the epithelial marker E-cadherin is significantly upregulated while the mesenchymal marker N-cadherin shows a down regulation upon knockdown of GSKIP, although not significant. This suggests activation of the Mesenchymal-Epithelial transition (MET), which is the reverse pathway of EMT, and explains the negative effect on the migration of these cells.

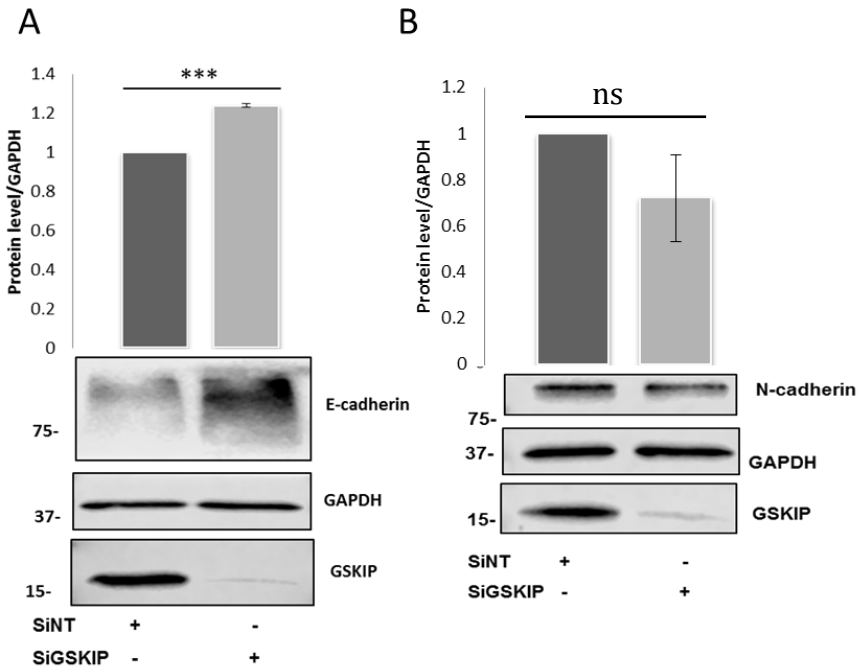

Figure 19: GSKIP Kd results in upregulation of E-cadherin. Semi-quantitative analysis of protein expression levels was carried out using ImageJ (n=3). Protein levels were normalized to the loading control, GAPDH (means ± SEM). Significant differences vs. NT control were determined using Students t-test (*= P <0.05 **= P <0.01 ***= P<0.001 ns=not significant)

The insignificant downregulation of N-cadherin can be attributed to the fact that A549 are cells of a mixed invasiveness status, expressing varying levels of E-cadherin and N-cadherin (Kim et al., 2014). Stimulation with TGFβ1 followed by flow cytometry sorting will allow the separation between the highly-invasive and non-invasive A549 cells (Sun et al., 2014) and amplification of the MET phenotype induced by GSKIP Kd. In addition, the insignificance in downregulation of N-cadherin can be attributed to insufficient n number, and may increase after additional repetitions.

3.4.2 GSKIP Kd results in SNAIL and ZEB1 downregulation

Since E-cadherin expression is repressed during EMT by master regulators such as SNAIL and ZEB1 (see section 1.1.2), the protein expression levels of SNAIL and ZEB1 were evaluated *via* Western Blot after GSKIP Kd.

Figure 20 shows a significant downregulation of both ZEB1 and SNAIL protein expression levels upon GSKIP Kd, which explains the upregulation of E-Cadherin and migration inhibition. The observed double band of SNAIL corresponds to phosphorylated and unphosphorylated protein (Zhou et al., 2004b).

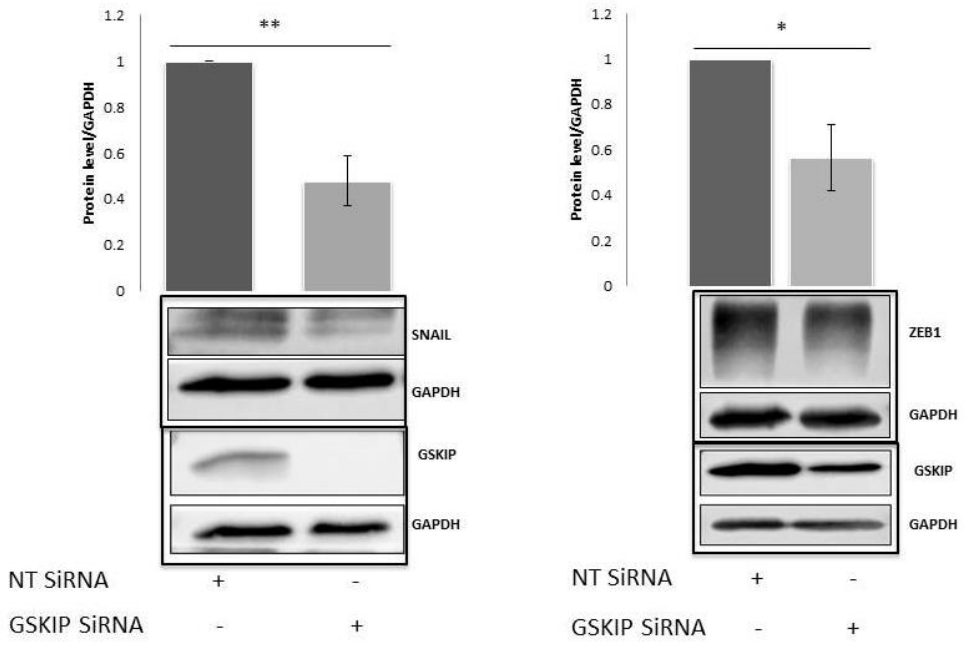

Figure 20: GSKIP Kd downregulates EMT master regulators. Semi-quantitative analysis of protein expression levels was carried out using ImageJ (n=3). Protein levels were normalized to the loading control, GAPDH (means ± SEM). Significant differences vs. NT control were determined using Students t-test (*= P <0.05 **= P <0.01 ***= P<0.001 ns=not significant)

ZEB1 expression is directly regulated by SNAIL, as well as by TGFβ (See section 1.1.3.1) and GPI/AMF signaling (See section 1.1.3.3). In addition, SNAIL expression is negatively regulated by GSK3β (See section 1.3) and positively regulated by PKA (See section 1.4.3). Therefore, one possible mechanism of GSKIP's regulation of EMT will be by influencing SNAIL directly either by preventing GSK3β's inhibition of SNAIL or mediating PKA's stabilizing phosphorylation or both (see figure 21).

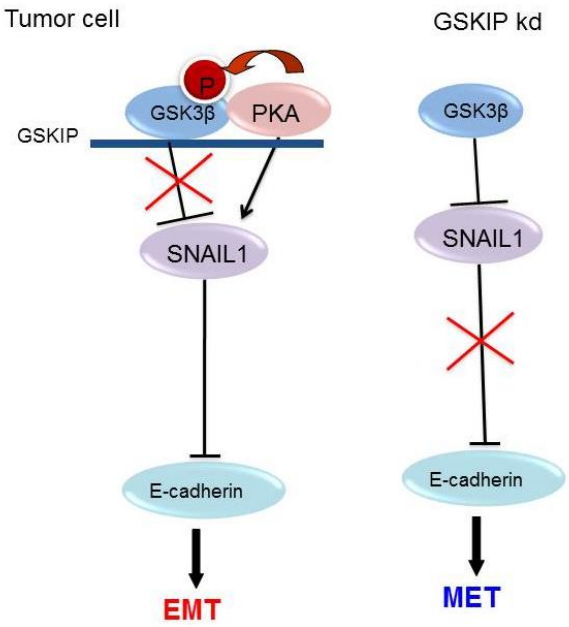

Figure 21: **Possible mechanism of GSKIP's regulation of EMT *via* SNAIL**. In tumor cells, GSKIP binds PKA and GSK3β facilitating GSK3β inhibition by PKA, thus preventing GSK3β from inhibiting SNAIL and promoting EMT. In addition PKA's stabilizing phosphorylation of SNAIL may be mediated by GSKIP. Upon Kd of GSKIP, GSK3β is free to inhibit SNAIL thus preventing EMT.

In addition, ZEB1 expression is directly regulated by GPI/AMF signaling (See section 1.1.3.3). Therefore, next GPI/AMF protein expression upon GSKIP Kd was evaluated by Western Blot.

3.4.3 GSKIP modulates EMT in A549 cells *via* GPI/AMF but not *via* NF-kB

Figure 22 shows that GPI/AMF protein levels are significantly reduced upon GSKIP knockdown further supporting the induction of MET.

However, the exact mechanism of EMT induction and regulation by GPI/AMF remains unclear (see section 1.1.3.3). GPI/AMF downregulation have been previously shown to correlate with MET induction characterized by upregulation of E-cadherin as well as downregulation of SNAIL and TGFβ (Niinaka et al., 2010), or SNAIL, GSK3β and β-catenin (Funasaka et al., 2007, 2009). And as demonstrated by (Ahmad et al., 2011) high protein levels of GPI/AMF in cancer cells increase NF-kB DNA binding, which results in transcriptional upregulation of ZEB1, subsequent E-cadherin repression and EMT induction.

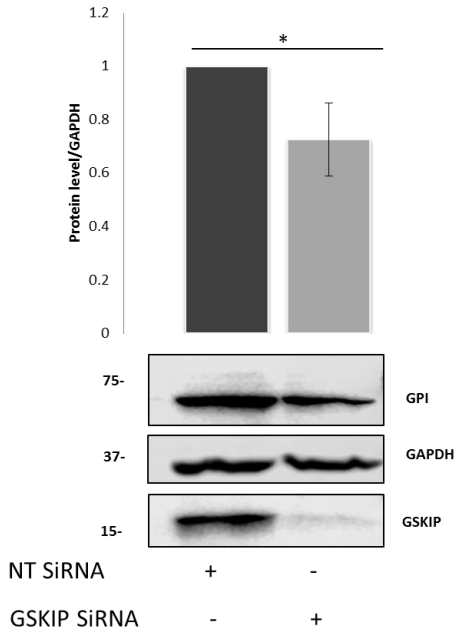

Figure 22: GSKIP Kd downregulates EMT inducer GPI/AMF. Semi-quantitative analysis of protein expression levels was carried out using ImageJ (n=3). Protein levels were normalized to the loading control, GAPDH (means ± SEM). Significant differences vs. NT control were determined using Student's t-test (*= P <0.05 **= P <0.01 ***= P<0.001 ns=not significant)

Since GSK3β is also known to regulate the NF-kB pathway it is possible that GSKIP may be involved in GPI/AMF regulation in cancer cells of EMT *via* NF-kB and ZEB1 (Figure 23). Under normal EMT conditions, GSKIP facilitates GSK3β inhibition by PKA which prevents GSK3β from inhibiting NF-kB activity. High NF-kB activity results in upregulation of ZEB1 which in turn inhibits E-cadherin thus promoting EMT. In addition GPI/AMF increases NF-kB DNA binding and it is plausible that GPI/AMF directly regulates GSK3β. Upon GSKIP Kd GSK3β is free to inhibit NF-kB and possibly GPI/AMF thus resulting in ZEB1 downregulation and reversal of EMT.

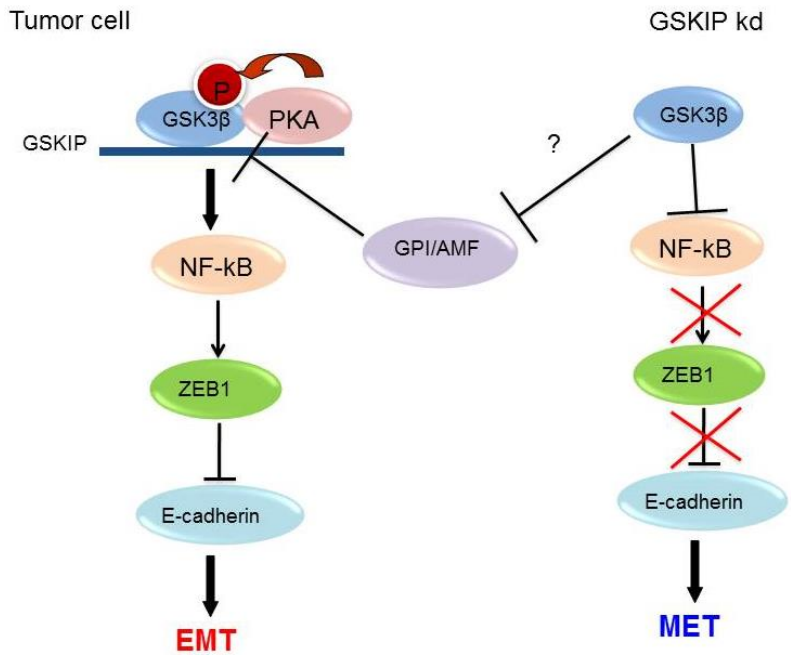

Figure 23: **Possible mechanism of GSKIP regulation of EMT *via* GPI/AMF**. In tumor cells, GSKIP binds PKA and GSK3β facilitating GSK3β inhibition by PKA, thus preventing GSK3β from inhibiting NF-kB. NF-kB activates ZEB1 which, in turn, inhibits E-cadherin thus promoting EMT. In addition GPI/AMF increases NF-kB DNA binding and it is plausible that GPI/AMF directly regulates GSK3β. Upon GSKIP Kd GSK3β inhibits NF-kB DNA binding and possibly GPI/AMF, thus resulting in ZEB1 downregulation and reversal of EMT.

In order to test whether GSKIP Kd results in lower NF-kB activity, *electrophoretic mobility shift assay* (EMSA) was performed in cooperation with Nadine Mikuda (AG Schederheit, MDC) on A549 cells transfected with either GSKIP siRNA or NT siRNA (control). However, the results showed no detectable NF-kB activity in the Kd or in the control samples (Supplementary figure 1). This suggests that NF-κB activity is too low to be detected without TNFα stimulation. Therefore, luciferase assays were performed using the NF-κB-dependent reporter, NF-κBtkluc.neo, kindly provided by AG Scheiderheit. However, luciferase assays showed very low NF-κB activity with or without TNFα stimulation (Supplementary figure 2). Furthermore, the NF-κB activity seems to be higher upon GSKIP Kd compared to NT control, but with high deviation between the three independent experiments. This potentially contradicts the observations made by (Ahmad et al., 2011), stating that downregulation of GPI/AMF protein expression levels result in reduced NF-κB activity. However, further experiments are needed to reach a definite conclusion. Therefore, in order to uncover the direct target protein/s of GSKIP which affects both GPI/AMF signaling and E-cadherin, a rescue of GSKIP after initial Kd was performed.

3.4.4 Re-expression of GSKIP rescues GPI/AMF

The rescue of GSKIP protein expression after Kd using FLAG-GSKIP WT as well as GSK3β-binding deficient (FLAG-GSKIP_L130P) and PKA-binding-deficient (FLAG-GSKIP_N42i) mutants was performed in A549 cells as described in section 2.2.1.5. Figure 24 shows re-expressing GSKIP WT and mut-GSKIP significantly rescue GSKIP Kd.

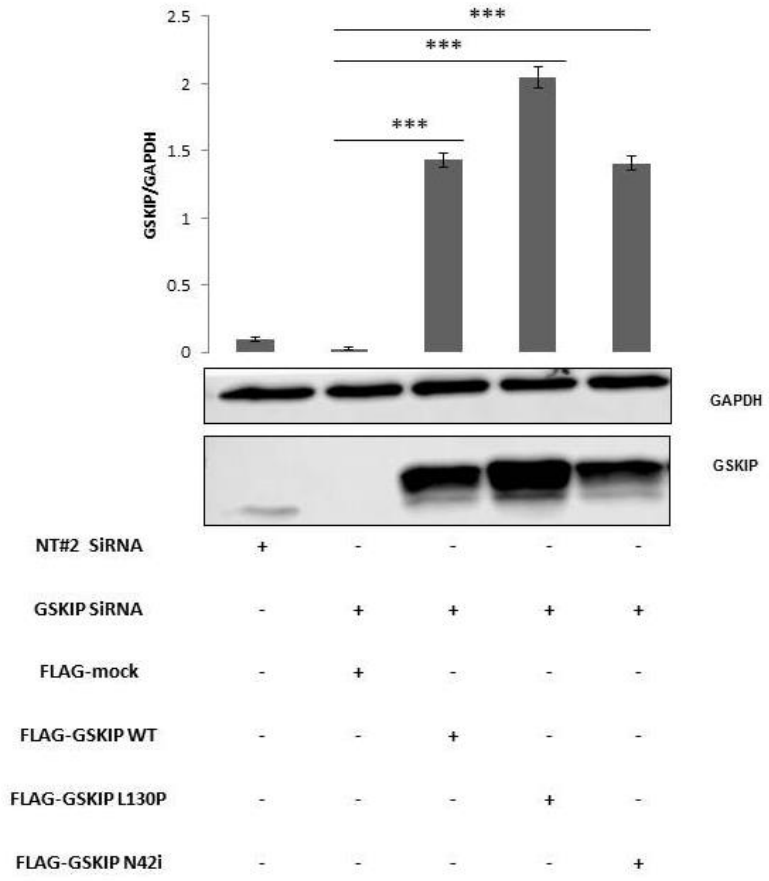

Figure 24: GSKIP re-expression rescues the Kd. Semi-quantitative analysis of protein expression levels was carried out using ImageJ (n=4). Protein levels were normalized to the loading control, GAPDH and to the mean protein expression of each independent experiment (means ± SEM). Significant differences vs. Kd were determined using Student's t-test (*= P <0.05 **= P <0.01 ***= P<0.001 ns=not significant)

After rescuing GSKIP's expression, GPI/AMF protein expression levels were evaluated *via* Western Blot. Figure 25 shows a significant rescue of GPI/AMF protein expression by re-expressing GSKIP WT as well as GSK3β and PKA binding deficient GSKIP. This indicates that GSKIP regulates GPI/AMF protein expression independent of binding to GSK3β or to PKA and argues against direct regulation of GPI/AMF by GSK3β (Figure 23). Since GPI/AMF is an inducer of EMT, rescue of GPI/AMF's protein expression may initiate the EMT cascade. However, re-expression of GSKIP failed to rescue protein expression of E-cadherin and migration inhibition caused by GSKIP Kd (Supplementary figures 3 and 4, respectively). This

may be attributed to the fact that E-cadherin is downstream in the EMT cascade and that the time interval between rescue and monitoring E-cadherin protein expression as well as wound closure (24 hrs) was insufficient to induce the protein expression necessary for reversal of the phenotype. However, due to the transient effect of GSKIP SiRNA (72 hrs), longer re-expression is not possible and stable Kd techniques such as shRNA or CRISP/CAS9 system should be used in future experiments.

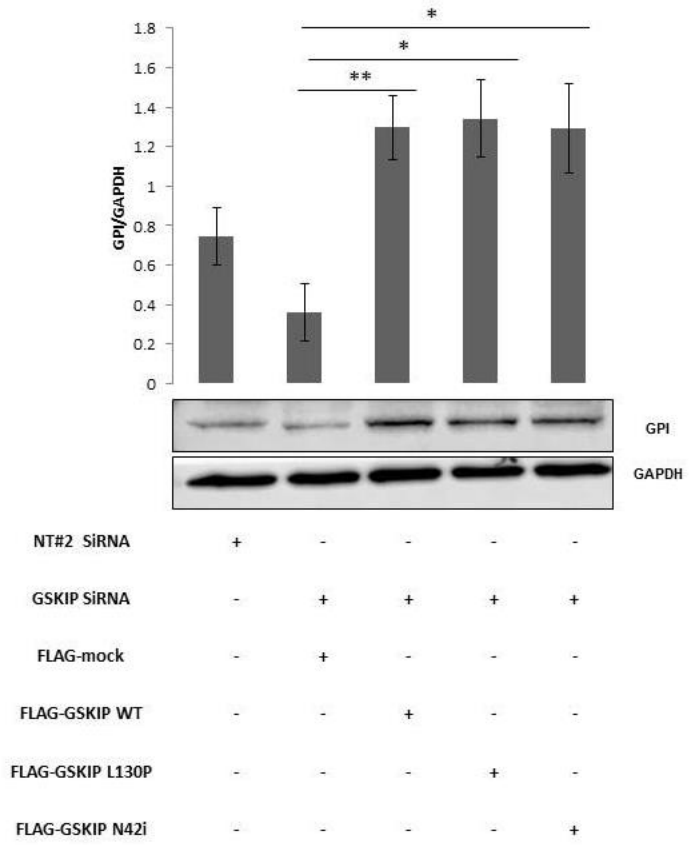

Figure 25: GSKIP re-expression rescues of GPI/AMF protein expression. Semi-quantitative analysis of protein expression levels was carried out using ImageJ (n=3). Protein levels were normalized to the loading control, GAPDH and to the mean protein expression of each independent experiment (means ± SEM). Significant differences vs. Kd were determined using Student's t-test (*= P <0.05 **= P <0.01 ***= P<0.001 ns=not significant)

Since regulation of EMT combines multiple signaling pathways as well as crosstalk between these pathways, a large scale screen of GSKIP target proteins was necessary to identify the pathway directly affected by GSKIP. To this end, proteomics analysis was performed on A549 using GSKIP SiRNA. The proteomics analysis was performed in cooperation with AG Kempa, using standard SILAC labeling and mass spectrometry (See section 2.2.3).

3.5 Proteomics analysis of A549 cells after GSKIP Kd

3.5.1 GSKIP Kd results in deregulation of metabolic and developmental proteins

1316 proteins were detected in proteomics assays. Out of these, 58 proteins showed upregulation/downregulation in the GSKIP knockdown samples compared to the control (Table 10). The cutoff for upregulation was set to 1.4 fold and for downregulation to 0.6fold for the average value of protein expression in GSKIP Kd normalized to protein expression in NT control sample. Using String 10 protein cluster analysis, 21 proteins were shown to participate in cellular metabolic processes (Figure 26) and 19 proteins were regulators of developmental processes (Figure 27). In order to validate the proteomics data the expression levels of four proteins were evaluated *via* Western Blot: AKAP12 (Gravin), MTPN, RAB27 CD44 and. Downregulation of AKAP12 and MTPN (Supplementary figure 5) as well as CD44 (Figure 28), were confirmed upon GSKIP Kd supporting the proteomics data. RAB27 showed upregulation inconsistent with proteomics data, making it a false positive (Supplementary figure 5).

Protein names	Gene names	siRNA-GSKIP2_x/y_Control2	siRNA-GSKIP1_x/y_Control1	Avg. siRNA-GSKIP_x/y_Control	PEP
NADH dehydrogenase [ubiquinone] 1 beta subcomplex subunit 1	NDUFB1	1.637058	4.879582	3.25832	2.01E-18
Carbonic anhydrase 12	CA12	2.67701	2.838632	2.757821	1.55E-34
OTU domain-containing protein 6B	OTUD6B	2.26841	2.466318	2.367364	1.31E-109
NADPH:adrenodoxin oxidoreductase, mitochondrial	FDXR	2.309731	1.97403	2.1418805	3.96E-98
Lamin-B1	LMNB1	1.898585	2.024015	1.9613	5.46E-198
Hematological and neurological expressed 1-like protein	HN1L	1.954991	1.855823	1.905407	1.53E-15
Erythrocyte band 7 integral membrane protein	STOM	1.992469	1.726409	1.859439	1.39E-48
40S ribosomal protein S27-like	RPS27L	1.839305	1.723776	1.7815405	4.58E-08
Ankycorbin	RAI14	1.6608	1.863353	1.7620765	3.89E-36
60 kDa SS-A/Ro ribonucleoprotein	TROVE2	1.863953	1.651034	1.7574935	1.14E-22
Cancer-related nucleoside-triphosphatase	NTPCR	1.804289	1.694261	1.749275	1.29E-39
Complexin-2	CPLX2	1.687273	1.801446	1.7443595	7.89E-20
Sideroflexin-1	SFXN1	1.954356	1.472528	1.713442	6.58E-60
Neudesin	NENF	2.020647	1.402489	1.711568	2.99E-15
Lysosome-associated membrane glycoprotein 2	LAMP2	1.851103	1.537137	1.69412	8.20E-14
Kinectin	KTN1	1.676741	1.643419	1.66008	4.07E-142
Tax1-binding protein 3	TAX1BP3	1.538841	1.685037	1.611939	4.72E-12
Protein SON	SON	1.45372	1.754542	1.604131	3.73E-20
Protein enabled homolog	ENAH	1.560033	1.619975	1.590004	2.99E-21
Calcineurin B homologous protein 1	CHP1	1.573252	1.562906	1.568079	2.13E-15
Succinyl-CoA ligase [GDP-forming] subunit beta, mitochondrial	SUCLG2	1.489124	1.627208	1.558166	4.00E-48
CD2-associated protein	CD2AP	1.680892	1.42019	1.550541	6.31E-24

Ensconsin	MAP7	1.507352	1.569604	1.538478	3.03E-20
pre-rRNA processing protein FTSJ3	FTSJ3	2.155927	0.9208608	1.5383939	2.11E-17
HCLS1-binding protein 3	HS1BP3	1.424843	1.639676	1.5322595	1.71E-29
Annexin A1	ANXA1	1.490699	1.572771	1.531735	0
Crk-like protein	CRKL	1.518489	1.53243	1.5254595	5.38E-35
Small acidic protein	SMAP	1.353267	1.634863	1.494065	4.12E-66
Fructose-2,6-bisphosphatase TIGAR	TIGAR	1.493848	1.493341	1.4935945	4.84E-30
Apoptosis regulator BAX	BAX	1.586566	1.375257	1.4809115	7.47E-30
Tubulin beta-2A chain;Tubulin beta-2B chain	TUBB2A;TUBB2B	1.475852	1.455809	1.4658305	7.82E-265
Catalase	CAT	1.542353	1.380576	1.4614645	1.55E-40
Glutaredoxin-related protein 5, mitochondrial	GLRX5	1.47107	1.441522	1.456296	7.52E-13
Serine/threonine-protein kinase 24;Serine/threonine-protein kinase 24 36 kDa subunit;Serine/threonine-protein kinase 24 12 kDa subunit	STK24	1.282603	1.628334	1.4554685	1.07E-29
Ras GTPase-activating protein-binding protein 1	G3BP1	1.409158	1.48925	1.449204	2.32E-85
Acyl-coenzyme A thioesterase 13	ACOT13	1.439254	1.430267	1.4347605	7.53E-15
Protein FAM107B	FAM107B	1.364659	1.468304	1.4164815	1.51E-19
CD44 antigen	CD44	0.7647355	0.4782885	0.621512	2.34E-31
Protein Dr1	DR1	0.5716775	0.6201586	0.5959181	2.34E-12
Probable ATP-dependent RNA helicase DDX17	DDX17	0.5880821	0.588212	0.5881471	1.04E-88
Dolichyl-diphosphooligosaccharide--protein glycosyltransferase subunit 1	RPN1	0.6107014	0.5591571	0.5849293	6.15E-101
Interferon-induced, double-stranded RNA-activated protein kinase	EIF2AK2	0.5534261	0.6135591	0.5834926	6.16E-35
Importin subunit alpha-2	KPNA2	0.5736055	0.5852709	0.5794382	1.72E-108
THO complex subunit 2	THOC2	0.6011869	0.5181544	0.5596707	1.84E-26
Myotrophin	MTPN	0.5346812	0.5347177	0.5346995	1.78E-36
PDZ and LIM domain protein 5	PDLIM5	0.5720129	0.4901454	0.5310792	2.68E-36
DNA topoisomerase 2-alpha	TOP2A	0.5731421	0.4744639	0.523803	6.55E-61
Glutamate dehydrogenase 1, mitochondrial;Glutamate dehydrogenase 2, mitochondrial	GLUD1;GLUD2	0.4876884	0.5154686	0.5015785	9.72E-87
Epsin-3	EPN3	0.4834045	0.4956484	0.4895265	2.64E-10
Hypoxanthine-guanine phosphoribosyltransferase	HPRT1	0.4808258	0.4798309	0.4803284	7.55E-47
Peptidyl-prolyl cis-trans isomerase FKBP10	FKBP10	0.5167466	0.4390533	0.4779	2.56E-26
Ras-related protein Rab-27B;Ras-related protein Rab-27A	RAB27B;RAB27A	0.4919718	0.3762916	0.4341317	9.88E-13
Transforming growth factor beta-1-induced transcript 1 protein	TGFB1I1	0.460246	0.3818254	0.4210357	3.42E-25
A-kinase anchor protein 12	AKAP12	0.3656977	0.3458077	0.3557527	9.10E-74
Nucleolar RNA helicase 2	DDX21	0.2675947	0.2612604	0.2644276	7.23E-91

Table 10: GSKIP Kd alters the expression of multiple proteins in A549 cells. Two GSKIP knockdown samples were evaluated against two control samples (NT SiRNA) and are shown in the first two columns. The third column shows the average ratio Kd/control of the two samples.The cutoff for upregulation upon GSKIP knockdown was set to 1.4 fold Kd/cntrl (red and yellow) and the cutoff for downregulation to 0.6 fold (green) for at least one of the two samples. Posterior error probabilities (PEP) values represent the probability of false positive.

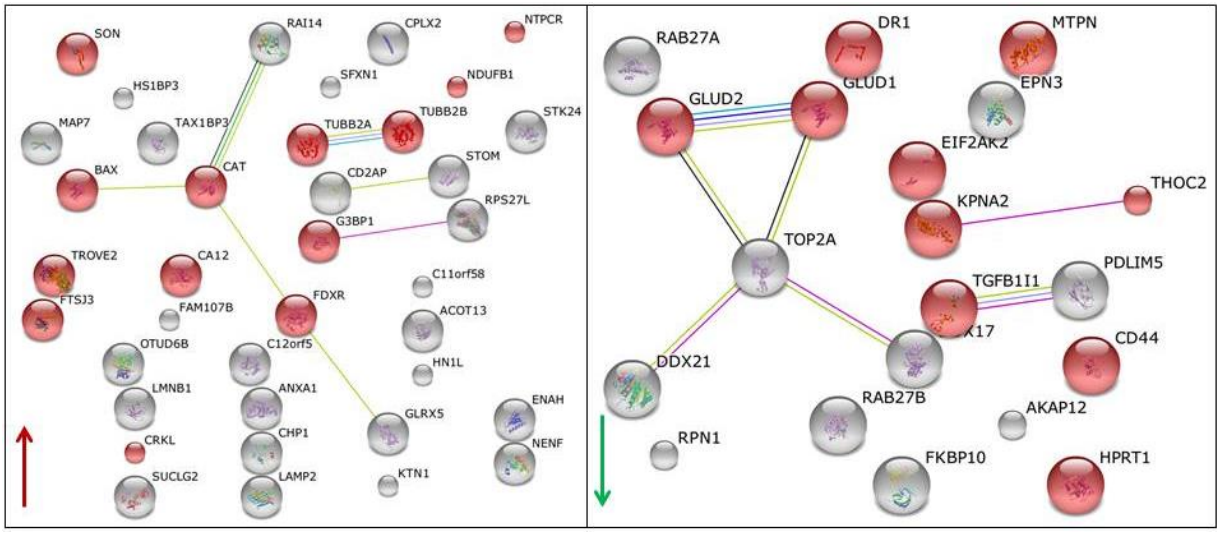

Figure 26: GSKIP Kd alters the expression of metabolic proteins. String network showing deregulated proteins upon GSKIP Kd and their interacting proteins. The proteins marked in red regulate metabolic processes. *Upregulated (left):* Apoptosis regulator (BAX), catalase (CAT), Protein SON (SON), NADPH:adrenodoxin oxidoreductase (FDXR), 60 kDa SS-A/Ro ribonucleoprotein (TROVE2), Carbonic anhydrase 12 (CA12), Crk-like protein (CRKL), Protein Dr1 (DR1), pre-rRNA processing protein (FTSJ3), Ras GTPase-activating protein-binding protein 1 (G3BP1), Cancer-related nucleoside-triphosphatase (NTPCR), Tubulin beta-2A chain (TUBB2A), NADH dehydrogenase [ubiquinone] 1 beta subcomplex subunit 1 (NDUFB1). *Downregulated (right):* Hypoxanthine-guanine phosphoribosyltransferase (HPRT1), Glutamate dehydrogenase 1;2 (GLUD1;2), Transforming growth factor beta-1-induced transcript 1 (TGFB1I1), Myotrophin (MTPN), Importin subunit alpha-2 (KPNA2), THO complex subunit 2 (THOC2), CD44 antigen (CD44), Interferon-induced, double-stranded RNA-activated protein kinase (EIF2AK2).

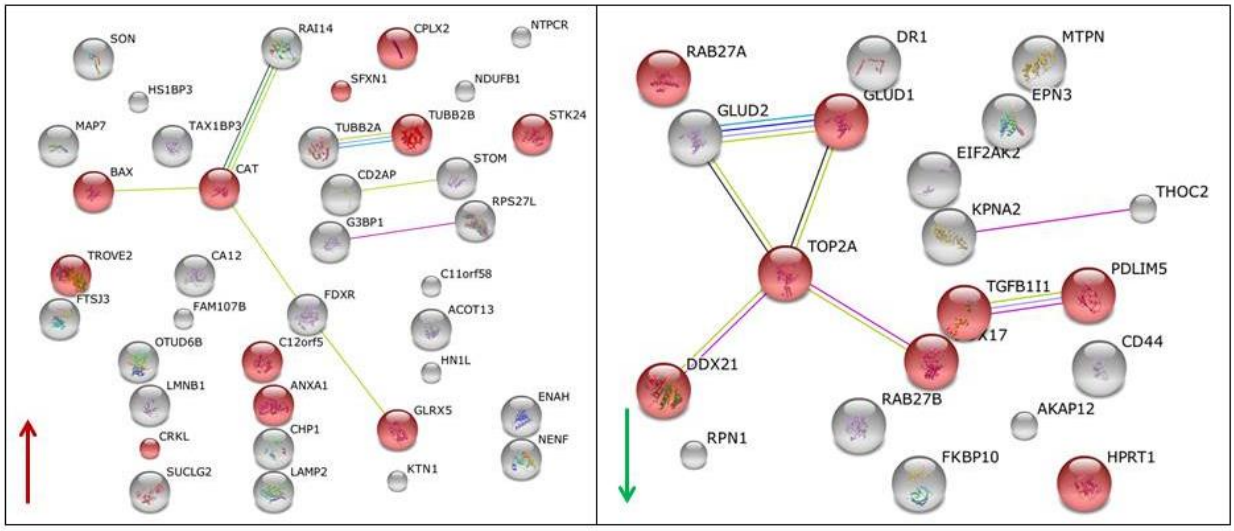

Figure 27: GSKIP Kd alters the expression of developmental-processes-related proteins. String network showing deregulated proteins upon GSKIP Kd and their interacting proteins. The proteins marked in red regulate developmental processes. *Upregulated (left):* Apoptosis regulator (BAX), catalase (CAT), 60 kDa SS-A/Ro ribonucleoprotein (TROVE2), Fructose-2,6-biphosphatase TIGAR (C12orf5), Annexin A1 (ANXA1), Crk-like protein (CRKL), Glutaredoxin-related protein 5 (GLRX5), Sideroflexin-1 (SFXN1), Serine/threonine-protein kinase 24 (STK24), Tubulin beta-2B chain (TUBB2B), Complexin-2 (CPLX2). *Downregulated (right):* DNA topoisomerase 2-alpha (TOP2A), Nucleolar RNA helicase 2 (DDX21), PDZ and LIM domain protein 5 (PDLIM5), Ras-related protein Rab-27A (RAB27A), Ras-related protein Rab-27B (RAB27B), Hypoxanthine-guanine phosphoribosyltransferase (HPRT1), Glutamate dehydrogenase 1 (GLUD1), Transforming growth factor beta-1-induced transcript 1 (TGFB1I1).

3.5.2 GSKIP Kd results in TGFβ and CD44 downregulation

Table 10 shows many proteins deregulated by GSKIP Kd that have important regulatory roles in tumorigenesis. For example CD44, its expression positively correlates with EMT (see section 1.1.1) and TGFβ1I1 (Transforming growth factor beta-1-induced transcript 1 protein), which positively regulates EMT by preventing the inhibition of TGFβ signaling and is itself induced by TGFβ (see section 1.1.3.1). Since TGFβ1I1 coding gene is induced by TGFβ, TGFβ protein expression levels were evaluated *via* Western Blot upon GSKIP Kd.

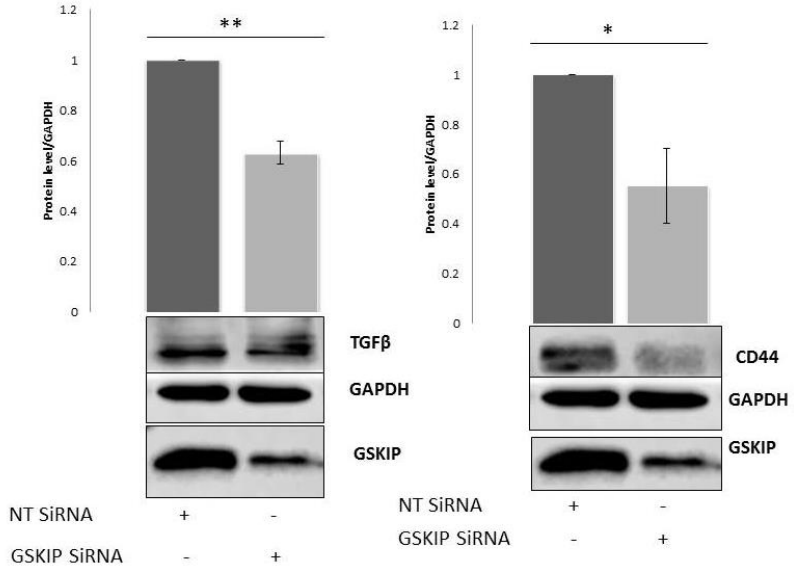

Figure 28: GSKIP Kd downregulates EMT proteins TGFβ and CD44. Semi-quantitative analysis of protein expression levels was carried out using ImageJ (n=3). Protein levels were normalized to the loading control, GAPDH (means ± SEM). Significant differences vs. NT control were determined using Student's t-test (*= P <0.05 **= P <0.01 ***= P<0.001 ns=not significant)

Figure 28 shows that, both TGFβ and CD44 are significantly downregulated after GSKIP Kd. Since TGFβ is the major EMT inducer in A549 cells and a promoter of both SNAIL and ZEB1 expression, downregulation of TGFβ signaling explains the negative effect on motility as well as on SNAIL, ZEB1 and E-cadherin protein levels. Due to crosstalk between TGFβ signaling with GPI/AMF signaling, reduced TGFβ may influence GPI/AMF protein levels (Figure 29).

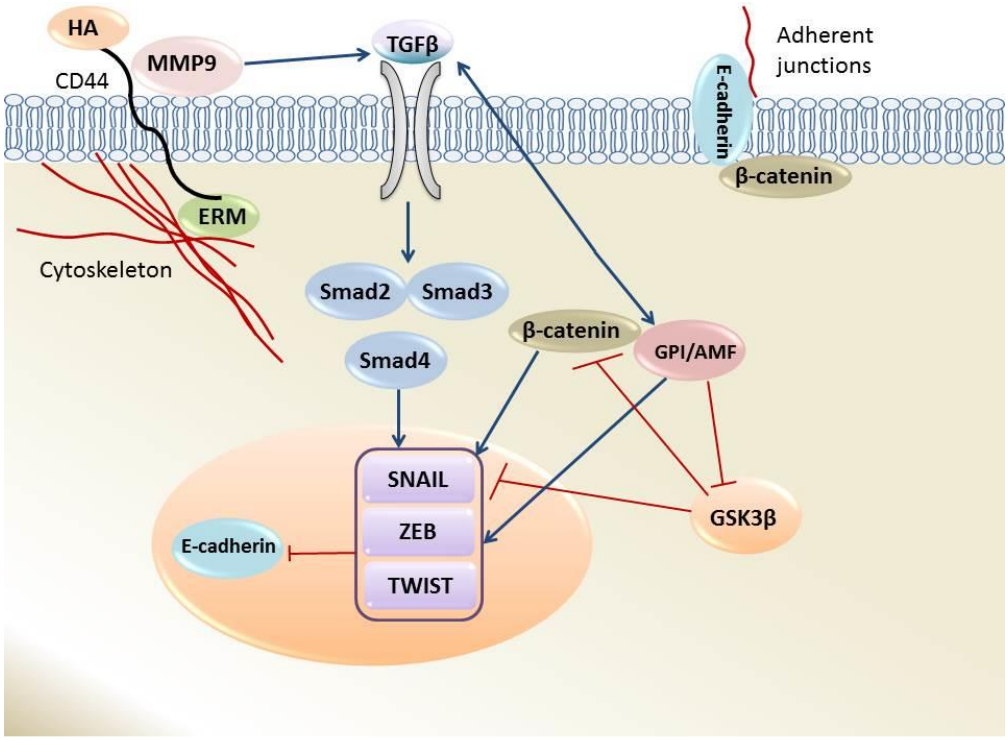

Figure 29: **Schematic representation of TGFβ, CD44 and GPI/AMF crosstalk.** Upon HA binding to the extracellular domain of CD44, CD44 becomes associated with MMP9, which promotes EMT by activating TGFβ and loss of adherent junctions. Also, CD44 is associated with ERM proteins in the cytoplasm, which cross link the actin cytoskeleton with ECM thus promoting migration. Active TGFβ induces transcription of SNAIL, TWIST and ZEB which suppress E-cadherin. This suppression results in degradation of adherent junctions and enhanced migration. GPI/AMF and β-catenin also contributes to upregulation of SNAIL, ZEB and TWIST. β-catenin is inhibited by GSK3β together with SNAIL and GPI/AMF inhibits GSK3β and activates TGFβ by a yet unknown mechanism, most likely involving a positive feedback loop, since TGFβ was also shown to result in increased levels of GPI/AMF.

Since CD44 is a major actin cytoskeleton cross-linker protein, downregulation of CD44 correlates with reduced motility (see section 1.1.1). This may suggest that reduced CD44 expression would have an affect the structure and perhaps distribution of actin. Therefore next immunofluorescence microscopy assays were performed on A549 cells.

3.5.3 GSKIP Kd alters the distribution of actin cytoskeleton in A549 cells

The immunofluorescence assays were performed as described in materials and methods (see section 2.2.7). Figure 30 demonstrates qualitative differences in the actin cytoskeleton upon GSKIP Kd compared to NT control. The overall signal from actin appears to be lower in the Kd compared to negative control. However this observation requires quantification. In addition, upon Kd the actin appears to be more globular as opposed to more linear in the NT control, which may indicate a reduction in stress fiber formation required for EMT. This needs to be confirmed by quantification. In addition, the reduction in CD44 protein levels upon GSKIP Kd may have resulted in reduced binding between CD44 and ERM proteins (see

section 1.1.1 and figure 29) preventing actin reorganization, thus attenuating directional cell motility. However, this hypothesis needs further confirmation by immunoprecipitation.

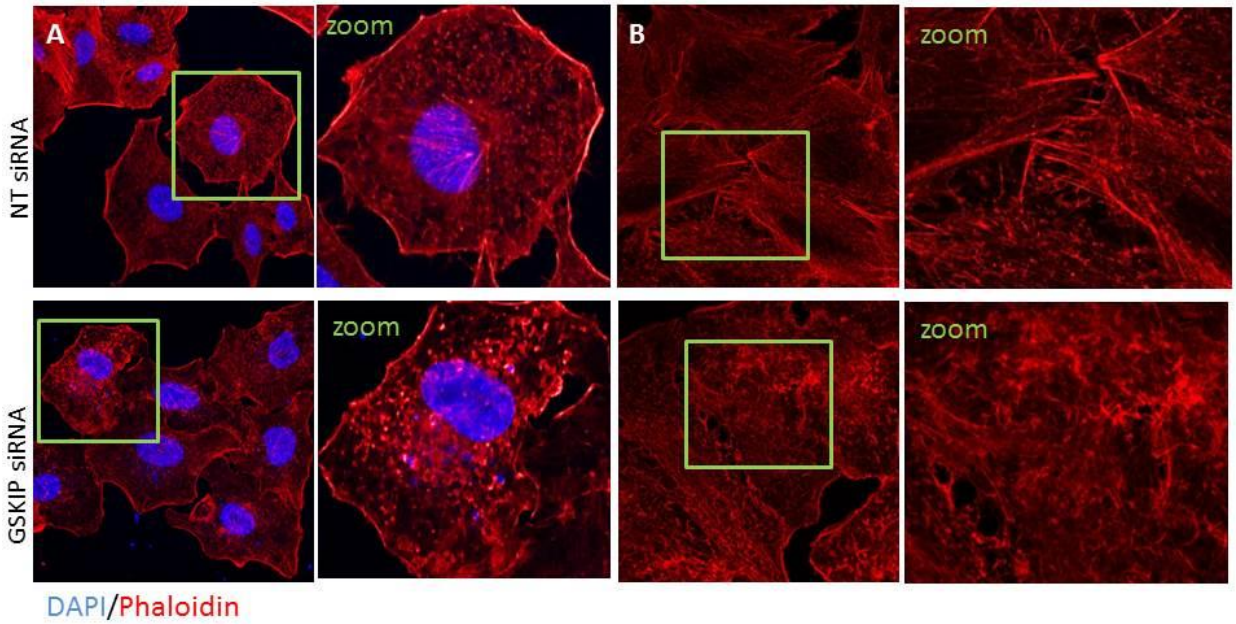

Figure 30: GSKIP Kd alters actin cytoskeleton in A549 cells. Representative images (n=4) from two independent experiments (A and B) showing Immunofluorescent staining of A549 cells treated with GSKIP SiRNA (bottom panel) or NT SiRNA as a negative control (upper panel). Original size images (right hand side) and zoom of the rectangular area (left hand side). Blue: DAPI nuclear staining, Red: Phaloidin actin cytoskeleton staining.

3.6 GSKIP Kd alters metabolic function of A549 cells

Since GSKIP Kd affects the expression of many metabolic proteins (Figure 26) as well as GPI/AMF, a protein involved in metabolism and GSK3β and PKA regulate metabolic pathways, GSKIP may influence metabolic pathways in cancer cells. Upon induction of EMT, cancer cells switch to catabolic metabolism and upregulate the TCA cycle and OXPHOS, presumably *via* upregulation of PDH activity (see section 1.2.3). Since upon GSKIP Kd A549 cells exhibited a more epithelial phenotype compared to control, their metabolism might be more anabolic than catabolic. In order to examine this, TCA cycle metabolites and mitochondrial OXPHOS were evaluated in A549 cells. In addition, since PDH was not detected by the proteomics analysis its protein expression was evaluated *via* WB.

3.6.1 GSKIP Kd results in reduced PDH activity in A549 cells

Figure 31 shows that upon GSKIP Kd PDH protein levels significantly decrease, suggesting a reduced TCA cycle flux and subsequent reduced OXPHOS rates (see section 1.2.3).

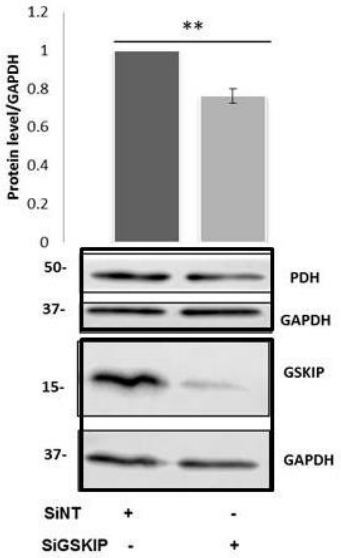

Figure 31: GSKIP Kd downregulates PDH. Semi-quantitative analysis of protein expression levels was carried out using ImageJ (n=3). Protein levels were normalized to the loading control, GAPDH (means ± SEM). Significant differences vs. NT control were evaluated using Student's t-test (*= P <0.05 **= P <0.01 ***= P<0.001 ns=not significant)

In order to confirm that PDH downregulation is reflected in reduced TCA cycle flux, metabolomics analysis were performed on A549 cells transfected with GSKIP siRNA in collaboration with K. Hiller, University of Luxembourg. 24 hours after siRNA transfection the cells were incubated for 24 hours in unlabeled medium or medium supplemented with either $^{13}C_6$-glucose or $^{13}C_5$-glutamine (See section 2.2.4) and ^{13}C Mass isotopomer distribution (MID) were measured for different metabolites *via* GC-MS. The results confirm reduced PDH activity and a switch to anabolic metabolism in A549 cells upon GSKIP Kd (Figures 32-34).

Figure 32 shows the conversion of $^{13}C_6$-glucose to pyruvate in glycolysis and the subsequent incorporation of labeled pyruvate into the TCA cycle *via* pyruvate dehydrogenase (PDH) and pyruvate carboxylase (PC). The labeled pyruvate is converted to TCA cycle intermediates with different carbon-labeling represented by ^{13}C isotopologs (M0-M5) and depicted in the atom-resolved map (Sellers et al., 2015). PDH activity generates [$^{13}C2$] acetyl-CoA (labelled on both carbon atoms) subsequently resulting in M2 citrate (Figure 32B), which is decreased in GSKIP Kd. This reduction indicates reduced pyruvate uptake into the TCA cycle by PDH, presumably due to reduced PDH protein levels.

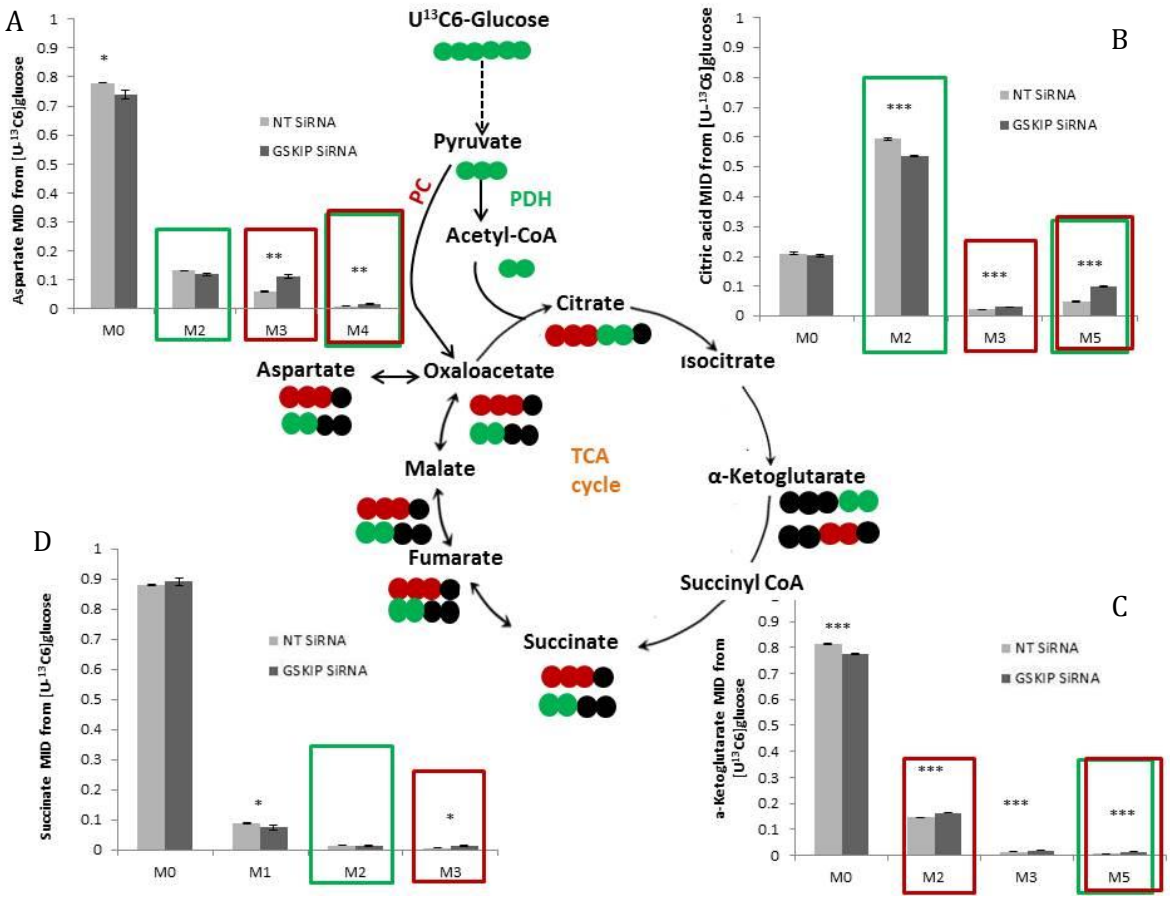

Figure 32: GSKIP Kd results in reduced PDH activity (labelled glucose metabolism). ^{13}C Mass isotopomer distributions (MID) derived from $^{13}C_6$-glucose were determined by GC-MS (n=3, means ± SEM). Significant differences vs. NT control were evaluated using Student's t-test (*= P <0.05 **= P <0.01 ***= P<0.001). The ^{13}C isotopologs of TCA cycle metabolites produced *via* PDH activity (Carbon atoms are tracked by green dots in the atom-resolved map and green rectangles in the bar graphs) and *via* PC (tracked by red dots in the atom-resolved map and red rectangles in the bar graphs) are shown. A. Aspartate isotopologs B. Citric acid isotopologs, C.a-Ketoglutarate isotopologs, D. Succinate isotopologs. Black dots indicate unlabeled carbon atoms.

Reduced M2 citrate levels could be attributed to lower glucose uptake, however Figure 33 shows no significant change in glucose uptake between the GSKIP Kd cells and control. Therefore, low M2 citrate can only be cause by low levels of PDH. Future experiments will aim to determine the cause of this downregulation.

PC activity yields [$^{13}C3$] oxaloacetate (labelled on three carbon atoms) leading to M3-labeled citrate, whereas M5 isotopologues of citrate reflect the combined carbon contribution of PC and PDH to citrate. Figure 34B shows that both M3 and M5 citrate isotopologs are increased in GSKIP Kd cells, suggesting that the combined activity of PDH and PC is increased. This suggests that PC protein expression is increased. PC protein levels are upregulated by 30 % as indicated in the proteomics analysis, confirming the metabolomics results.

The observation made for citrate is further supported by isotopologs of TCA downstream metabolites α-ketoglutarate (Figure 32C), succinate (Figure 32D) and aspartate (Figure 32A); reduced PDH activity upon GSKIP Kd is reflected by M2-labelled succinate and M2-labeled aspartate, the mild increase in PC activity is reflected in M2 α-ketoglutarate and M3-labeled succinate and aspartate, while the increase in combined PDH+PC activity is shown by M5-labeled α-ketoglutarate and aspartate. Taken together these results indicate that GSKIP Kd shifts the A549 metabolism to a more anabolic metabolism, supporting the inhibition of migration (see section 1.2.3).

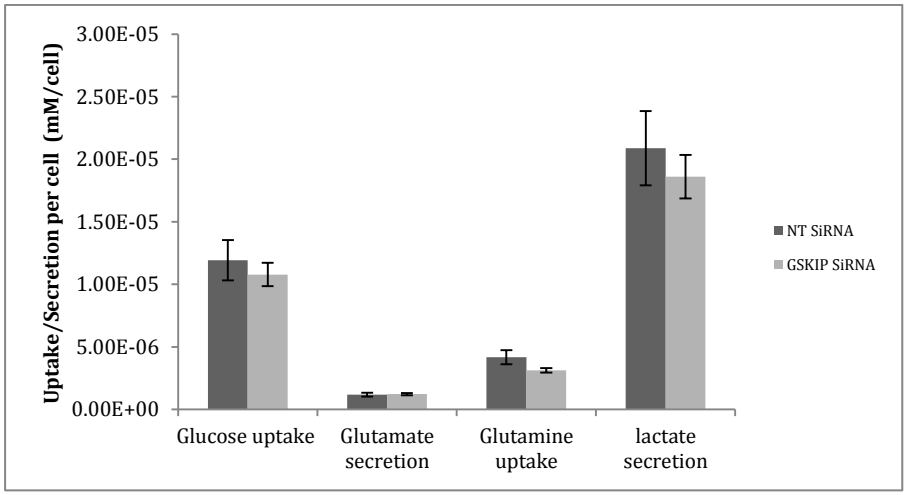

Figure 33: **GSKIP Kd does not affect metabolites uptake and secretion rates**. Cell specific uptake and secretion of glucose/glutamine and lactate/glutamate levels were measured at the end of culture and normalized to viable cell density. (n=3, means ± SEM). Significant differences vs. NT control were evaluated using Student's t-test (*= P <0.05 **= P <0.01 ***= P<0.001). No significant differences were found for all uptake/secretion values.

This switch to a more anabolic metabolism was confirmed by isotopologs derived from $^{13}C_5$-glutamine metabolism. Glutamine metabolism can take place in an oxidative or reductive manner (see Figure 34). Initial biochemical reactions are shared between the oxidative and reductive glutamine metabolism pathways: glutaminase generates glutamate from glutamine which subsequently is metabolized to α-ketoglutarate by glutamate dehydrogenase. Under oxidative conditions glutamine derived α-ketoglutarate is fed into the TCA cycle and oxidatively decarboxylated to succinyl-CoA (DeBerardinis et al., 2007) producing oxaloacetate and finally citrate. This is evidenced by M4-labelled citrate in Figure 34A, which is reduced upon GSKIP Kd, due to fusion of M4-labelled oxaloacetate to unlabeled acetyl-CoA. Unlabeled acetyl-CoA is also reduced due to lower PDH leading to reduced M4 labelling in citrate. Furthermore, unlabeled citrate (M0), which is produced when unlabeled oxaloacetate is fused to unlabeled acetyl-CoA, is increased in the Kd. This can be attributed to a mild increase

in PC activity or to higher citrate production by PC, since PC uses unlabeled pyruvate and CO_2 to form unlabeled oxaloacetate. Also, unlabeled α-ketoglutarate (M0), which is formed from unlabeled citrate, is increased in GSKIP Kd cells (Figure 34B), supporting the observed mild increase in PC activity. Due to increased oxaloacetate formed by PC from unlabeled pyruvate resulting after fusion with unlabeled acetyl-CoA in unlabeled citrate, which is then converted to α -ketoglutarate. Consequently α-ketoglutarate M4 is decreased in Kd. The observations made for citrate and α-ketoglutarate are further supported by isotopologs of TCA downstream metabolites succinate (Figure 34C) and aspartate (Figure 34D); lower PDH activity and eventually increase in PC activity, suggesting a more anabolic metabolism pattern.

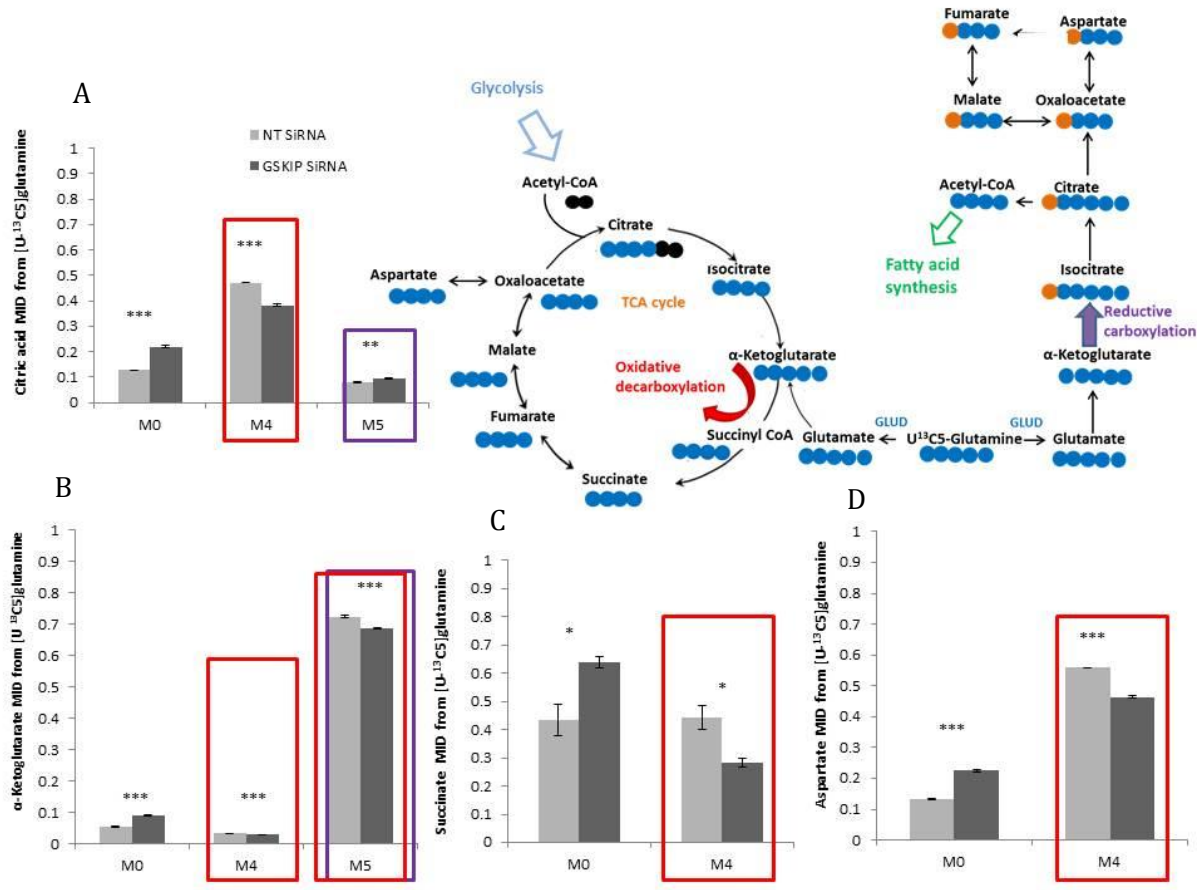

Figure 34: GSKIP Kd results in reduced PDH activity (labeled glutamine metabolism). ^{13}C Mass isotopomer distributions (MID) derived from $^{13}C_5$-glutamine were determined by GC-MS (n=3, means ± SEM). Significant differences vs. NT control were evaluated using Student's t-test (*= P <0.05 **= P <0.01 ***= P<0.001). The ^{13}C isotopologs of TCA cycle metabolites produced *via* oxidative decarboxylation of glutamine (carbon atoms are tracked by blue dots in the atom-resolved map and red rectangles in the bar graphs) and *via* reductive carboxylation (tracked by blue-orange dots in the atom-resolved map and purple rectangles in the bar graphs) are shown. A-citric acid isotopologs, B- α-ketoglutarate isotopologs, C-succinate isotopologs, D-aspartate isotopologs. Black dots indicate unlabeled carbon atoms.

Under reductive conditions α-ketoglutarate is carboxylated to isocitrate by isocitrate dehydrogenase and converted to citrate (Des Rosiers et al., 1995; Yoo et al., 2008). Glutamine derived citrate can then serve as carbon source for lipogenesis (Holleran et al., 1995). M5

labelled citrate (Figure 34A) derives from reductive carboxylation and is increased upon GSKIP Kd. Since M5-labelled citrate is then converted to acetyl-CoA and used in lipogenesis, this increase could indicate upregulation of lipogenesis, which is necessary for proliferation of more anabolic and less-migrating cells, while induction of EMT suppresses lipogenesis (see section1.2.3).

3.6.2 GSKIP Kd results in lower OXPHOS rate

The metabolomics data in the previous section collectively demonstrate that upon GSKIP Kd A549 cells switch to a more anabolic metabolism associated with reduced migration. The consequences of lower TCA flux caused by reduced PDH activity are downregulation of OXPHOS, which is an additional feature of anabolic metabolism. In order to determine whether OXPHOS rates were affected by GSKIP Kd, Seahorse XF24 experiments were performed on A549 cells as described in section 2.2.1.9.

Figure 35A shows that baseline respiration, indicated by oxygen consumption rate (OCR) of GSKIP Kd cells is significantly lower compared to the NT control. In addition, GSKIP Kd cells show significantly lower maximum respiratory capacity (Figure 35B). Furthermore, mitochondrial reserve capacity is significantly downregulated upon GSKIP Kd (Figure 35C). These results indicate that GSKIP Kd cells have reduced levels of OXPHOS compared to the control. This is in line with the observation of Caneba *et al*., namely that lower migration rate coincided with lower OCR (Caneba, 2012). Finally, the mitochondrial Respiratory Control Rate (RCR) was measured (Fig. 35D) and no significant difference was observed. This indicates that mitochondrial integrity was not affected by GSKIP Kd and the decreased OCR is a result of signaling alterations and not physiological damage to the mitochondria.

Although mitochondrial function was clearly affected, no significant differences were observed in glycolysis rates between GSKIP Kd cells and control (Supplementary figure 4), indicating that the cells become less catabolic but do not upregulate anabolic metabolism to a high enough extent to promote proliferation. This statement is further supported by unchanged levels of Lactate secretion (Figure 33), which should be higher in proliferating cells as well as by unchanged viability (Figure 16), which also would be higher. This may indicate that during the transient GSKIP Kd, the A549 cells are transitioning to a yet undetermined state. Future experiments will require longer observation times of cellular proliferation, viability, metabolism and migration after GSKIP Kd, which will necessitate stable Kd.

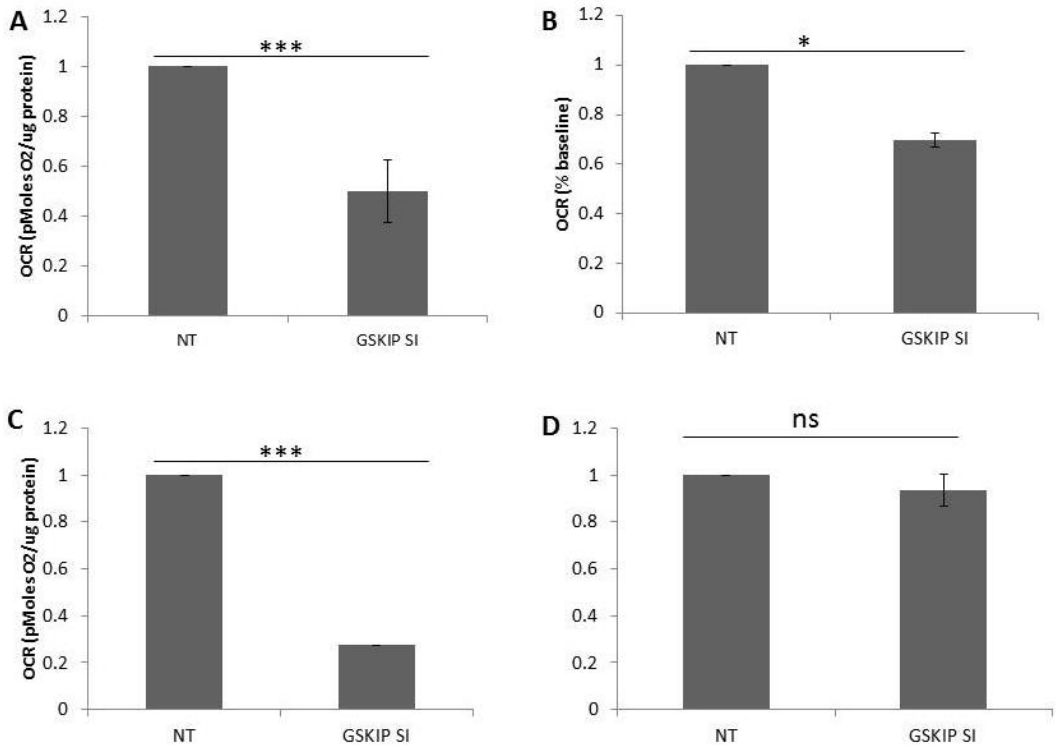

Figure 35: GSKIP Kd reduces OXPHOS in A549 cells. Oxygen consumption rate (OCR) was measured using Seahorse XF24 Analyzer. A. Basal respiration. B. Maximum respiratory capacity (OCR after injection of FCCP). C. Mitochondrial reserve capacity (OCR after injection of FCCP minus basal OCR). D. Respiratory control ratio indicating the overall mitochondrial efficacy (Basal OCR/ OCR after injection of Oligomycin). (n=3, means ± SEM). Significant differences vs. NT control were evaluated using Student#s t-test (*=P <0.05 **= P <0.01 ***= P<0.001).

3.7 GSKIP interacts with SMYD2 and GDF5OS in HEK293 cells

Identifying new interaction partners of GSKIP in cancer cells may contribute to understanding its function. Proteomics analysis, performed on MCF-7 breast carcinoma cell line that was intended to discover novel PKA substrates, revealed GDF5OS protein to be phosphorylated by PKA. Growth and differentiation factor 5 opposite strand (GDF5OS) is a small protein of unknown function (28kDa) which is predicted to be localized in the mitochondria. GSKIP's interaction with GDF5OS was evaluated by immunoprecipitation as described in section 2.2.2.5. In addition, GSKIP is predicted to interact with SMYD2 (see section 1.6.3), which was identified to methylate tumor suppressors p53 and Rb thus inhibiting their functions (Wang et al., 2011). Since p53 tumor suppressor is directly regulated by GSK3β in the induction of intrinsic apoptosis in the mitochondria (see section 1.3.2) and SMYD2 was found to interact with GSK3β (Skroblin, 2011), SMYD2's predicted interaction with GSKIP was evaluated by immuniprecipitation.

Figure 36 shows that both SMYD2 (lane A) and GDF5OS (lane B) co-immunoprecipitate with

GSKIP, indicating physical interaction between GSKIP and the two proteins.

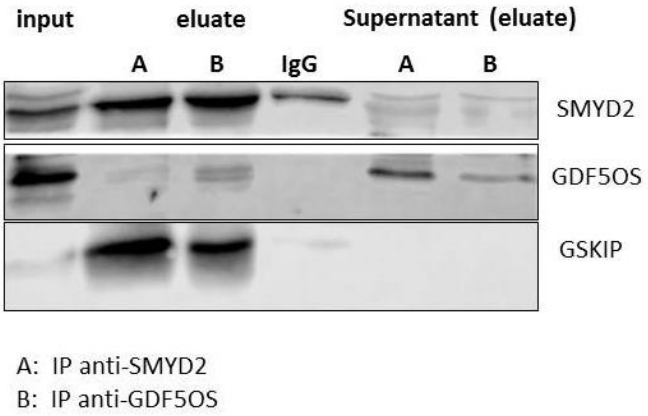

Figure 36: GSKIP interacts with SMYD2 and GDF5OS. Immunoprecipitation (IP) assay of GSKIP with SMYD2 (lane A) and GDF5OS (lane B) in HEK293 cells (n=3). GSKIP co- immunoprecipitates with both SMYD2 and GDF5OS (eluate fraction, lanes A and B, respectively) and not with the IgG control.

In order to evaluate the exact region of SMYD2 and GDF5OS that interacts with GSKIP peptide spots containing the entire protein sequence of SMYD2 (Figure 37) and GDF5OS (Figure 38) were synthesized and incubated with His-tagged GSKIP or with blocking buffer alone, as a negative control, as described in section 2.2.2.6.

Figure 37 shows that GSKIP binds to SMYD2 peptides in spots D14-16 in a specific manner. The common sequence to the three spots is highlighted in red, and represents the probable binding sequence between GSKIP and SMYD2.

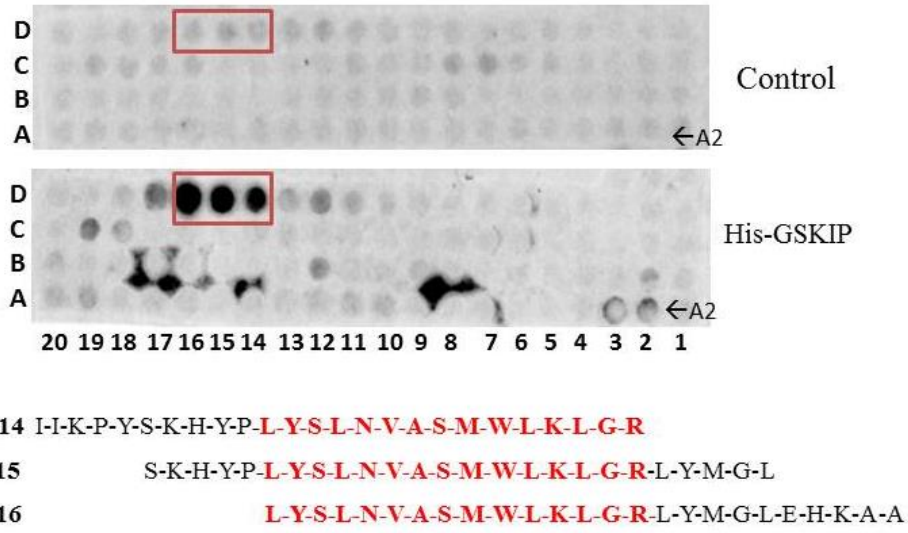

Figure 37: Probable binding sequence of GSKIP to SMYD2. Peptide spot arrays containing SMYD2-derived 25-mer peptides were incubated with HIS-GSKIP (lower membrane) and Blocking buffer alone (upper membrane), following incubation with GSKIP antibody (n=3). Results show strong binding of GSKIP to peptides D14-16. The sequences of peptides D14-16 are shown below and the common sequence between the three peptides is highlighted in red.

Figure 40 shows that GSKIP binds to GDF5OS peptide K4-K7, K9, K14, K20 and L19 in a specific manner. However, some unspecific binding to GDF5OS peptides was also detected.

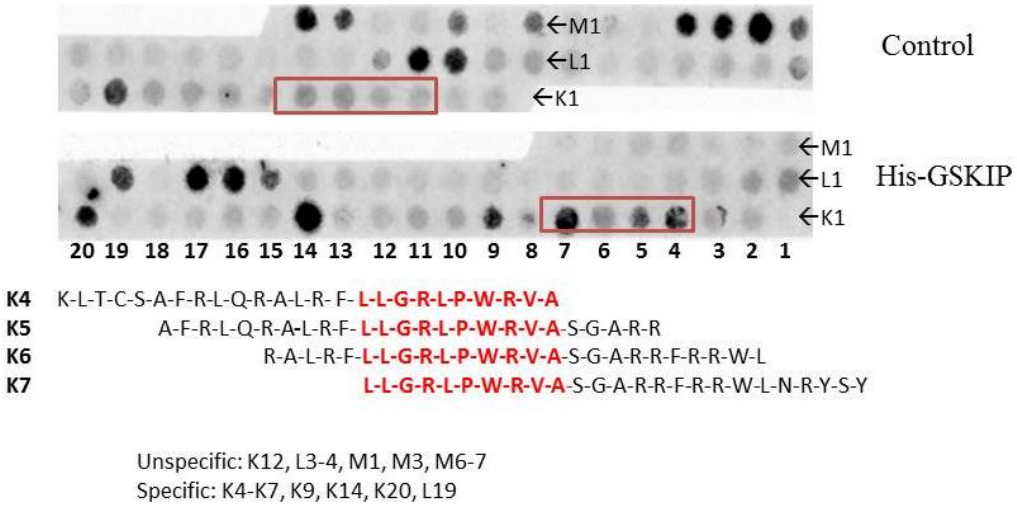

Figure 38: **Probable binding sequence of GSKIP to GDF5OS.** Peptide spot arrays containing GDF5OS-derived 25-mer peptides were incubated with Blocking buffer alone (upper membrane) and HIS-GSKIP (lower membrane), following incubation with GSKIP antibody (n=3). Results show unspecific binding to the control membrane as well as specific binding of GSKIP to peptides K4-7. The sequences of peptides K4-7are shown below and the common sequence between the four peptides highlighted in red. Unspecific and specific binding peptides are listed below.

Collectively these results indicate that GSKIP physically interacts with both SMYD2 and GDF5OS in HEK293 cells and future experiments will aim to elucidate the functional significance of the GSKIP-SMYD2 and GSKIP-GDF5OS complex formation.

4. Discussion

Induction of the EMT signaling cascade in cancer cells signifies a first step in generation of usually fatal distant metastasis. The process of EMT induction is accompanied by metabolic changes, where cancer cells switch between anabolic, proliferation-related metabolism, and catabolic, metastasis-associated metabolism. This metabolic switch allows cancer to survive under conditions of ECM-detachment required for metastasis and requires extensive regulation and crosstalk between metabolic and EMT-related proteins. This cooperation between the two signaling pathways provides a therapeutic opportunity, since targeting one of these signaling pathways may have an impact on the second pathway. Therefore, understanding the regulatory mechanism of EMT, metabolic reprogramming and in particular the mechanisms of cooperation between these signaling pathways, can contribute to the development of novel and more effective cancer treatments. The cooperation between EMT and metabolic reprogramming is achieved largely *via* multifunctional proteins that regulate both signaling pathways. Two such multifunctional proteins are GSK3β and PKA, and GSKIP is known to bind PKA and GSK3β and facilitate GSK3β's inhibitory phosphorylation by PKA. GSKIP is ubiquitously expressed in various tumor tissues and is a potential regulator of tumorigenic signaling pathways *via* PKA, GSK3β and other predicted interaction partners, such as SMYD2. However, GSKIP's role in cancer progression remains largely unclear.

The current PhD project demonstrates for the first time the roles of GSKIP in the regulation of two tumorigenic processes, EMT and metabolic reprogramming of A549 lung carcinoma cells. Upon GSKIP Kd the cells lose their migratory ability, which is indicative of reduced metastatic potential. Moreover, GSKIP Kd results in downregulation of EMT inducers, such as TGFβ and GPI/AMF, as well their downstream targets and EMT master regulators, such as SNAIL, ZEB1 and E-cadherin. Furthermore, GSKIP Kd results in downregulation of metabolic protein PDH and consequent metabolic switch from catabolic metabolism, thus nominating GSKIP as a coupling agent between metabolism and EMT regulation.

The data obtained in this project suggests the possible mechanisms by which GSKIP regulates these complex tumorigenic pathways and discusses the future work required for the exact elucidation of these mechanisms. Moreover, the data obtained in this project suggests GSKIP to function as a tumor promoter, thus nominating GSKIP as a possible therapeutic target in lung cancer. However, the direct target/s of GSKIP regulation remain unknown, therefore this project raises the "chicken or the egg" question– Which pathway is affected first by GSKIP, EMT or metabolism?

In addition, this project supports the interaction of GSKIP with the tumor promoter SMYD2 and identifies a novel interaction partner with an unknown function, GDF5OS, thus contributing to elucidation of SMYD2's and GDF5OS's functional roles. The following passages will discuss in detail the results of this research.

4.1 GSKIP links metabolic reprograming and EMT

This work has demonstrated that upon Kd of GSKIP, migration of A549 cells is significantly impaired and this impairment is attributed to the significant reduction in protein expression levels of E-cadherin's transcriptional repressors, ZEB1and SNAIL. SNAIL is negatively regulated by GSK3β and on the other hand positively regulated by PKA. Therefore, the downregulation of SNAIL may be a consequence of increased activity of GSK3β upon GSKIP Kd, since GSKIP is not able to facilitate GSK3β's inhibition by PKA. GSK3β phosphorylates SNAIL multiple times and one or more of these phosphorylation events may be GSKIP-dependent (Figure 39). In addition, the reduction in SNAIL protein expression upon GSKIP Kd can be attributed to PKA. It is plausible that GSKIP facilitates PKA's stabilizing phosphorylation of SNAIL which is abrogated upon GSKIP Kd (Figure 39). Future experiments need to be conducted to test this hypothesis (see outlook section). In addition, GSKIP Kd results in a significant reduction in the potent EMT inducer TGFβ, which is a positive regulator of SNAIL. The possibility that GSKIP regulates TGFβ signaling in A549 cells is suggested not only by SNAIL and ZEB1, but also by TGFβ1I1 downregulation upon GSKIP Kd, all downstream targets of TGFβ. The exact mechanism of this regulation remains to be elucidated; GSKIP may positively regulate TGFβ1I1, which will result in Smad7 upregulation and inhibition of TGFβ by a negative feedback mechanism. Alternatively, GSKIP may positively regulate PKA in EMT induction, by either facilitating PKA's interaction with Smad3 and Smad4, or with STAT3 (see section 1.4.3). Future experiments need to evaluate these possibilities.

Since the upregulation of ZEB1 protein expression upon EMT induction is a direct consequence of SNAIL protein expression upregulation, ZEB1 downregulation upon GSKIP Kd can be attributed directly to SNAIL (Figure 39). Moreover, downregulation of GPI/AMF and subsequent MET induction characterized by downregulation of SNAIL and ZEB1 protein expression levels is in accordance with previous studies (Funasaka and Raz, 2007; Niinaka, 2010; Tsutsumi et al., 2004). However, the mechanism by which GSKIP regulates GPI/AMF and consequently ZEB1, remains to be elucidated; The reduction in NF-kB DNA binding activity upon GPI/AMF downregulation was not observed, in contrast to observations made by

Ahmad *et al*. (Ahmad and Aboukameel, 2011) and although re-expression of GSKIP rescued GPI/AMF protein expression, it failed to rescue E-cadherin or migration inhibition during the observed time interval. The current work indicates that the possible mechanism of EMT regulation by GSKIP is likely to involve crosstalk between GPI/AMF and TGFβ signaling as well as GSK3β and PKA (Figure 39). In the proposed model, GSKIP promotes both TGFβ and GPI/AMF signaling in A549 cells and this effect is abrogated upon GSKIP Kd. TGFβ and GPI/AMF signaling positively regulate each other and activate the EMT transcriptional program *via* SNAIL and ZEB1. Whether GSKIP acts directly or indirectly (*via* PKA or GSK3β) on TGFβ, GPI/AMF or on SNAIL remains to be elucidated.

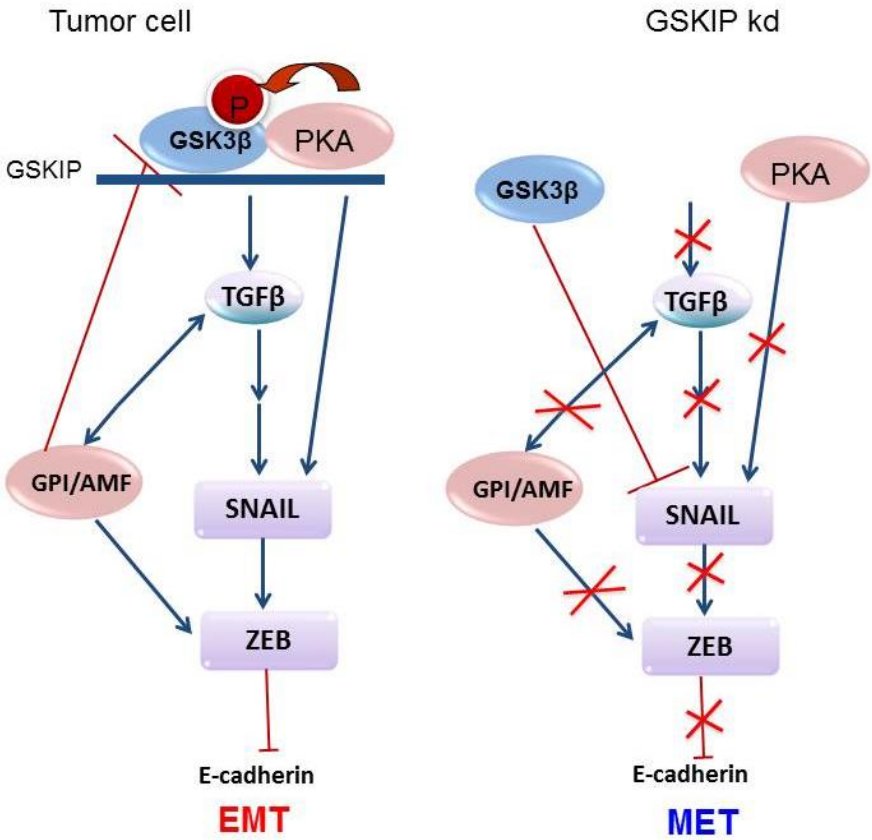

Figure 39: **Proposed mechanism of EMT regulation by GSKIP.** In the presence of GSKIP (left) GSKIP promotes TGFβ signaling and active TGFβ induces transcription of SNAIL and ZEB which suppress E-cadherin. This suppression results in degradation of adherent junctions and enhanced migration. GPI/AMF also contributes to upregulation of SNAIL, ZEB1 and TGFβ signaling by a yet unknown mechanism. PKA stabilizes SNAIL and GSK3β' inhibitory activity on SNAIL is blocked by both PKA and GPI/AMF, thus promoting EMT. Upon GSKIP Kd (right) SNAIL is inhibited by GSK3β and PKA-mediated stabilization of SNAIL is lost. TGFβ and GPI/AMF activity is reduced due to GSKIP's absence, resulting in downregulation of SNAIL and ZEB1 protein expression and consequently upregulation of E-cadherin and MET.

The induction of MET upon GSKIP Kd was also shown to correlate with downregulation of CD44 protein expression, which is in accordance with previous observations (Gao, 2015).

Since CD44 is known to regulate TGFβ signaling, this regulation might be mediated by GSKIP. Moreover, preliminary immunofluorescence experiments have shown alterations in the actin cytoskeleton distribution upon GSKIP Kd, which correlates with attenuation of migration and CD44 downregulation. The proteomics analysis revealed AKAP12, to be downregulated upon GSKIP Kd is (-0.36 fold). Although, AKAP12 was shown to function as a negative regulator of EMT and tumour growth (section 1.5.2) (Akakura and Gelman, 2012; Akakura et al., 2010; Gelman, 2010), in melanoma mouse model silencing of AKAP12 *in vivo* was shown to reduce tumor growth and EMT (Finger et al., 2015), corresponding to observations made in this work upon GSKIP Kd. The prospect of GSKIPs cooperation with other AKAPs to synergistically regulate PKA and other ligands in tumorigenesis may have therapeutic implications on targeting AKAPs, and merits further investigation. The conclusions from these observations are that GSKIP is an important mediator of motility in A549 cells and affects multiple EMT-regulators by a yet to be determined mechanism.

In addition to the induction of MET, GSKIP Kd induced a metabolic switch from catabolic to anabolic metabolism in A549 cells. This switch was demonstrated by downregulation of PDH protein expression and subsequent reduction in TCA cycle flux and OXPHOS. These results support previous studies demonstrating that highly invasive cancer cells upregulate OXPHOS and TCA cycle flux (Caneba, 2012; Cha, 2015; Ward and Thompson, 2012) and upregulate PDH (Sun et al., 2014). The mild upregulation of PC activity upon GSKIP Kd was demonstrated in metabolomics assays and PC protein expression levels were slightly upregulated (+1.3 fold) in the proteomics data set. This upregulation further confirms the switch to a more anabolic metabolism in accordance with previous studies, demonstrating significantly upregulated PC in early stage highly-proliferative lung cancer cells (Sellers et al., 2015). However, since PC is only mildly upregulated and increased proliferation expected of anabolic cancer cells was not observed upon GSKIP Kd in this work or in previous studies (LeBleu et al., 2014), it is unclear at this point whether GSKIP Kd would result in increased proliferation further down the line or not. Implementation of stable Kd is required to test this hypothesis as well as confirmation of PC upregulation *via* WB.

In addition, the negative correlation between EMT and lipogenesis (Jiang et al., 2015) was indicated in this project, showing possible upregulation of lipogenesis upon GSKIP characteristic of anabolic metabolism. The possible upregulation of lipogenesis is further supported by upregulation of protein expression of TIGAR (see details in the next section)

upon GSKIP Kd, a protein that upregulates the PPP (Bensaad et al., 2006), which results in higher levels of NADPH necessary for lipogenesis. In contrast, upregulation of reductive glutamine metabolism, which is another source of NADPH (DeBerardinis et al., 2007) was not observed upon GSKIP Kd. Furthermore, downregulation of GLUD1;2 (-0.5fold) upon GSKIP Kd in the proteomics data, may indicate a downregulation of reductive glutamine metabolism, but further metabolomics assay using other labeled metabolites than glucose and glutamine are required to confirm this hypothesis.

In addition, two of the highest scoring upregulated proteins upon GSKIP Kd are NADH Dehydrogenase (Ubiquinone) 1 Beta Subcomplex, NDUFB1 (+3.25fold) and Carbonic anhydrase 12, CA12 (+2.75), both metabolic proteins. Carbonic anhydrase 12 is a transmembrane metabolism and EMT-related protein that catalyzes the reversible hydration of CO_2 in mitochondria and its expression was found to correlate with favorable prognosis in invasive breast cancer patients (Watson et al., 2003). CA12 upregulation upon GSKIP Kd may indicate that CA12 is a favorable prognosis marker in lung cancer as well. In contrast to CA12, little is known about the role of NDUFB1 in cancer progression. NDUFB1 is a subunit of mitochondrial complex I, and functions to transfer electrons from NADH to ubiquinone as well as to pump protons from the mitochondrial matrix to the intermembrane space, which results in increased membrane potential across the inner mitochondrial membrane (Chandra and Singh, 2011). Although no data is available on protein expression of NDUFB1 in cancer, another subunit of complex I GRIM-19, was shown to have pro-apoptotic activity in breast cancer cells (Angell et al., 2000). Therefore, overexpression of NDUFB1 may share this pro-apoptotic function. In addition, further investigation into the potential regulation of CA12 and NDUFB1by GSKIP may provide additional insight into the cross talk between EMT and metabolic reprogramming signaling.

However, the exact mechanism of GSKIP regulation of EMT and metabolic proteins as well as the direct target of GSKIP remain unknown. The multitude of various possible targets of GSKIP raises the possible of GSKIP targeting microRNAs and thus able to regulate whole clusters of protein post-translationally. GSKIP is predicted to interact with microRNAs 19a and 19b by the PicTar algorithm (Figure 40). MicroRNAs (miRNAs) are endogenous ~22 nt RNAs that negatively regulate translation in many biological processes, including proliferation, development, EMT, metabolism and apoptosis (Bartel, 2004; Chen et al., 2012; Krützfeldt and Stoffel, 2006). miR19a was shown to regulate EMT in A549 cells (Li et al., 2015), proliferation and apoptosis in prostate cancer (Lu et al., 2015), TCA cycle enzyme citrate

synthase (Chen et al., 2012) and together with miR19b, drug resistance in gastric cancer (Wang et al., 2013). Taken together, these results suggest GSKIP as a potential master regulator of cancer related gene clusters *via* miRNAs.

PicTar WEB INTERFACE

Choose Species: vertebrate

Choose Dataset: target predictions for all human microRNAs based on conservation in mammals (human, chimp, mouse, rat, dog)

Gene ID: C14orf129

PicTar score: 3.22 primates: 3.31
rodents: 3.10 dog: 3.25 chicken: 0.00
fishes: 0.00

Org	PicTar score	PicTar score per species	microRNA	Probabilities	Free Energies kcal/mol	Structure of predicted duplex
hs	3.22	3.3	hsa-miR-19a	0.96	-23.1	UAG UAGAUUUGCACA : GUC AUCUAAACGUGU
pt	3.22	3.31	hsa-miR-19a	0.96	-23.1	UAG UAGAUUUGCACA : GUC AUCUAAACGUGU
mm	3.22	3.1	hsa-miR-19a	0.96	-22.1	UAGAUUUGCACA : AUCUAAACGUGU
rn	3.22	3.11	hsa-miR-19a	0.96	-22.1	UAGAUUUGCACA : AUCUAAACGUGU
cf	3.22	3.25	hsa-miR-19a	0.96	-23.1	UAG UAGAUUUGCACA : GUC AUCUAAACGUGU

PicTar score: 3.22 primates: 3.31
rodents: 3.10 dog: 3.25 chicken: 0.00
fishes: 0.00

Org	PicTar score	PicTar score per species	microRNA	Probabilities	Free Energies kcal/mol	Structure of predicted duplex
hs	3.22	3.3	hsa-miR-19b	0.96	-20.2	UAG GAUUUGCACA : GUC CUAAACGUGU
pt	3.22	3.31	hsa-miR-19b	0.96	-20.2	UAG GAUUUGCACA : GUC CUAAACGUGU
mm	3.22	3.1	hsa-miR-19b	0.96	-19.1	UAG GAUUUGCACA : GUC CUAAACGUGU
rn	3.22	3.11	hsa-miR-19b	0.96	-19.1	UAG GAUUUGCACA : GUC CUAAACGUGU
cf	3.22	3.25	hsa-miR-19b	0.96	-20.2	UAG GAUUUGCACA : GUC CUAAACGUGU

Figure 40: GSKIP is predicted to interact with miR19. microRNAs (miRs) predicted to interact with GSKIP in primates of various species as predicted by PicTar, an algorithm for the identification of microRNA targets (http://pictar.mdc-berlin.de/). Left to right: species (Org), PicTar overall score for the gene-miR interaction, PicTar score for the gene-miR interaction per species, name of miR, probabilities for the interaction, Free energy of the gene-miR interaction, structure of the predicted gene-miR duplex. *Homo-sapiens* (hs), *Pan troglodytes* (pt), *Mus musculus* (mm), *Rattus norvegicus (rn), canisfamiliaris (cf)*

4.2 GSKIP is a potential pro-survival protein

In addition to the above mentioned EMT-related and metabolic proteins already verified to be part of the GSKIP regulatory network, the proteomics data presented here reveals additional suspects. Since deregulation of development-related proteins such as TGFβ and Wnt-related proteins, is frequently associated with EMT and tumor growth, these potential targets of GSKIP require further insight. Additional downregulated proteins upon GSKIP Kd include DNA topoisomerase 2-alpha, TOP2A (-0.52fold) and nuclear RNA helicase, DDX12 (-0.26fold) upon GSKIP Kd is intriguing. TOP2A is a nuclear DNA replication regulator and proliferation marker and its overexpression correlates with poor prognosis and drug resistance in various cancers (De Resende et al., 2013; Dingemans et al., 1999; Wong et al., 2009). Similarly, DDX21, a nucleolar protein involved in ribosome RNA processing, was found to be highly overexpressed in breast tumor tissue (Zhang et al., 2014). Therefore, this downregulation of TOP2A and DDX21 protein expression upon GSKIP Kd suggests suppression of tumor growth and may potentially sensitize A549 cells to chemotherapy or stress-induced apoptosis.

This sensitization prospect correlates with an apparent induction of tumor suppressor p53-regulated cascade upon GSKIP Kd, evidenced in the proteomics data by upregulated apoptosis regulator BAX (+1.48fold), Fructose 2,6-biphosphatase TIGAR (+1.49fold) and ferredoxin reductase FDXR (+2.14fold), all p53 induced proteins. TIGAR is a p53-inducible protein activated by low levels of stress and may play a role in the pro-survival tumor-suppressor function of p53, such as cell cycle arrest in order to allow for DNA repair. However in the event that such a repair is not possible or upon persistent high stress levels, TIGAR is downregulated and pro-apoptotic cascade is activated by p53 (Bensaad et al., 2006). This is supported by upregulation of the pro-apoptotic BAX, the mitochondrial protein BAX, which regulates apoptosis and its protein expression levels is positively regulated by GSK3β (see section 1.3.2), either *via* phosphorylation (Linseman, 2004) or *via* activation of p53 (Beurel and Jope, 2006). BAX's upregulation upon GSKIP Kd can be attributed to a more active GSK3β and may signify the initial step in intrinsic apoptosis. However, since no difference in viability between GSKIP Kd and control was observed during 72 hours, future experiments need to examine apoptosis in a stable Kd. It is possible that the observed time interval after Kd was sufficient to initiate the protein expression of pro-apoptotic proteins but not stuffiest to execute the complete apoptotic program, which would be evident by viability assays. Another evidence of p53 induction upon GSKIP Kd is FDXR, which is a mitochondrial protein induced by p53 in response to DNA damage and was shown sensitize cancer cells to apoptosis (Liu and

Chen, 2002). The upregulation of p53-inducible proteins may be a consequence of reduced GSKIP-mediated GSK3β inhibition, rendering GSK3β more available to activate p53. Preliminary experiments (n=1) on A549 cells showed an upregulation of GSK3β-phosphorylated p53 protein expression level however, this requires additional repetitions. Alternatively, the interaction of GSK3β and GSKIP with p53 inhibitor SMYD2 may be responsible for p53 signaling upregulation. The implications of this upregulation may be induction of intrinsic apoptosis of cancer cells by silencing of GSKIP, which is an attractive therapeutic strategy and must be investigated further.

4.3 GSKIP binds to SMYD2 in a direct and specific manner

SMYD2 was previously shown to interfere with the pro-apoptotic functions of tumor suppressor p53 and Rb (Wang et al., 2011), to directly interact with GSK3β (Skroblin, 2011) and to interact with GSKIP in the human liver by Y2H assay (Wang et al., 2014), however the exact interaction site between GSKIP and SMYD2 was never evaluated.
The results of this work have possible implications of GSKIP expression on p53-induced apoptosis. In addition, GSK3β interacts with p53, SMYD2 and GSKIP, which would grant GSKIP access to both SMYD2 and p53. Therefore, a confirmation of direct interaction between SMYD2 and GSKIP was performed. The results showed that GSKIP binds directly and specifically to a region of AA 376-391 (L-Y-S-L-N-V-A-S-M-W-L-K-L-G-R) of SMYD2. The consequences of complex formation between GSKIP and SMYD2 are speculative at this point and further research is necessary to determine the structural and functional aspects of this complexation. However, taken together with the induction of pro-apoptotic protein expression and EMT suppression upon GSKIP Kd in A549 cells, it is plausible that GSKIP is required for SMYD2-mediated suppression of p53 and its absence provides for GSK3β-mediated p53 activation.

4.4 GSKIP interacts with a novel PKA substrate GDF5OS

The prospect that GSKIP, mainly a cytosolic protein, directly binds to a predicted mitochondrial protein is intriguing, especially due to GSKIP's above mentioned roles in mitochondrial TCA cycle and OXPHOS regulation. In addition, the fact that GSK3β regulates p53-induced apoptosis in the mitochondria (Beurel and Jope, 2006; Chiara and Rasola, 2013) together with the potential roles of GSKIP, which regulates GSK3β's activity, in the

mitochondrial intrinsic apoptosis pathway (see section 4.2) may necessitate the involvement of additional interaction partners such as GDF5OS. However, since the function of GDF5OS is unknown and its mitochondrial localization has not been verified to date, this hypothesis requires further research. In addition, the possibility that GDF5OS is a PKA substrate may contribute to elucidation of cAMP/PKA signaling regulatory roles in the mitochondria. cAMP signaling in mitochondria and PKA phosphorylation of mitochondrial proteins is a fairly new field and gaining further insight may be therapeutically beneficial for treatment of cancer as well as neurodegenerative and metabolic disorders (Valsecchi et al., 2013).

4.5 GSKIP an oncoprotein?

The results of this work demonstrate GSKIP as a multifunctional protein involved in EMT, metabolic reprograming and possibly apoptosis regulation. The less-tumorigenic phenotype resulting from GSKIP Kd in A549 cells indicates that GSKIP is an oncoprotein. However, due to the transient Kd conditions employed, this conclusion is only speculative. GSKIP's role in GSK3β regulation as well as its ubiquitous expression in various tumor tissues and cells, increases the probability of GSKIP's context and cell type depended tumor-promoting and tumor-suppressing actions, similarly to GSK3β. The possible negative regulation of p53 that is strongly suggested in this work by the upregulation of protein expression of pro-apoptotic BAX in proteomics data as well as by GSKIP's direct interaction with GSK3β and SMYD2, strengthens GSKIP perspective role as an oncoprotein. The oncoprotein function is further supported by EMT reversal and reduced catabolic metabolism in the absence of GSKIP, which is known to sensitize cancer cells to anoikis. Moreover, the absence of GSKIP suggests possible negative affect on drug resistance ability of A549 cells as evidenced by FDXR upregulation in the proteomics data. Collectively these results indicate a tumor-promoting function of GSKIP and nominate GSKIP as a perspective target in cancer therapy.

5. Outlook

Mechanism of GSKIP's regulation in tumorigenesis

In order to answer the question of GSKIP's potential role as an oncoprotein, stable Kd has to be established in a tumor cell line model. This can be done by short hairpin RNA interference or the CRISP/CAS9 system. Stable Kd would allow prolonged observation time of cellular behavior, morphology and signaling. In addition, re-expression of GSKIP under stable Kd conditions may prove successful in rescuing the migratory and metabolic phenotype, thus contributing to mechanistic understanding of GSKIP's regulatory network.

In addition, the transition from mesenchymal to epithelial state of GSKIP Kd cells demonstrated in this work can be made more prominent, which will allow for more distinct differences in protein expression levels between the control and the KD cells. The induction of mesenchymal state can be achieved by stimulating A549 cells with recombinant TGFβ followed by isolation of mesenchymal cells from the epithelial ones by flow cytometry cell sorting, using mesenchymal and epithelial markers such as E-cadherin and N-cadherin. The mesenchymal, highly invasive cell population can then be transfected with control and GSKIP siRNAs, thus ensuring a more distinct anti-metastatic phenotype induction. This experimental setup will allow for a more distinct observation of GSKIP Kd's effect on the protein expression levels and contribute to elucidation of afflicted the regulatory pathways.

Additional experiments must be performed on the mesenchymal clones upon GSKIP Kd, including immunofluorescent microscopy assays with quantification of the actin cytoskeleton intensity and distribution as well as localization of migratory regulators and possible targets of GSKIP, such as CD44, ERM and E-cadherin. Moreover, evaluation of GSKIP's suggested impact on metastatic ability requires evaluation of not only migration ability but also invasion. Chemotaxis assays using Transwell inserts coated with matrigel will allow the evaluation of invasion capabilities of cancer cells. In addition to the already mentioned possible targets of GSKIP, many other developmental and metabolic proteins showed deregulation upon GSKIP Kd. Future work should confirm their regulation by GSKIP also in other cancer cell lines and attempt to elucidate the underlining regulatory mechanism. Moreover, the predicted interaction between GSKIP and microRNAs 19a and 19b, should be evaluated since the prospect of post-translational regulatory roles of GSKIP would explain the multitude of affected targets and tumorigenic signalling pathways and may be therapeutically relevant.

GSKIP's scaffolds

The evaluation of complex formation by immunoprecipitation is a valuable strategy in elucidation of GSKIP regulatory mechanism. Complex formation evaluation should be performed on GSKIP Kd cells with regards to PKA-SNAIL-GSK3β as well CD44-ERM, both of which regulate EMT. In addition, the possibility of complexation between GSKIP, GSK3β, SMYD2 and perhaps p53 and Rb proteins, is intriguing for therapeutic reasons and should be evaluated. In addition, the formation of GSKIP-GDF5OS and possibly the GSKIP-PKA-GDF5OS complexes, requires further investigation with regards to specific binding region, the sub-cellular localization and the physiological relevance of this complexation, which may elucidate the yet unknown function of GDF5OS.

Targeting GSKIP *in vivo*

The results of this research nominate GSKIP as a target in cancer therapy and future work should focus on targeting GSKIP in an animal cancer model. While, silencing GSKIP *in vitro* allows for elucidation of regulatory mechanism, the effects of GSKIP silencing on *in vivo* tumor growth holds therapeutic promise. However, transitioning from *in vitro* to an *in vivo* system poses numerous challenges, such as heterogeneity of tumors' inner and outer microenvironment leading to sub-classification of tumors from the same type of cancer. This phenotypic and functional diversity can result from patient-specific mutations in prominent oncogenes as well as individual environmental factors, which can affect not only the type and subclass of cancer but also the ability to develop chemo-resistance to specific treatments. Since, GSKIP is a potential multi-functional regulator of tumorigenesis in A549 lung cancer cells, targeting GSKIP in Non-small cell lung carcinoma tumors may prove to be effective. However, GSKIP's multi-functionality in EMT, metabolic reprograming and possibly survival, proliferation and drug resistance, suggests that targeting GSKIP *in vivo* should be sustained, for example using controlled delivery systems for siRNA delivery, in order to prevent toxic or tumor-promoting side-effects. Moreover, in order to predict the possible implications of GSKIP's targeting *in vivo*, its role in heterogeneous and extreme tumor micro-environment must be evaluated. This includes evaluation of GSKIP's functions under conditions of hypoxia and lactate-induced acidic environment, characteristic of highly proliferating tumors. In addition, cell type and intracellular compartment-specific effects of GSKIP silencing, must be taken into account for designing an effective and safe targeting formulation.

6. Summary

The onset of EMT is one of the hallmarks of tumorigenesis, which involves a complex cascade of multiple intracellular signaling pathways and extracellular cross talk, its activation in cancer cells signifies a first step in generation of usually fatal distant metastasis. Therefore, elucidating the regulatory elements of EMT signaling is of great therapeutic value.

GSK3β is a multifunctional kinase implicated in EMT regulation as well as other tumorigenic signaling pathways, such as Wnt signaling and glycogen metabolism. One of the regulatory proteins of GSK3β is PKA, a kinase activated by cAMP. Deregulation of cAMP/PKA signaling pathway is implicated in tumorigenic metabolic reprogramming and EMT. PKA can inhibit GSK3β by direct phosphorylation and this phosphorylation is facilitated by the AKAP GSKIP *via* direct binding to PKA and GSK3β. Since GSKIP is able to regulate GSK3β activity *via* PKA as well as PKA activity spatially and temporally, elucidating GSKIP's exact function in tumorigenesis is compelling.

The principle cell model for studying GSKIP's function in this work was A549 lung carcinoma cells. GSKIP Kd in A549 cells significantly inhibits cell migration without affecting cell viability. In addition, GSKIP Kd results in a significant increase in the protein expression levels of E-cadherin and a significant decrease in protein expression levels of its transcriptional repressors, ZEB1and SNAIL. A significant reduction in potent EMT inducers, such as TGFβ and GPI/AMF and actin cytoskeleton regulator CD44, was also observed upon GSKIP Kd. This modulation explains the reduced migration and indicates a role of GSKIP in EMT regulation.

In addition to its regulation of EMT, GPI/AMF regulates metabolism and together with GSK3β's and PKA's intricate roles in metabolic pathways, GSKIP's role in metabolism was evaluated. The results show that upon GSKIP Kd cells downregulate their dependence on mitochondrial energy production *via* OXPHOS. This downregulation was attributed to reduced TCA cycle flux due to reduced PDH activity. These results indicate that upon GSKIP Kd A549 cells switch from catabolic metabolism, characterizing invasive cells, to anabolic metabolism.

In summary, the current research demonstrates for the first time GSKIP's involvement in EMT and metabolism regulation in cancer cells, thus implicating GSKIP as a potential coupling agent between metabolic reprograming of cancer cells and EMT, and proposes GSKIP as a potential therapeutic target.

7. Zusammenfassung

Die Epitheliale Mesenchymale Transition (EMT) kennzeichnet die Tumorgenese und gilt als erster Schritt der Metastasenbildung. Die Transition der Krebszellen wird durch verschiedene intrazelluläre Signalwege gesteuert. Die Beschreibung elementarer regulatorischer Komponenten dieser Signalwege hat somit einen großen therapeutischen Wert.
GSK3ß ist eine multifunktionale Kinase, die neben EMT auch andere tumorinduzierende Signalwege reguliert; z.B. den Wnt-Signalweg und den Glycogenmetabolismus. GSK3β wird durch PKA, einer durch cAMP aktivierten Proteinkinase, phosphoryliert. Eine Dysregulation des cAMP/PKA Signalwegs führt während der Tumorgenese zu einer metabolischen Umprogrammierung und EMT. Die Phosphorylierung von GSK3β durch PKA wird durch die Assoziation des AKAPs GSKIP erleichtert, ein Gerüstprotein das sowohl PKA als auch GSK3β bindet. Neben der Phosphorylierung von GSK3β reguliert GSKIP auch die räumliche und zeitliche Organisation von PKA, was die Rolle von GSKIP in der Tumorgenese in den Fokus rückt / interessant macht.
Als zugrunde liegendes Zellmodell zur Analyse der GSKIP-Funktion wurde die Zelllinie A549, gewonnen aus einem Lungenkarzinom, verwendet. Es konnte gezeigt werden, dass ein GSKIP Kd / eine Reduktion der GSKIP-Expression die Zellmigration signifikant inhibiert ohne dabei die Zellviabilität zu beeinflussen. Darüberhinaus konnte gezeigt werden, dass der GSKIP Kd eine signifikant erhöhte Expressionsrate von E-cadherin und eine signifikant reduzierte Expressionsrate von ZEB1 und SNAIL, zwei Transkriptions-Repressoren, bewirkt. Die signifikante Reduktion von EMT induzierenden Faktoren wie TGFβ, GPI/AMF und der Regulator des Aktin-Cytoskeletts CD44 wurde ebenfalls durch die reduzierte GSKIP-Expression hervorgerufen und erklärt die reduzierte Migrationsrate. Dies weist eine mögliche relevante Rolle von GSKIP in der Regulation von EMT auf.
GPI/AMF reguliert neben EMT auch den Metabolismus und zusammen mit der Rolle von GSK3β und PKA in metabolischen Signalwegen wurde die Rolle von GSKIP experimentell untersucht. Es konnte gezeigt werden, dass die reduzierte GSKIP-Expression in der Zelle die mitochondriale Energieproduktion über OXPHOS reduziert. Dem liegt ein reduzierter Zitronensäurezyklus durch verminderte PDH Aktivität zugrunde. Es lässt sich folgern, dass eine reduzierte GSKIP-Expression in A549 Zellen zu einem Wechsel vom katabolischen Metabolismus zum anabolischen Metabolismus führt, ein Kennzeichen von invasiven Zellen.

Zusammengefasst lässt sich sagen, dass in dieser Arbeit zum ersten Mal die Rolle von GSKIP in EMT und in der Regulation des Metabolismus in Krebszellen beschrieben wurde. Nachfolgende Untersuchungen können sich auf die Signalwege fokussieren, die diese zwei Phänotypen mittels metabolischer Experimente und Proteomics-Analysen charakterisieren. Unser Ansatz kann Mechanismen der EMT und die Regulation der metabolischen Reprogrammierung in der Tumorgenese beschreiben und GSKIP als potentielles therapeutisches Zielprotein in Betracht ziehen.

8. Bibliography

Ahmad, A., and Aboukameel, A. (2011). Phosphoglucose Isomerase/Autocrine Motility Factor mediates epithelial-mesenchymal transition regulated by miR-200 in breast cancer cells. Cancer Res. *9*, 3400–3409.

Ahmad, A., Aboukameel, A., Kong, D., Wang, Z., Sethi, S., Chen, W., Sarkar, F.H., and Raz, A. (2011). Phosphoglucose Isomerase/Autocrine Motility Factor Mediates Epithelial-Mesenchymal Transition Regulated by miR-200 in Breast Cancer Cells. Cancer Res. *71*, 3400–3409.

Akakura, S., and Gelman, I.H. (2012). Pivotal Role of AKAP12 in the Regulation of Cellular Adhesion Dynamics: Control of Cytoskeletal Architecture, Cell Migration, and Mitogenic Signaling. J. Signal Transduct. *2012*, e529179.

Akakura, S., Nochajski, P., Gao, L., Sotomayor, P., Matsui, S., and Gelman, I.H. (2010). Rb-dependent cellular senescence, multinucleation and susceptibility to oncogenic transformation through PKC scaffolding by SSeCKS/AKAP12. Cell Cycle *9*, 4656–4665.

American Cancer Society (2015). Cancer Facts & Figures 2015.

Angell, J.E., Lindner, D.J., Shapiro, P.S., Hofmann, E.R., and Kalvakolanu, D.V. (2000). Identification of GRIM-19, a Novel Cell Death-regulatory Gene Induced by the Interferon- and Retinoic Acid Combination, Using a Genetic Approach. J. Biol. Chem. *275*, 33416–33426.

Azhar, M., Schultz, J.E.J., Grupp, I., Dorn, G.W., Meneton, P., Molin, D.G.M., Gittenberger-de Groot, A.C., and Doetschman, T. (2003). Transforming growth factor beta in cardiovascular development and function. Cytokine Growth Factor Rev. *14*, 391–407.

Bartel, D.P. (2004). MicroRNAs: genomics, biogenesis, mechanism, and function. Cell *116*, 281–297.

Bensaad, K., Tsuruta, A., Selak, Calvo Vidal, Nakano, Bartrons, Gottlieb, and Vousden (2006). TIGAR, a p53-Inducible Regulator of Glycolysis and Apoptosis. Cell 107–120.

Bergmann, M., Barnes, P.J., and Newton, R. (2000). Molecular Regulation of Granulocyte Macrophage Colony-Stimulating Factor in Human Lung Epithelial Cells by Interleukin (IL)-1 β, IL-4, and IL-13 Involves Both Transcriptional and Post-Transcriptional Mechanisms. Am. J. Respir. Cell Mol. Biol. *22*, 582–589.

Beurel, E. (2006). The paradoxical pro- and anti-apoptotic actions of GSK3 in the intrinsic and extrinsic apoptosis signaling pathways. Prog Neurobiol 173–189.

Beurel, E., and Jope, R.S. (2006). The paradoxical pro- and anti-apoptotic actions of GSK3 in the intrinsic and extrinsic apoptosis signaling pathways. Prog. Neurobiol. *79*, 173–189.

Bhat, R.V., and Budd, S.L. (2002). GSK3β Signalling: Casting a Wide Net in Alzheimer’s Disease. Neurosignals *11*, 251–261.

Blackhall, F.H., Merry, C.L., Davies, E.J., and Jayson, G.C. (2001). Heparan sulfate proteoglycans and cancer. Br. J. Cancer *85*, 1094.

Bossis, I., and Stratakis, C.A. (2004). Minireview: *PRKAR1A* : Normal and Abnormal Functions. Endocrinology *145*, 5452–5458.

Bradford, M.M. (1976). A Rapid and Sensitive Method for the Quantitation of Microgram Quantities of Protein Utilizing the Principle of Protein-Dye Binding. Anal. Biochem. 248–254.

Brand (2011). Assessing mitochondrial dysfunction in cells. Biochem J 297–312.

Bruystens, J.G.H., Wu, J., Fortezzo, A., Kornev, A.P., Blumenthal, D.K., and Taylor, S.S. (2014). PKA RIα Homodimer Structure Reveals an Intermolecular Interface with Implications for Cooperative cAMP Binding and Carney Complex Disease. Structure *22*, 59–69.

Caneba (2012). Pyruvate uptake is increased in highly invasive ovarian cancer cells under anoikis conditions for anaplerosis, mitochondrial function and migration. Am J Physiol Endocrinol Metab E1036–E1052.

Caneba, C.A., Bellance, N., Yang, L., Pabst, L., and Nagrath, D. (2012). Pyruvate uptake is increased in highly invasive ovarian cancer cells under anoikis conditions for anaplerosis, mitochondrial function, and migration. AJP Endocrinol. Metab. *303*, E1036–E1052.

Caretta, A., and Mucignat-Caretta, C. (2011). Protein Kinase A in Cancer. Cancers *3*, 913–926.

Caspi, M. (2008). Nuclear GSK-3 b inhibits the canonical Wnt signalling pathwayin a b - catenin phosphorylation-independent manner. Oncogene 3546–3555.

Cha, Y.H. (2015). Catabolic metabolism during cancer EMT. Arch. Pharm. Res. *38*, 313–320.

Chandra, D., and Singh, K.K. (2011). Genetic insights into OXPHOS defect and its role in cancer. Biochim. Biophys. Acta BBA - Bioenerg. *1807*, 620–625.

Chen, B., Li, H., Zeng, X., Yang, P., Liu, X., Zhao, X., and Liang, S. (2012). Roles of microRNA on cancer cell metabolism. J Transl Med *10*, 228.

Chiara, F., and Rasola, A. (2013). GSK-3 and mitochondria in cancer cells. Front. Oncol. *3*.

Cho, E.-A., Kim, E.-J., Kwak, S.-J., and Juhnn, Y.-S. (2014). cAMP signaling inhibits radiation-induced ATM phosphorylation leading to the augmentation of apoptosis in human lung cancer cells. Mol. Cancer *13*, 1–15.

Chou, C.-H., Lin, C.-C., Yang, M.-C., Wei, C.-C., Liao, H.-D., Lin, R.-C., Tu, W.-Y., Kao, T.-C., Hsu, C.-M., Cheng, J.-T., et al. (2012). GSK3beta-Mediated Drp1 Phosphorylation Induced Elongated Mitochondrial Morphology against Oxidative Stress. PLoS ONE *7*, e49112.

Chou, H.-Y., Howng, S.-L., Cheng, T.-S., Hsiao, Y.-L., Lieu, A.-S., Loh, J.-K., Hwang, S.-L., Lin, C.-C., Hsu, C.-M., Wang, C., et al. (2006). GSKIP Is Homologous to the Axin GSK3β Interaction Domain and Functions as a Negative Regulator of GSK3β †. Biochemistry (Mosc.) *45*, 11379–11389.

Chowdhury, S., Howell, G.M., Rajput, A., Teggart, C.A., Brattain, L.E., Weber, H.R., Chowdhury, A., and Brattain, M.G. (2011). Identification of a Novel TGFβ/PKA Signaling Transduceome in Mediating Control of Cell Survival and Metastasis in Colon Cancer. PLoS ONE *6*, e19335.

Cox, J., and Mann, M. (2008). MaxQuant enables high peptide identification rates, individualized p.p.b.-range mass accuracies and proteome-wide protein quantification. Nat. Biotechnol. *26*, 1367–1372.

Cross, D. (1995). Inhibition of glycogen synthase kinase-3 by insulin mediated by protein kinase B. Nature *378*, 785–789.

Das, R., Abu-Abed, M., and Melacini, G. (2006). Mapping allostery through equilibrium perturbation NMR spectroscopy. J. Am. Chem. Soc. *128*, 8406–8407.

Dave, N., Guaita-Esteruelas, S., Gutarra, S., Frias, A., Beltran, M., Peiro, S., and de Herreros, A.G. (2011). Functional Cooperation between Snail1 and Twist in the Regulation of ZEB1 Expression during Epithelial to Mesenchymal Transition. J. Biol. Chem. *286*, 12024–12032.

DeBerardinis, R.J., Mancuso, A., Daikhin, E., Nissim, I., Yudkoff, M., Wehrli, S., and Thompson, C.B. (2007). Beyond aerobic glycolysis: transformed cells can engage in glutamine metabolism that exceeds the requirement for protein and nucleotide synthesis. Proc. Natl. Acad. Sci. *104*, 19345–19350.

Deming, P.B., Campbell, S.L., Stone, J.B., Rivard, R.L., Mercier, A.L., and Howe, A.K. (2015). Anchoring of Protein Kinase A by ERM (Ezrin-Radixin-Moesin) Proteins Is Required for Proper Netrin Signaling through DCC (Deleted in Colorectal Cancer). J. Biol. Chem. *290*, 5783–5796.

De Resende, M.F., Vieira, S., Chinen, L.T., Chiappelli, F., da Fonseca, F.P., Guimarães, G.C., Soares, F.A., Neves, I., Pagotty, S., Pellionisz, P.A., et al. (2013). Prognostication of prostate cancer based on TOP2A protein and gene assessment: TOP2A in prostate cancer. J Transl Med *11*, 1–9.

Derynck, R., Muthusamy, B.P., and Saeteurn, K.Y. (2014). Signaling pathway cooperation in TGF-β-induced epithelial–mesenchymal transition. Curr. Opin. Cell Biol. *31*, 56–66.

Des Rosiers, C., Di Donato, L., Comte, B., Laplante, A., Marcoux, C., David, F., and Fernandez, C. (1995). Isotopomer analysis of citric acid cycle and gluconeogenesis in rat liver. J. Biol. Chem. *270*, 10027–10036.

Dingemans, A.-M.C., Witlox, M.A., Stallaert, R.A., van der Valk, P., Postmus, P.E., and Giaccone, G. (1999). Expression of DNA topoisomerase IIα and topoisomerase IIβ genes predicts survival and response to chemotherapy in patients with small cell lung cancer. Clin. Cancer Res. *5*, 2048–2058.

Diviani, D., and Scott, J.D. (2001). AKAP signaling complexes at the cytoskeleton. J. Cell Sci. *114*, 1431–1437.

Dong, H., Claffey, K.P., Brocke, S., and Epstein, P.M. (2015). Inhibition of breast cancer cell migration by activation of cAMP signaling. Breast Cancer Res. Treat. *152*, 17–28.

Elbashir, S.M., Lendeckel, W., and Tuschl, T. (2001). RNA interference is mediated by 21- and 22-nucleotide RNAs. Genes Dev. *15*, 188–200.

Eldar-Finkelman, H. Phosphorylation of insulin receptor substrate 1 by glycogen synthase kinase 3 impairs insulin action. Proc Natl Acad Sci USA *18*, 9660–9664.

Fang, X., Yu, S.X., Lu, Y., Bast, R.C., Woodgett, J.R., and Mills, G.B. (2000). Phosphorylation and inactivation of glycogen synthase kinase 3 by protein kinase A. Proc. Natl. Acad. Sci. *97*, 11960–11965.

Feng, X.-H., and Derynck, R. (2005). Specificity and versatility in TGF-β signaling through Smads. Annu Rev Cell Dev Biol *21*, 659–693.

Ferrari, S. (2006). Protein kinases controlling the onset of mitosis. Cell. Mol. Life Sci. *63*, 781–795.

Finger, E.C., Castellini, L., Rankin, E.B., Vilalta, M., Krieg, A.J., Jiang, D., Banh, A., Zundel, W., Powell, M.B., and Giaccia, A.J. (2015). Hypoxic induction of AKAP12 variant 2 shifts PKA-mediated protein phosphorylation to enhance migration and metastasis of melanoma cells. Proc. Natl. Acad. Sci. *112*, 4441–4446.

Fire, A. (1999). RNA-triggered gene silencing. Trends Genet. *15*, 358–363.

Floor, S.L., Dumont, J.E., Maenhaut, C., and Raspe, E. (2012). Hallmarks of cancer: of all cancer cells, all the time? Trends Mol. Med. *18*, 509–515.

Forbes, B., and Ehrhardt, C. (2005). Human respiratory epithelial cell culture for drug delivery applications. Eur. J. Pharm. Biopharm. *60*, 193–205.

Frank, R. (2002). The SPOT-synthesis technique: synthetic peptide arrays on membrane supports—principles and applications. J. Immunol. Methods *267*, 13–26.

Frank, B., Wiestler, M., Kropp, S., Hemminki, K., Spurdle, A.B., Sutter, C., Wappenschmidt, B., Chen, X., Beesley, J., Hopper, J.L., et al. (2008). Association of a Common AKAP9 Variant With Breast Cancer Risk: A Collaborative Analysis. JNCI J. Natl. Cancer Inst. *100*, 437–442.

Fujiki, Y., Yagita, Y., and Matsuzaki, T. (2012). Peroxisome biogenesis disorders: Molecular basis for impaired peroxisomal membrane assembly In metabolic functions and biogenesis of peroxisomes in health and disease. Biochim. Biophys. Acta BBA - Mol. Basis Dis. *2012*, 1337–1342.

Funasaka, T., and Raz, A. (2007). The role of autocrine motility factor in tumor and tumor microenvironment. Cancer Metastasis Rev. *26*, 725–735.

Funasaka, T., Hu, H., Yanagawa, T., Hogan, V., and Raz, A. (2007). Down-regulation of phosphoglucose isomerase/autocrine motility factor results in mesenchymal-to-epithelial transition of human lung fibrosarcoma cells. Cancer Res. *67*, 4236–4243.

Funasaka, T., Hogan, V., and Raz, A. (2009). Phosphoglucose Isomerase/Autocrine Motility Factor Mediates Epithelial and Mesenchymal Phenotype Conversions in Breast Cancer. Cancer Res. *69*, 5349–5356.

Gancedo, J.M. (2013). Biological roles of cAMP: variations on a theme in the different kingdoms of life: Biological roles of cAMP. Biol. Rev. *88*, 645–668.

Gao, Y. (2015). Knockdown of CD44 inhibits the invasion and metastasis of hepatocellular carcinoma both in vitro and in vivo by reversing epithelial-mesenchymal transition. Oncotarget *6*, 7828–7837.

Gao, F., Al-Azayzih, A., and Somanath, P. (2015). Discrete functions of GSK3α and GSK3β isoforms in prostate tumor growth and micrometastasis. Oncotarget *6*, 5947–5962.

Gelman, I.H. (2010). Emerging Roles for SSeCKS/Gravin/AKAP12 in the Control of Cell Proliferation, Cancer Malignancy, and Barriergenesis. Genes Cancer *1*, 1147–1156.

Gold, M.G., Lygren, B., Dokurno, P., Hoshi, N., McConnachie, G., Taskén, K., Carlson, C.R., Scott, J.D., and Barford, D. (2006). Molecular Basis of AKAP Specificity for PKA Regulatory Subunits. Mol. Cell *24*, 383–395.

Goode, N. (1992). Differential Regulation of Glycogen Synthase Kinase-3P by Protein Kinase C Isotypes*. J. Biol. Chem. *257*, 16878–16882.

Gooding, J.M., Yap, K.L., and Ikura, M. (2004). The cadherin-catenin complex as a focal point of cell adhesion and signalling: new insights from three-dimensional structures. BioEssays *26*, 497–511.

Hanahan, D., and Weinberg, R.A. (2000). The hallmarks of cancer. Cell *100*, 57–70.

Hanahan, D., and Weinberg, R.A. (2011). Hallmarks of Cancer: The Next Generation. Cell *144*, 646–674.

Hanoune, J., and Defer, N. (2001). Regulation and role of adenylyl cyclase isoforms. Annu. Rev. Pharmacol. Toxicol. *41*, 145–174.

He, T.-C., Sparks, A.B., and Rago, C. (1996). Heiko Hermeking, Leigh Zawel, Luis T. da Costa, Patrice J. Morin, Bert Vogelstein, Kenneth W. Kinzler. J Biol Chem *271*, 9009.

Hedrick, E.D., Agarwal, E., Leiphrakpam, P.D., Haferbier, K.L., Brattain, M.G., and Chowdhury, S. (2013). Differential PKA activation and AKAP association determines cell fate in cancer cells. J. Mol. Signal. *8*, 10.

Hiller, K., Hangebrauk, J., Jäger, C., Spura, J., Schreiber, K., and Schomburg, D. (2009). MetaboliteDetector: Comprehensive Analysis Tool for Targeted and Nontargeted GC/MS Based Metabolome Analysis. Anal. Chem. *81*, 3429–3439.

Hirono, Y., Fushida, S., Yonemura, Y., Yamamoto, H., Watanabe, H., and Raz, A. (1996). Expression of autocrine motility factor receptor correlates with disease progression in human gastric cancer. Br. J. Cancer *74*, 2003.

Hochbaum, D., Hong, K., Barila, G., Ribeiro-Neto, F., and Altschuler, D.L. (2008). Epac, in Synergy with cAMP-dependent Protein Kinase (PKA), Is Required for cAMP-mediated Mitogenesis. J. Biol. Chem. *283*, 4464–4468.

Hoeflich, K.P. (2000). Requirement for glycogen synthase kinase-3 b in cell survival and NF- k B activation. Lett. Nat. *406*, 86–90.

Holleran, A.L., Briscoe, D.A., Fiskum, G., and Kelleher, J.K. (1995). Glutamine metabolism in AS-30D hepatoma cells. Evidence for its conversion into lipids via reductive carboxylation. Mol. Cell. Biochem. *152*, 95–101.

Hundsrucker, C. (2010). Glycogen synthase kinase 3β Interaction Protein Functions as an A-kinase Anchoring Protein. J Biol Chem *8*, 5507–5521.

Jerby, L., Wolf, L., Denkert, C., Stein, G.Y., Hilvo, M., Oresic, M., Geiger, T., and Ruppin, E. (2012). Metabolic Associations of Reduced Proliferation and Oxidative Stress in Advanced Breast Cancer. Cancer Res. *72*, 5712–5720.

Jiang, L., Deberardinis, R., and Boothman, D.A. (2015). The cancer cell "energy grid": TGF-β1 signaling coordinates metabolism for migration. Mol. Cell. Oncol. *2*, e981994.

Jiang, P., Enomoto, A., and Takahashi, M. (2009). Cell biology of the movement of breast cancer cells: Intracellular signalling and the actin cytoskeleton. Cancer Lett. *284*, 122–130.

Jiang, W.G., Raz, A., Douglas-Jones, A., and Mansel, R.E. (2006). Expression of autocrine motility factor (AMF) and its receptor, AMFR, in human breast cancer. J. Histochem. Cytochem. *54*, 231–241.

Jiang, Y., Trescott, L., Holcomb, J., Zhang, X., Brunzelle, J., Sirinupong, N., Shi, X., and Yang, Z. (2014). Structural Insights into Estrogen Receptor α Methylation by Histone Methyltransferase SMYD2, a Cellular Event Implicated in Estrogen Signaling Regulation. J. Mol. Biol. *426*, 3413–3425.

Jope, R.S. (2007). Glycogen Synthase Kinase-3 (GSK3): Inflammation, Diseases, and Therapeutics. Neurochem Res . *4-5*, 577–595.

Justus, C.R., Leffler, N., Ruiz-Echevarria, M., and Yang, L.V. (2014). In vitro Cell Migration and Invasion Assays. J. Vis. Exp.

Kim, C., Cheng, C.Y., Saldanha, S.A., and Taylor, S.S. (2007). PKA-I Holoenzyme Structure Reveals a Mechanism for cAMP-Dependent Activation. Cell *130*, 1032–1043.

Kim, I.G., Kim, S.Y., Choi, S.I., Lee, J.H., Kim, K.C., and Cho, E.W. (2014). Fibulin-3-mediated inhibition of epithelial-to-mesenchymal transition and self-renewal of ALDH+ lung cancer stem cells through IGF1R signaling. Oncogene *33*, 3908–3917.

Koppenol, W.H., Bounds, P.L., and Dang, C.V. (2011). Otto Warburg's contributions to current concepts of cancer metabolism. Nat Rev Cancer *11*, 325–337.

Krützfeldt, J., and Stoffel, M. (2006). MicroRNAs: A new class of regulatory genes affecting metabolism. Cell Metab. *4*, 9–12.

Kulikov, R. (2005). Glycogen synthase kinase 3-dependent phosphorylation of Mdm2 regulates p53 abundance. Mol Cell Biol *16*, 7170–7180.

Lamouille, S., Xu, J., and Derynck, R. (2014). Molecular mechanisms of epithelial–mesenchymal transition. Nat. Rev. Mol. Cell Biol. *15*, 178–196.

Langeberg, L.K., and Scott, J.D. (2015). Signalling scaffolds and local organization of cellular behaviour. Nat. Rev. Mol. Cell Biol. *16*, 232–244.

LeBleu, V.S., O'Connell, J.T., Gonzalez Herrera, K.N., Wikman, H., Pantel, K., Haigis, M.C., de Carvalho, F.M., Damascena, A., Domingos Chinen, L.T., Rocha, R.M., et al. (2014). PGC-1α mediates mitochondrial biogenesis and oxidative phosphorylation in cancer cells to promote metastasis. Nat. Cell Biol. *16*, 992–1003.

Lefkimmiatis, K., and Zaccolo, M. (2014). cAMP signaling in subcellular compartments. Pharmacol. Ther. *143*, 295–304.

Legg, J.W., Lewis, C.A., Parsons, M., Ng, T., and Isacke, C.M. (2002). A novel PKC-regulated mechanism controls CD44–ezrin association and directional cell motility. Nat. Cell Biol. *4*, 399–407.

Li, J., Yang, S., Yan, W., Yang, J., Qin, Y.-J., Lin, X.-L., Xie, R.-Y., Wang, S.-C., Jin, W., Gao, F., et al. (2015). MicroRNA-19 triggers epithelial-mesenchymal transition of lung cancer cells accompanied by growth inhibition. Lab Invest *95*, 1056–1070.

Lin, C.-C., Chou, C.-H., Howng, S.-L., Hsu, C.-Y., Hwang, C.-C., Wang, C., Hsu, C.-M., and Hong, Y.-R. (2009). GSKIP, an inhibitor of GSK3Î², mediates the N-cadherin/Î²-catenin pool in the differentiation of SH-SY5Y cells. J. Cell. Biochem. *108*, 1325–1336.

Linseman, D.A. (2004). Glycogen Synthase Kinase-3 Phosphorylates Bax and Promotes Its Mitochondrial Localization during Neuronal Apoptosis. J. Neurosci. *24*, 9993–10002.

Liu, G., and Chen, X. (2002). The ferredoxin reductase gene is regulated by the p53 family and sensitizes cells to oxidative stress-induced apoptosis. Oncogene 7195–7204.

Liu, Y., Hu, H., Wang, K., Zhang, C., Wang, Y., Yao, K., Yang, P., Han, L., Kang, C., Zhang, W., et al. (2014). Multidimensional analysis of gene expression reveals TGFB1I1-induced EMT contributes to malignant progression of astrocytomas. Oncotarget *5*, 12593.

Liu, Z., Liu, D., Bojdani, E., El-Naggar, A.K., Vasko, V., and Xing, M. (2010). IQGAP1 Plays an Important Role in the Invasiveness of Thyroid Cancer. Clin. Cancer Res. *16*, 6009–6018.

Löffler, I., Grün, M., Böhmer, F.D., and Rubio, I. (2008). Role of cAMP in the promotion of colorectal cancer cell growth by Prostaglandin E2. BMC Cancer *8*, 380.

Logue, J.S., Whiting, J.L., Tunquist, B., Sacks, D.B., Langeberg, L.K., Wordeman, L., and Scott, J.D. (2011). AKAP220 Protein Organizes Signaling Elements That Impact Cell Migration. J. Biol. Chem. *286*, 39269–39281.

Lu, K., Liu, C., Tao, T., Zhang, X., Zhang, L., Sun, C., Wang, Y., Chen, S., Xu, B., and Chen, M. (2015). MicroRNA-19a regulates proliferation and apoptosis of castration-resistant prostate cancer cells by targeting BTG1. FEBS Lett. *589*, 1485–1490.

Maccario, H. (2007). PTEN is destabilized by phosphorylation on Thr366. Biochem J *3*, 439–444.

MacPherson, M.R., Molina, P., Souchelnytskyi, S., Wernstedt, C., Martin-Pérez, J., Portillo, F., and Cano, A. (2010). Phosphorylation of serine 11 and serine 92 as new positive regulators of human Snail1 function: potential involvement of casein kinase-2 and the cAMP-activated kinase protein kinase A. Mol. Biol. Cell *21*, 244–253.

Martinez, J., Patkaniowska, A., Urlaub, H., Lührmann, R., and Tuschl, T. (2002). Single-stranded antisense siRNAs guide target RNA cleavage in RNAi. Cell *110*, 563–574.

McCubrey, J.A., Steelman, L.S., Bertrand, F.E., Davis, N.M., Sokolosky, M., Abrams, S.L., Montalto, G., D'Assoro, A.B., Libra, M., Nicoletti, F., et al. (2014). GSK-3 as potential target for therapeutic intervention in cancer. Oncotarget *5*, 2881.

McKenzie, A.J., Campbell, S.L., and Howe, A.K. (2011). Protein Kinase A Activity and Anchoring Are Required for Ovarian Cancer Cell Migration and Invasion. PLoS ONE *6*, e26552.

Medina, M., Garrido, J.J., and Wandosell, F.G. (2011). Modulation of GSK-3 as a Therapeutic Strategy on Tau Pathologies. Front. Mol. Neurosci. *4*.

Mehlen, P., and Furne, C. (2005). Netrin-1: when a neuronal guidance cue turns out to be a regulator of tumorigenesis. Cell. Mol. Life Sci. *62*, 2599–2616.

Mercado-Pimentel, M.E., and Runyan, R.B. (2007). Multiple Transforming Growth Factor-β Isoforms and Receptors Function during Epithelial-Mesenchymal Cell Transformation in the Embryonic Heart. Cells Tissues Organs *185*, 146–156.

Montminy, M. (1997). Transcriptional regulation by cyclic AMP. Annu. Rev. Biochem. *66*, 807–822.

Moustakas, A. (2005). Non-Smad TGF- signals. J. Cell Sci. *118*, 3573–3584.

Mu, Y., Gudey, S.K., and Landström, M. (2012). Non-Smad signaling pathways. Cell Tissue Res. *347*, 11–20.

Mukai, F., Ishiguro, K., Sano, Y., and Fujita, S.C. (2002). Alternative splicing isoform of tau protein kinase I/glycogen synthase kinase 3β. J. Neurochem. *81*, 1073–1083.

Nauert, Rigas, and Lester (2003). Identification of an IQGAP1/AKAP79 complex in beta-cells. J Cell Biochem *1*, 97–108.

Naviglio, S., Caraglia, M., Abbruzzese, A., Chiosi, E., Di Gesto, D., Marra, M., Romano, M., Sorrentino, A., Sorvillo, L., Spina, A., et al. (2009). Protein kinase A as a biological target in cancer therapy. Expert Opin. Ther. Targets *13*, 83–92.

Naviglio, S., Di Gesto, D., Illiano, F., Chiosi, E., Giordano, A., Illiano, G., and Spina, A. (2010). Leptin potentiates antiproliferative action of cAMP elevation via protein kinase A down-regulation in breast cancer cells. J. Cell. Physiol. *225*, 801–809.

Nawshad, A., LaGamba, D., and Hay, E.. (2004). Transforming growth factor β (TGFβ) signalling in palatal growth, apoptosis and epithelial mesenchymal transformation (EMT). Arch. Oral Biol. *49*, 675–689.

Neary, C.L., Nesterova, M., Cho, Y.S., Cheadle, C., Becker, K.G., and Cho-Chung, Y.S. (2004). Protein kinase A isozyme switching: eliciting differential cAMP signaling and tumor reversion. Oncogene *23*, 8847–8856.

Niinaka (2010). Silencing of Autocrine Motility Factor Induces Mesenchymal to-Epithelial Transition and Suppression of Osteosarcoma Pulmonary Metastasis. Cancer Res. *22*, 9483–9493.

Niinaka, Y., Harada, K., Fujimuro, M., Oda, M., Haga, A., Hosoki, M., Uzawa, N., Arai, N., Yamaguchi, S., Yamashiro, M., et al. (2010). Silencing of Autocrine Motility Factor Induces Mesenchymal-to-Epithelial Transition and Suppression of Osteosarcoma Pulmonary Metastasis. Cancer Res. *70*, 9483–9493.

Nikoulina, S. (2000). Potential role of glycogen synthase kinase-3 in skeletal muscle insulin resistance of type 2 diabetes. Diabetes *2*, 263–271.

O'Brien, J., Wilson, I., Orton, T., and Pognan, F. (2000). Investigation of the Alamar Blue (resazurin) fluorescent dye for the assessment of mammalian cell cytotoxicity. Eur. J. Biochem. *267*, 5421–5426.

Omori, K., and Kotera, J. (2007). Overview of PDEs and Their Regulation. Circ. Res. *100*, 309–327.

Ong, S.-E., Blagoev, B., Kratchmarova, I., Kristensen, D.B., Steen, H., Pandey, A., and Mann, M. (2002). Stable isotope labeling by amino acids in cell culture, SILAC, as a simple and accurate approach to expression proteomics. Mol. Cell. Proteomics *1*, 376–386.

Orian-Rousseau, V. (2010). CD44, a therapeutic target for metastasising tumours. Eur. J. Cancer *46*, 1271–1277.

Paoli, P., Giannoni, E., and Chiarugi, P. (2013). Anoikis molecular pathways and its role in cancer progression. Biochim. Biophys. Acta BBA - Mol. Cell Res. *1833*, 3481–3498.

Peinado, H. (2007). Snail, Zeb and bHLH factors in tumour progression: an alliance against the epithelial phenotype? Nat. Rev. 415–428.

Pignatelli, J., Tumbarello, D.A., Schmidt, R.P., and Turner, C.E. (2012). Hic-5 promotes invadopodia formation and invasion during TGF- -induced epithelial-mesenchymal transition. J. Cell Biol. *197*, 421–437.

Polakis, P. (2007). The many ways of Wnt in cancer. Curr. Opin. Genet. Dev. 45–51.

Ralston, S.H. (2006). Genetic regulation of bone mass and susceptibility to osteoporosis. Genes Dev. *20*, 2492–2506.

Ramelot, T.A., Cort, J.R., and Xiao, R. (Unpublished work). NMR Structure of the human C14orf129 gene product, HSPC210. Northeast Structural Genomics target HR969. PDB 1SGO.

Rayasam, G.V., Tulasi, V.K., Sodhi, R., Davis, J.A., and Ray, A. (2009). Glycogen synthase kinase 3: more than a namesake. Br. J. Pharmacol. *156*, 885–898.

Reya, T., and Clevers, H. (2005). Wnt signalling in stem cells and cancer. Nature *434*, 843–850.

Ridley, A.J. (2011). Life at the Leading Edge. Cell *145*, 1012–1022.

Sahlgren, C., Gustafsson, M.V., Jin, S., Poellinger, L., and Lendahl, U. (2008). Notch signaling mediates hypoxia-induced tumor cell migration and invasion. Proc. Natl. Acad. Sci. *105*, 6392–6397.

Sapio, L., Di Maiolo, F., Illiano, M., Esposito, A., Chiosi, E., Spina, A., and Naviglio, S. (2014). Targeting protein kinase A in cancer therapy: An update.

Schächterle, C., Christian, F., Fernandes, J.M.P., and Klussmann, E. (2015). Screening for Small Molecule Disruptors of AKAP–PKA Interactions. In cAMP Signaling, M. Zaccolo, ed. (New York, NY: Springer New York), pp. 151–166.

Schlessinger, K., and Hall, A. (2004). GSK-3β sets Snail's pace. Nat. Cell Biol. *6*, 913–915.

Sellers, K., Fox, M.P., Bousamra, M., Slone, S.P., Higashi, R.M., Miller, D.M., Wang, Y., Yan, J., Yuneva, M.O., Deshpande, R., et al. (2015). Pyruvate carboxylase is critical for non–small-cell lung cancer proliferation. J. Clin. Invest. *125*, 687–698.

Shaikh, D., Zhou, Q., Chen, T., Ibe, J.C.F., Raj, J.U., and Zhou, G. (2012). cAMP-dependent protein kinase is essential for hypoxia-mediated epithelial–mesenchymal transition, migration, and invasion in lung cancer cells. Cell. Signal. *24*, 2396–2406.

Skalhegg, B.S., and Tasken, K. (2000). Specificity in the cAMP/PKA signaling pathway. Differential expression, regulation, and subcellular localization of subunits of PKA. Front Biosci *5*, D678–D693.

Skroblin, P. (2011). Glycogen synthase kinase 3β interaction protein is a novel A-kinase anchoring protein that integrates PKA and GSK3β signalling. Freie Universität Berlin, Germany.

Skroblin, P., Grossmann, S., Schäfer, G., Rosenthal, W., and Klussmann, E. (2010). Mechanisms of Protein Kinase A Anchoring. In International Review of Cell and Molecular Biology, (Elsevier), pp. 235–330.

Smith, F.D., Langeberg, L.K., Cellurale, C., Pawson, T., Morrison, D.K., Davis, R.J., and Scott, J.D. (2010). AKAP-Lbc enhances cyclic AMP control of the ERK1/2 cascade. Nat. Cell Biol. *12*, 1242–1249.

Spina, A., Di Maiolo, F., Esposito, A., Sapio, L., Chiosi, E., Sorvillo, L., and Naviglio, S. (2012). cAMP Elevation Down-Regulates *β* 3 Integrin and Focal Adhesion Kinase and Inhibits Leptin-Induced Migration of MDA-MB-231 Breast Cancer Cells. BioResearch Open Access *1*, 324–332.

Su, B., Gao, L., Meng, F., Guo, L.-W., Rothschild, J., and Gelman, I.H. (2013). Adhesion-mediated cytoskeletal remodeling is controlled by the direct scaffolding of Src from FAK complexes to lipid rafts by SSeCKS/AKAP12. Oncogene *32*, 2016–2026.

Sun, Y.-J. (1999). The Crystal Structure of a Multifunctional Protein: Phosphoglucose Isomerase/Autocrine Motility Factor/Neuroleukin. Proc. Natl. Acad. Sci. *10*, 5412–5417.

Sun, Y., Daemen, A., Hatzivassiliou, G., Arnott, D., Wilson, C., Zhuang, G., Gao, M., Liu, P., Boudreau, A., Johnson, L., et al. (2014). Metabolic and transcriptional profiling reveals pyruvate dehydrogenase kinase 4 as a mediator of epithelial-mesenchymal transition and drug resistance in tumor cells. Cancer Metab. *2*, 20.

Tanji, C. (2002). A-Kinase Anchoring Protein AKAP220 Binds to Glycogen Synthase Kinase-3beta (GSK-3beta) and Mediates Protein Kinase A-dependent Inhibition of GSK-3beta. J. Biol. Chem. *277*, 36955–36961.

Taylor, S.S., Zhang, P., Steichen, J.M., Keshwani, M.M., and Kornev, A.P. (2013). PKA: Lessons learned after twenty years. Biochim. Biophys. Acta BBA - Proteins Proteomics *1834*, 1271–1278.

Thiery, J.P. (2002). Epithelial–mesenchymal transitions in tumour progression. Nat. Rev. Cancer *2*, 442–454.

Tomasetti, C., and Vogelstein, B. (2015). Variation in cancer risk among tissues can be explained by the number of stem cell divisions. Science *347*, 78–81.

Troeger, J. (2012). A-kinase anchoring proteins as potential drug targets. Br. J. Pharmacol. 420–433.

Tröger, J., Moutty, M.C., Skroblin, P., and Klussmann, E. (2012). A-kinase anchoring proteins as potential drug targets: AKAPs as novel drug targets. Br. J. Pharmacol. *166*, 420–433.

Tsutsumi, S., Yanagawa, T., Shimura, T., Kuwano, H., and Raz, A. (2004). Autocrine motility factor signaling enhances pancreatic cancer metastasis. Clin. Cancer Res. *10*, 7775–7784.

Tumbarello, D.A., and Turner, C.E. (2007). Hic-5 contributes to epithelial-mesenchymal transformation through a RhoA/ROCK-dependent pathway. J. Cell. Physiol. *211*, 736–747.

Uhlén, M., Fagerberg, L., Hallström, B.M., Lindskog, C., Oksvold, P., Mardinoglu, A., Sivertsson, Å., Kampf, C., Sjöstedt, E., Asplund, A., et al. (2015). Tissue-based map of the human proteome. Science *347*, 1260419.

Valsecchi, F., Ramos-Espiritu, L.S., Buck, J., Levin, L.R., and Manfredi, G. (2013). cAMP and Mitochondria. Physiology *28*, 199–209.

Walsh, D. (1994). Multiple pathway signal transduction by the cAMP-dependent protein kinase. Faseb J *15*, 1227–1236.

Wang, F., Li, T., Zhang, B., Li, H., Wu, Q., Yang, L., Nie, Y., Wu, K., Shi, Y., and Fan, D. (2013). MicroRNA-19a/b regulates multidrug resistance in human gastric cancer cells by targeting PTEN. Biochem. Biophys. Res. Commun. *434*, 688–694.

Wang, H., Song, K., Krebs, T.L., Yang, J., and Danielpour, D. (2008). Smad7 is inactivated through a direct physical interaction with the LIM protein Hic-5/ARA55. Oncogene *27*, 6791–6805.

Wang, J., Huo, K., Ma, L., Tang, L., Li, D., Huang, X., Yuan, Y., Li, C., Wang, W., Guan, W., et al. (2014). Toward an understanding of the protein interaction network of the human liver. Mol. Syst. Biol. *7*, 536–536.

Wang, L., Li, L., Zhang, H., Luo, X., Dai, J., Zhou, S., Gu, J., Zhu, J., Atadja, P., Lu, C., et al. (2011). Structure of Human SMYD2 Protein Reveals the Basis of p53 Tumor Suppressor Methylation. J. Biol. Chem. *286*, 38725–38737.

Wang, S.-P., Wang, W.-L., Chang, Y.-L., Wu, C.-T., Chao, Y.-C., Kao, S.-H., Yuan, A., Lin, C.-W., Yang, S.-C., Chan, W.-K., et al. (2009). p53 controls cancer cell invasion by inducing the MDM2-mediated degradation of Slug. Nat. Cell Biol. *11*, 694–704.

Ward, P.S., and Thompson, C.B. (2012). Metabolic Reprogramming: A Cancer Hallmark Even Warburg Did Not Anticipate. Cancer Cell *21*, 297–308.

Watson, P.H., Chia, S.K., Wykoff, C.C., Han, C., Leek, R.D., Sly, W.S., Gatter, K.C., Ratcliffe, P., and Harris, A.L. (2003). Carbonic anhydrase XII is a marker of good prognosis in invasive breast carcinoma. Br. J. Cancer *88*, 1065–1070.

White, C.D., Brown, M.D., and Sacks, D.B. (2009). IQGAPs in cancer: A family of scaffold proteins underlying tumorigenesis. FEBS Lett. *583*, 1817–1824.

Wirtenberger, M., Tchatchou, S., Hemminki, K., Klaes, R., Schmutzler, R.K., Bermejo, J.L., Chen, B., Wappenschmidt, B., Meindl, A., Bartram, C.R., et al. (2006). Association of genetic variants in the Rho guanine nucleotide exchange factor AKAP13 with familial breast cancer. Carcinogenesis *27*, 593–598.

Wong, W., and Scott, J.D. (2004). AKAP signalling complexes: focal points in space and time. Nat. Rev. Mol. Cell Biol. *5*, 959–970.

Wong, N., Yeo, W., Wong, W.-L., Wong, N.L.-Y., Chan, K.Y.-Y., Mo, F.K.-F., Koh, J., Chan, S.L., Chan, A.T.-C., Lai, P.B.-S., et al. (2009). TOP2A overexpression in hepatocellular carcinoma correlates with early age onset, shorter patients survival and chemoresistance. Int. J. Cancer *124*, 644–652.

Woodgett, J.R. (1990). Molecular cloning and expression of glycogen synthase kinase-3/factor A. EMBO J. *9*, 2431.

Wu, J., Brown, S.H.J., von Daake, S., and Taylor, S.S. (2007). PKA Type II Holoenzyme Reveals a Combinatorial Strategy for Isoform Diversity. Science *318*, 274–279.

Wu, M., Neilson, A., Swift, A.L., Moran, R., Tamagnine, J., Parslow, D., Armistead, S., Lemire, K., Orrell, J., Teich, J., et al. (2006). Multiparameter metabolic analysis reveals a close link between attenuated mitochondrial bioenergetic function and enhanced glycolysis dependency in human tumor cells. AJP Cell Physiol. *292*, C125–C136.

Wu, Y., Deng, J., Rychahou, P.G., Qiu, S., Evers, B.M., and Zhou, B.P. (2009). Stabilization of Snail by NF-κB Is Required for Inflammation-Induced Cell Migration and Invasion. Cancer Cell *15*, 416–428.

Xie, Y., Yan, J., Cutz, J.-C., Rybak, A.P., He, L., Wei, F., Kapoor, A., Schmidt, V.A., Tao, L., and Tang, D. (2012). IQGAP2, A candidate tumour suppressor of prostate tumorigenesis. Biochim. Biophys. Acta BBA - Mol. Basis Dis. *1822*, 875–884.

Xu, J., Lamouille, S., and Derynck, R. (2009a). TGF-β-induced epithelial to mesenchymal transition. Cell Res. *19*, 156–172.

Xu, J., Lamouille, S., and Derynck, R. (2009b). TGF-β-induced epithelial to mesenchymal transition. Cell Res. *19*, 156–172.

Yang, Y. (2006). Regulation of Transforming Growth Factor- 1-Induced Apoptosis and Epithelial-to-Mesenchymal Transition by Protein Kinase A and Signal Transducers and Activators of Transcription 3. Cancer Res. *66*, 8617–8624.

Yang, H., Li, G., Wu, J.-J., Wang, L., Uhler, M., and Simeone, D.M. (2013). Protein Kinase A Modulates Transforming Growth Factor- Signaling through a Direct Interaction with Smad4 Protein. J. Biol. Chem. *288*, 8737–8749.

Yoneda, A., Lendorf, M.E., Couchman, J.R., and Multhaupt, H.A. (2012). Breast and Ovarian Cancers A Survey and Possible Roles for the Cell Surface Heparan Sulfate Proteoglycans. J. Histochem. Cytochem. *60*, 9–21.

Yoo, H., Antoniewicz, M.R., Stephanopoulos, G., and Kelleher, J.K. (2008). Quantifying Reductive Carboxylation Flux of Glutamine to Lipid in a Brown Adipocyte Cell Line. J. Biol. Chem. *283*, 20621–20627.

Yook, J.I., Li, X.-Y., Ota, I., Hu, C., Kim, H.S., Kim, N.H., Cha, S.Y., Ryu, J.K., Choi, Y.J., Kim, J., et al. (2006). A Wnt–Axin2–GSK3β cascade regulates Snail1 activity in breast cancer cells. Nat. Cell Biol. *8*, 1398–1406.

Yoon, Y.-K., Kim, H.-P., Han, S.-W., Oh, D.Y., Im, S.-A., Bang, Y.-J., and Kim, T.-Y. (2010). *KRAS* mutant lung cancer cells are differentially responsive to MEK inhibitor due to AKT or STAT3 activation: Implication for combinatorial approach. Mol. Carcinog. *49*, 353–362.

Yu, Q., and Stamenkovic, I. (1999). Localization of matrix metalloproteinase 9 to the cell surface provides a mechanism for CD44-mediated tumor invasion. Genes Dev. *13*, 35–48.

Zhang, L., Duan, C.J., Binkley, C., Li, G., Uhler, M.D., Logsdon, C.D., and Simeone, D.M. (2004). A Transforming Growth Factor -Induced Smad3/Smad4 Complex Directly Activates Protein Kinase A. Mol. Cell. Biol. *24*, 2169–2180.

Zhang, Y., Baysac, K.C., Yee, L.-F., Saporita, A.J., and Weber, J.D. (2014). Elevated DDX21 regulates c-Jun activity and rRNA processing in human breast cancers. Breast Cancer Res. *16*, 449.

Zhou, B.P., Deng, J., Xia, W., Xu, J., Li, Y.M., Gunduz, M., and Hung, M.-C. (2004a). Dual regulation of Snail by GSK-3β-mediated phosphorylation in control of epithelial–mesenchymal transition. Nat. Cell Biol. *6*, 931–940.

Zhou, B.P., Deng, J., Xia, W., Xu, J., Li, Y.M., Gunduz, M., and Hung, M.-C. (2004b). Dual regulation of Snail by GSK-3β-mediated phosphorylation in control of epithelial–mesenchymal transition. Nat. Cell Biol. *6*, 931–940.

9. Publications

Articles

- Alessandro Dema, **Ekaterina Perets**, Maike Svenja Schulz, Veronika Anita Deàk and Enno Klussmann „ Pharmacological targeting of AKAP-directed compartmentalized cAMP signalling", Cellular signaling, 2015.

- Micha Friedemann Schröter, Alessandro Dema, **Ekaterina Perets**, Philipp Skroblin, Marie Christine Moutty, Veronika Deak, Walter Birchmeier, and Enno Klussmann, „GSKIP and AKAP220 are AKAPs that regulate Wnt signaling by compartmentalizing distinct pools of GSK3β" (in revision) 2015.

- B.H. Laster, C. Isaacson, **E. Perets**, M. Msamra, E. Priel, J. Kalef-Ezra, J. Kost, "Keeping those telomers short! An innovative intratumoral long-term drug delivery system," Journal of Cancer Research and Clinical oncology (2014).

Poster presentations

- **E. Perets**, W. Rosenthal, E. Klussmann, "A potential role of the anchoring protein GSKIP in tumorigenesis", CMD & Transcard retreat, Neuruppin, Germany, November 26-28, 2014
- **Ekaterina Perets**, Walter Rosenthal and Enno Klussmann, "A potential role of the anchoring protein GSKIP in tumorigenesis", 15th MDC/ FMP PhD Retreat, Kremmen, Germany, August 29-31, 2013.
- **E. Perets**, W. Rosenthal, E. Klussmann, "A potential role of the anchoring protein GSKIP in tumorigenesis", Cancer Biology BRIC 10-year anniversary symposium, Copenhagen, Denmark, August 22-23, 2013.

10. Supplementary Data

10.1 Supplementary figures

10.1.1 Electrophoretic shift assay

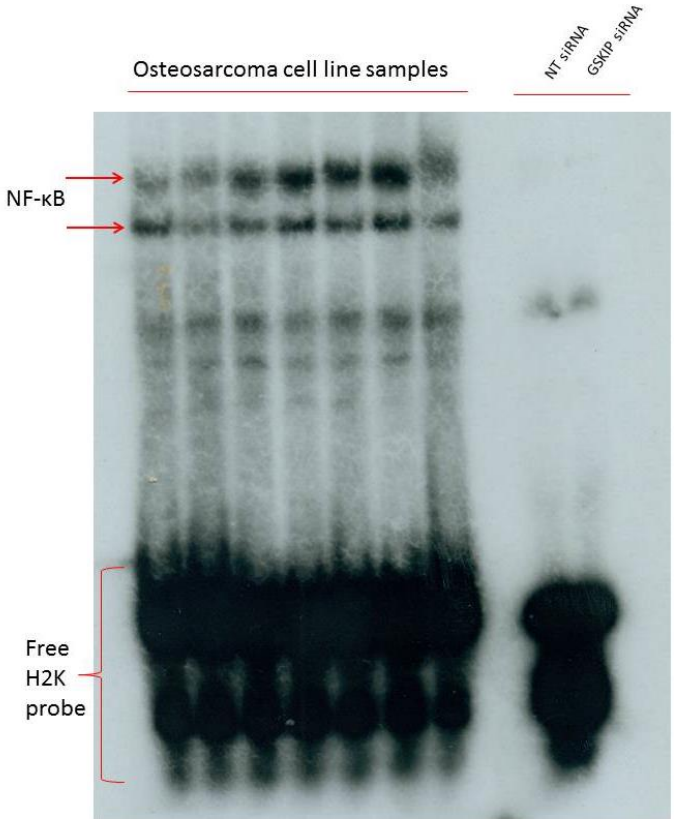

Supplementary figure 1: A549 cells show no detectable NFkB DNA binding activity. A549 cells were transfected with GSKIP siRNA or with NT siRNA (control) and lysed after 48 hours. The gel electrophoresis mobility shift assay (EMSA) assay was performed on A549 samples (left) and osteosarcoma cell line samples by using ^{32}P-labeled dsDNA probe containing NF-κB binding sites derived from the MHC class I H2K gene (5′CAGGCTGGGGATTCCCATCTCCACAGTTTCACTTC-3′). Protein lysates and nucleic acid were mixed subjected to electrophoresis under native conditions through agarose gel. After electrophoresis, the distribution of species containing nucleic acid was determined by autoradiography of ^{32}P-labeled nucleic acid. Protein-DNA complexes migrate more slowly (top) than the corresponding free DNA of the H2K probe (bottom). The osteosarcoma cell lines show a clear binding of NF-kB subunits to DNA (top left) while the A549 samples show no detectable DNA binding (n=1).

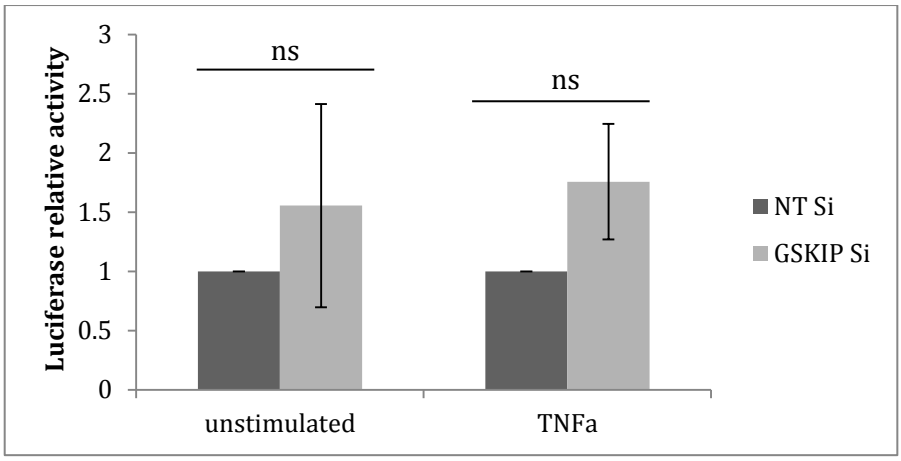

Supplementary figure 2: GSKIP does not affect NF-κB luciferase activity. A549 cells were transfected with GSKIP siRNA or with siGENOME Non-Targeting siRNA #3 (GE Healthcare, Chalfont St Giles, UK) (control) and 24 hrs later transfected with the NF-kB–dependent reporter, 6NF-kBtkluc.neo (Bergmann et al., 2000) driving the luciferase gene, together with pRL-SV40 vector encoding renilla luciferase which was used as an internal standard. 24 hrs later cells were either stimulated with TNFa (kindly provided by AG Scjeiderheit) or left unstimulated. The cells were lysed 6 h later and luciferase activity was measured using the Dual Luciferase Assay Kit (Promega, Fitchburg, USA) and a Centro XS3 LB 960 luminometer (Berthold technologies, Bad Wildbad, Germany). Activity of the 6NF-kBtkluc.neo vectors was normalized to activity of the pRL-SV40 (Luciferase relative activity). Luciferase relative activity was set to 1 for the NT control and GSKIP Kd activity was normalized to NT control (n=3, means ± SEM). Significant differences vs. NT control were evaluated using Student's t-test (*= P <0.05 **= P <0.01 ***= P<0.001 ns=not significant)

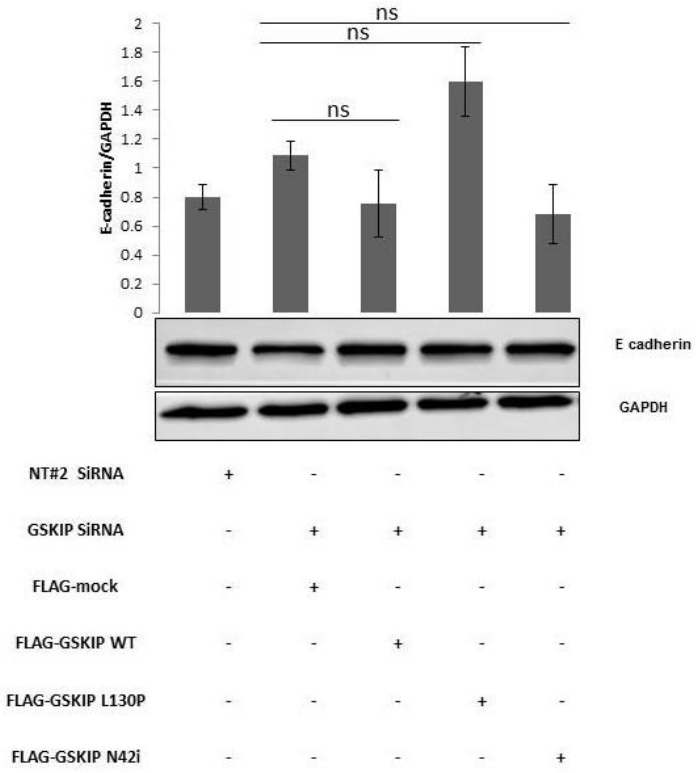

Supplementary figure 3: GSKIP re-expression of does not rescue E-cadherin. Semi-quantitative analysis of protein expression levels was carried out using ImageJ (n=3). Protein levels were normalized to the loading control, GAPDH (means ± SEM). Significant differences vs. Kd were determined using Student's t-test (*= P <0.05 **= P <0.01 ***= P<0.001 ns=not significant)

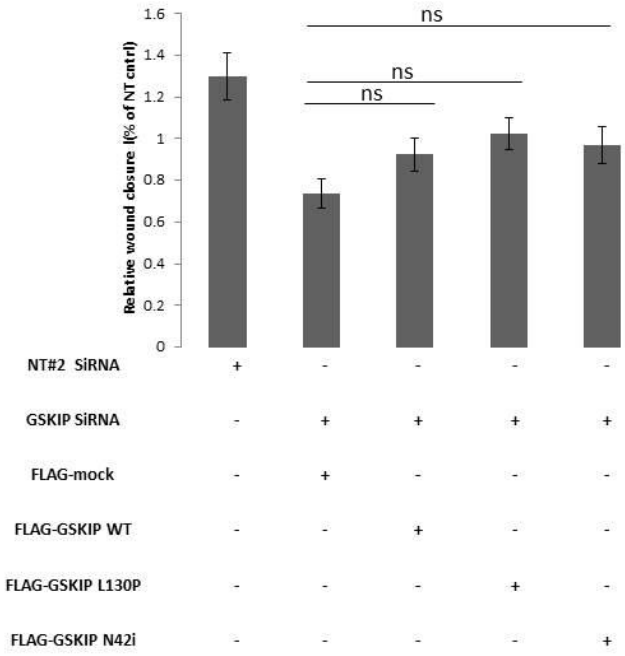

Supplementary figure 4: GSKIP re-expression of does not rescue migration of A549 cells. Semi-quantitative analysis of wound area was done by ImageJ (n=3, means ± SEM). Wound areas of each sample were normalized to the mean wound area of each independent experiment Significant difference vs. Kd were determined using Student's t-test (*= P <0.05 **= P <0.01 ***= P<0.001 ns=not significant)

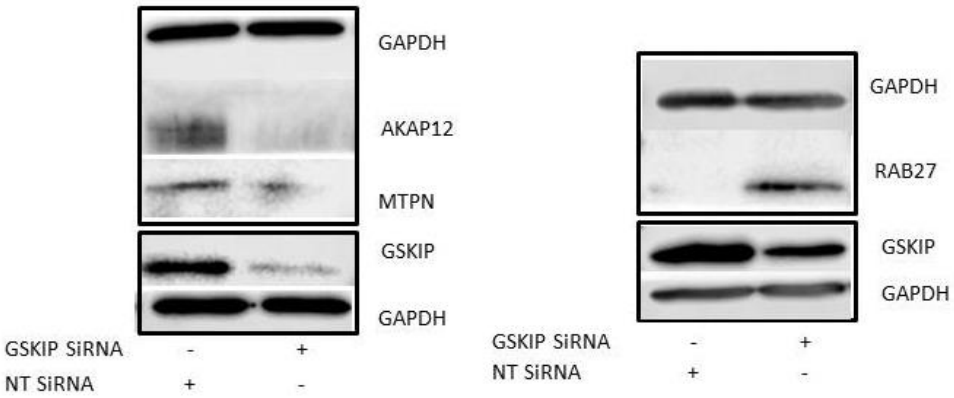

Supplementary figure 5: Verification of selected proteins from proteomics data affected by GSKIP Kd. A549 cells were transfected with GSKIP siRNA and lysed after 48 hours. Western Blot assay was performed as described in section 2.2.2.3 using antibodies for GSKIP, GAPDH, MTPN, AKAP12 and RAB27 (n=2).

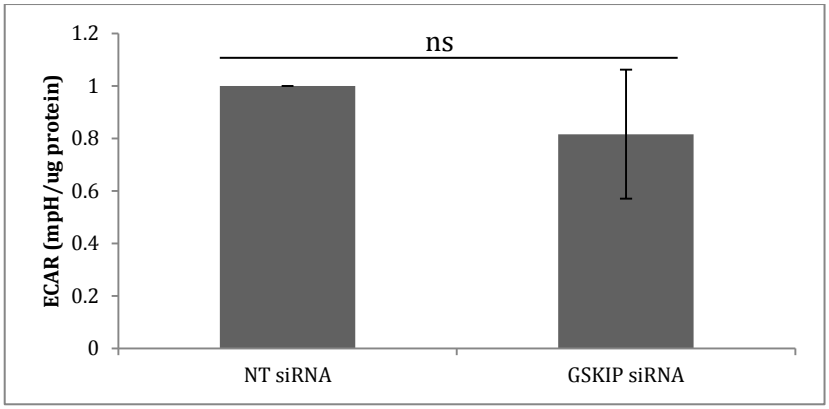

Supplementary figure 6: GSKIP Kd does not affect glycolysis. Extracellular acidification rate (ECAR) was measured using Seahorse XF24 Analyzer and normalized to protein level as described in section 2.2.1.9. The graph shows area under the curve of baseline ECAR of GSKIP Kd and NT control A549 cells. Data are expressed as means ± SEM (n=3). Significant differences were evaluated using students t-test (*- P <0.05, **- P <0.01, ***- P<0.001, ns-not significant).

10.2 Supplementary tables

Peptide spots were synthesized as described in materials and methods and contained the entire sequence of SMYD2 and GDF5OS. Each peptide contained 25 Amino acids of the protein sequence with a five AA-Shift.

SMYD2

Position	MolWeight	Sequence
A 1	2658.385	M-R-A-E-G-L-G-G-L-E-R-F-C-S-P-G-K-G-R-G-L-R-A-L-Q
A 2	2642.412	L-G-G-L-E-R-F-C-S-P-G-K-G-R-G-L-R-A-L-Q-P-F-Q-V-G
A 3	2748.454	R-F-C-S-P-G-K-G-R-G-L-R-A-L-Q-P-F-Q-V-G-D-L-L-F-S
A 4	2663.390	G-K-G-R-G-L-R-A-L-Q-P-F-Q-V-G-D-L-L-F-S-C-P-A-Y-A
A 5	2783.461	L-R-A-L-Q-P-F-Q-V-G-D-L-L-F-S-C-P-A-Y-A-Y-V-L-T-V
A 6	2772.347	P-F-Q-V-G-D-L-L-F-S-C-P-A-Y-A-Y-V-L-T-V-N-E-R-G-N
A 7	2879.261	D-L-L-F-S-C-P-A-Y-A-Y-V-L-T-V-N-E-R-G-N-H-C-E-Y-C
A 8	2965.320	C-P-A-Y-A-Y-V-L-T-V-N-E-R-G-N-H-C-E-Y-C-F-T-R-K-E
A 9	2948.362	Y-V-L-T-V-N-E-R-G-N-H-C-E-Y-C-F-T-R-K-E-G-L-S-K-C
A10	2945.315	N-E-R-G-N-H-C-E-Y-C-F-T-R-K-E-G-L-S-K-C-G-R-C-K-Q
A11	2973.285	H-C-E-Y-C-F-T-R-K-E-G-L-S-K-C-G-R-C-K-Q-A-F-Y-C-N
A12	2925.376	F-T-R-K-E-G-L-S-K-C-G-R-C-K-Q-A-F-Y-C-N-V-E-C-Q-K
A13	2922.263	G-L-S-K-C-G-R-C-K-Q-A-F-Y-C-N-V-E-C-Q-K-E-D-W-P-M
A14	3044.311	G-R-C-K-Q-A-F-Y-C-N-V-E-C-Q-K-E-D-W-P-M-H-K-L-E-C
A15	2985.288	A-F-Y-C-N-V-E-C-Q-K-E-D-W-P-M-H-K-L-E-C-S-P-M-V-V
A16	3020.322	V-E-C-Q-K-E-D-W-P-M-H-K-L-E-C-S-P-M-V-V-F-G-E-N-W
A17	2961.266	E-D-W-P-M-H-K-L-E-C-S-P-M-V-V-F-G-E-N-W-N-P-S-E-T
A18	2843.362	H-K-L-E-C-S-P-M-V-V-F-G-E-N-W-N-P-S-E-T-V-R-L-T-A
A19	2814.474	S-P-M-V-V-F-G-E-N-W-N-P-S-E-T-V-R-L-T-A-R-I-L-A-K
A20	2904.561	F-G-E-N-W-N-P-S-E-T-V-R-L-T-A-R-I-L-A-K-Q-K-I-H-P
B 1	2841.583	N-P-S-E-T-V-R-L-T-A-R-I-L-A-K-Q-K-I-H-P-E-R-T-P-S
B 2	2867.707	V-R-L-T-A-R-I-L-A-K-Q-K-I-H-P-E-R-T-P-S-E-K-L-L-A
B 3	2959.686	R-I-L-A-K-Q-K-I-H-P-E-R-T-P-S-E-K-L-L-A-V-K-E-F-E
B 4	2958.582	Q-K-I-H-P-E-R-T-P-S-E-K-L-L-A-V-K-E-F-E-S-H-L-D-K
B 5	2954.524	E-R-T-P-S-E-K-L-L-A-V-K-E-F-E-S-H-L-D-K-L-D-N-E-K
B 6	2981.596	E-K-L-L-A-V-K-E-F-E-S-H-L-D-K-L-D-N-E-K-K-D-L-I-Q
B 7	2884.471	V-K-E-F-E-S-H-L-D-K-L-D-N-E-K-K-D-L-I-Q-S-D-I-A-A
B 8	2949.487	S-H-L-D-K-L-D-N-E-K-K-D-L-I-Q-S-D-I-A-A-L-H-H-F-Y

B 9	2891.482	L-D-N-E-K-K-D-L-I-Q-S-D-I-A-A-L-H-H-F-Y-S-K-H-L-G
B10	2880.408	K-D-L-I-Q-S-D-I-A-A-L-H-H-F-Y-S-K-H-L-G-F-P-D-N-D
B11	2794.397	S-D-I-A-A-L-H-H-F-Y-S-K-H-L-G-F-P-D-N-D-S-L-V-V-L
B12	2896.455	L-H-H-F-Y-S-K-H-L-G-F-P-D-N-D-S-L-V-V-L-F-A-Q-V-N
B13	2721.311	S-K-H-L-G-F-P-D-N-D-S-L-V-V-L-F-A-Q-V-N-C-N-G-F-T
B14	2814.258	F-P-D-N-D-S-L-V-V-L-F-A-Q-V-N-C-N-G-F-T-I-E-D-E-E
B15	2733.321	S-L-V-V-L-F-A-Q-V-N-C-N-G-F-T-I-E-D-E-E-L-S-H-L-G
B16	2737.258	F-A-Q-V-N-C-N-G-F-T-I-E-D-E-E-L-S-H-L-G-S-A-I-F-P
B17	2707.240	C-N-G-F-T-I-E-D-E-E-L-S-H-L-G-S-A-I-F-P-D-V-A-L-M
B18	2729.202	I-E-D-E-E-L-S-H-L-G-S-A-I-F-P-D-V-A-L-M-N-H-S-C-C
B19	2636.280	L-S-H-L-G-S-A-I-F-P-D-V-A-L-M-N-H-S-C-C-P-N-V-I-V
B20	2679.275	S-A-I-F-P-D-V-A-L-M-N-H-S-C-C-P-N-V-I-V-T-Y-K-G-T
C 1	2732.334	D-V-A-L-M-N-H-S-C-C-P-N-V-I-V-T-Y-K-G-T-L-A-E-V-R
C 2	2743.367	N-H-S-C-C-P-N-V-I-V-T-Y-K-G-T-L-A-E-V-R-A-V-Q-E-I
C 3	2739.470	P-N-V-I-V-T-Y-K-G-T-L-A-E-V-R-A-V-Q-E-I-K-P-G-E-E
C 4	2814.433	T-Y-K-G-T-L-A-E-V-R-A-V-Q-E-I-K-P-G-E-E-V-F-T-S-Y
C 5	2881.500	L-A-E-V-R-A-V-Q-E-I-K-P-G-E-E-V-F-T-S-Y-I-D-L-L-Y
C 6	2911.438	A-V-Q-E-I-K-P-G-E-E-V-F-T-S-Y-I-D-L-L-Y-P-T-E-D-R
C 7	3025.503	K-P-G-E-E-V-F-T-S-Y-I-D-L-L-Y-P-T-E-D-R-N-D-R-L-R
C 8	3144.508	V-F-T-S-Y-I-D-L-L-Y-P-T-E-D-R-N-D-R-L-R-D-S-Y-F-F
C 9	3111.396	I-D-L-L-Y-P-T-E-D-R-N-D-R-L-R-D-S-Y-F-F-T-C-E-C-Q
C10	3056.295	P-T-E-D-R-N-D-R-L-R-D-S-Y-F-F-T-C-E-C-Q-E-C-T-T-K
C11	3015.305	N-D-R-L-R-D-S-Y-F-F-T-C-E-C-Q-E-C-T-T-K-D-K-D-K-A
C12	2986.340	D-S-Y-F-F-T-C-E-C-Q-E-C-T-T-K-D-K-D-K-A-K-V-E-I-R
C13	2867.372	T-C-E-C-Q-E-C-T-T-K-D-K-D-K-A-K-V-E-I-R-K-L-S-D-P
C14	2799.469	E-C-T-T-K-D-K-D-K-A-K-V-E-I-R-K-L-S-D-P-P-K-A-E-A
C15	2851.548	D-K-D-K-A-K-V-E-I-R-K-L-S-D-P-P-K-A-E-A-I-R-D-M-V
C16	2954.613	K-V-E-I-R-K-L-S-D-P-P-K-A-E-A-I-R-D-M-V-R-Y-A-R-N
C17	2946.527	K-L-S-D-P-P-K-A-E-A-I-R-D-M-V-R-Y-A-R-N-V-I-E-E-F
C18	3054.630	P-K-A-E-A-I-R-D-M-V-R-Y-A-R-N-V-I-E-E-F-R-R-A-K-H
C19	3120.641	I-R-D-M-V-R-Y-A-R-N-V-I-E-E-F-R-R-A-K-H-Y-K-S-P-S
C20	3103.657	R-Y-A-R-N-V-I-E-E-F-R-R-A-K-H-Y-K-S-P-S-E-L-L-E-I
D 1	3003.538	V-I-E-E-F-R-R-A-K-H-Y-K-S-P-S-E-L-L-E-I-C-E-L-S-Q

D 2	2948.474	R-R-A-K-H-Y-K-S-P-S-E-L-L-E-I-C-E-L-S-Q-E-K-M-S-S
D 3	2877.319	Y-K-S-P-S-E-L-L-E-I-C-E-L-S-Q-E-K-M-S-S-V-F-E-D-S
D 4	2935.343	E-L-L-E-I-C-E-L-S-Q-E-K-M-S-S-V-F-E-D-S-N-V-Y-M-L
D 5	3028.267	C-E-L-S-Q-E-K-M-S-S-V-F-E-D-S-N-V-Y-M-L-H-M-M-Y-Q
D 6	2929.218	E-K-M-S-S-V-F-E-D-S-N-V-Y-M-L-H-M-M-Y-Q-A-M-G-V-C
D 7	3017.249	V-F-E-D-S-N-V-Y-M-L-H-M-M-Y-Q-A-M-G-V-C-L-Y-M-Q-D
D 8	2996.275	N-V-Y-M-L-H-M-M-Y-Q-A-M-G-V-C-L-Y-M-Q-D-W-E-G-A-L
D 9	2980.273	H-M-M-Y-Q-A-M-G-V-C-L-Y-M-Q-D-W-E-G-A-L-Q-Y-G-Q-K
D10	2904.390	A-M-G-V-C-L-Y-M-Q-D-W-E-G-A-L-Q-Y-G-Q-K-I-I-K-P-Y
D11	3055.516	L-Y-M-Q-D-W-E-G-A-L-Q-Y-G-Q-K-I-I-K-P-Y-S-K-H-Y-P
D12	2995.549	W-E-G-A-L-Q-Y-G-Q-K-I-I-K-P-Y-S-K-H-Y-P-L-Y-S-L-N
D13	3013.541	Q-Y-G-Q-K-I-I-K-P-Y-S-K-H-Y-P-L-Y-S-L-N-V-A-S-M-W
D14	2976.630	I-I-K-P-Y-S-K-H-Y-P-L-Y-S-L-N-V-A-S-M-W-L-K-L-G-R
D15	2939.544	S-K-H-Y-P-L-Y-S-L-N-V-A-S-M-W-L-K-L-G-R-L-Y-M-G-L
D16	2863.513	L-Y-S-L-N-V-A-S-M-W-L-K-L-G-R-L-Y-M-G-L-E-H-K-A-A
D17	2771.487	V-A-S-M-W-L-K-L-G-R-L-Y-M-G-L-E-H-K-A-A-G-E-K-A-L
D18	2708.578	L-K-L-G-R-L-Y-M-G-L-E-H-K-A-A-G-E-K-A-L-K-K-A-I-A
D19	2684.465	L-Y-M-G-L-E-H-K-A-A-G-E-K-A-L-K-K-A-I-A-I-M-E-V-A
D20	2681.432	E-H-K-A-A-G-E-K-A-L-K-K-A-I-A-I-M-E-V-A-H-G-K-D-H
E 1	2734.437	G-E-K-A-L-K-K-A-I-A-I-M-E-V-A-H-G-K-D-H-P-Y-I-S-E
E 2	2847.521	K-K-A-I-A-I-M-E-V-A-H-G-K-D-H-P-Y-I-S-E-I-K-Q-E-I
E 3	2873.427	I-A-I-M-E-V-A-H-G-K-D-H-P-Y-I-S-E-I-K-Q-E-I-E-S-H

Supplementary table 1: Human SMYD2 peptide spots. 25 Amino acids with 5 AA-Shift

GDF5OS

Position	MolWeight	Sequence
K 2	2911.524	M-I-Q-S-S-Q-P-M-S-L-K-L-T-C-S-A-F-R-L-Q-R-A-L-R-F
K 3	2917.651	Q-P-M-S-L-K-L-T-C-S-A-F-R-L-Q-R-A-L-R-F-L-L-G-R-L
K 4	2970.722	K-L-T-C-S-A-F-R-L-Q-R-A-L-R-F-L-L-G-R-L-P-W-R-V-A
K 5	2965.747	A-F-R-L-Q-R-A-L-R-F-L-L-G-R-L-P-W-R-V-A-S-G-A-R-R
K 6	3108.832	R-A-L-R-F-L-L-G-R-L-P-W-R-V-A-S-G-A-R-R-F-R-R-W-L
K 7	3148.743	L-L-G-R-L-P-W-R-V-A-S-G-A-R-R-F-R-R-W-L-N-R-Y-S-Y
K 8	3083.632	P-W-R-V-A-S-G-A-R-R-F-R-R-W-L-N-R-Y-S-Y-T-V-L-S-S
K 9	3113.606	S-G-A-R-R-F-R-R-W-L-N-R-Y-S-Y-T-V-L-S-S-W-P-E-R-A
K10	3140.693	F-R-R-W-L-N-R-Y-S-Y-T-V-L-S-S-W-P-E-R-A-L-I-S-L-K

K11	3042.604	N-R-Y-S-Y-T-V-L-S-S-W-P-E-R-A-L-I-S-L-K-N-R-S-R-F
K12	2938.651	T-V-L-S-S-W-P-E-R-A-L-I-S-L-K-N-R-S-R-F-L-V-R-P-N
K13	3049.716	W-P-E-R-A-L-I-S-L-K-N-R-S-R-F-L-V-R-P-N-T-R-N-R-A
K14	3034.640	L-I-S-L-K-N-R-S-R-F-L-V-R-P-N-T-R-N-R-A-F-S-W-T-C
K15	3021.569	N-R-S-R-F-L-V-R-P-N-T-R-N-R-A-F-S-W-T-C-R-A-A-R-S
K16	2995.627	L-V-R-P-N-T-R-N-R-A-F-S-W-T-C-R-A-A-R-S-K-P-R-P-R
K17	2944.579	T-R-N-R-A-F-S-W-T-C-R-A-A-R-S-K-P-R-P-R-R-S-T-A-L
K18	2885.531	F-S-W-T-C-R-A-A-R-S-K-P-R-P-R-R-S-T-A-L-P-R-S-Q-A
K19	2815.550	R-A-A-R-S-K-P-R-P-R-R-S-T-A-L-P-R-S-Q-A-S-S-S-R-H
K20	2894.501	K-P-R-P-R-R-S-T-A-L-P-R-S-Q-A-S-S-S-R-H-S-W-A-E-F
L 1	2932.542	R-S-T-A-L-P-R-S-Q-A-S-S-S-R-H-S-W-A-E-F-L-K-F-R-K
L 2	2984.472	P-R-S-Q-A-S-S-S-R-H-S-W-A-E-F-L-K-F-R-K-S-F-Q-M-S
L 3	2972.424	S-S-S-R-H-S-W-A-E-F-L-K-F-R-K-S-F-Q-M-S-N-T-S-Q-P
L 4	2970.434	S-W-A-E-F-L-K-F-R-K-S-F-Q-M-S-N-T-S-Q-P-D-P-S-R-P
L 5	2894.435	L-K-F-R-K-S-F-Q-M-S-N-T-S-Q-P-D-P-S-R-P-G-T-E-R-T
L 6	2666.224	S-F-Q-M-S-N-T-S-Q-P-D-P-S-R-P-G-T-E-R-T-S-S-K-A-A
L 7	2612.261	N-T-S-Q-P-D-P-S-R-P-G-T-E-R-T-S-S-K-A-A-G-C-R-P-L
L 8	2585.251	D-P-S-R-P-G-T-E-R-T-S-S-K-A-A-G-C-R-P-L-G-Q-L-D-S
L 9	2595.239	G-T-E-R-T-S-S-K-A-A-G-C-R-P-L-G-Q-L-D-S-F-S-W-A-A
L10	2555.259	S-S-K-A-A-G-C-R-P-L-G-Q-L-D-S-F-S-W-A-A-R-P-P-P-G
L11	2494.243	G-C-R-P-L-G-Q-L-D-S-F-S-W-A-A-R-P-P-P-G-A-A-G-L-A
L12	2487.207	G-Q-L-D-S-F-S-W-A-A-R-P-P-P-G-A-A-G-L-A-V-S-E-G-F
L13	2687.434	F-S-W-A-A-R-P-P-P-G-A-A-G-L-A-V-S-E-G-F-F-R-K-I-R
L14	2554.366	R-P-P-P-G-A-A-G-L-A-V-S-E-G-F-F-R-K-I-R-S-S-A-P-S
L15	2555.302	A-A-G-L-A-V-S-E-G-F-F-R-K-I-R-S-S-A-P-S-S-P-S-F-S
L16	2730.380	V-S-E-G-F-F-R-K-I-R-S-S-A-P-S-S-P-S-F-S-R-A-L-M-S
L17	2805.394	F-R-K-I-R-S-S-A-P-S-S-P-S-F-S-R-A-L-M-S-N-T-Y-L-C
L18	2624.214	S-S-A-P-S-S-P-S-F-S-R-A-L-M-S-N-T-Y-L-C-F-L-T-T-G
L19	2778.347	S-P-S-F-S-R-A-L-M-S-N-T-Y-L-C-F-L-T-T-G-P-R-S-S-R
L20	2873.417	R-A-L-M-S-N-T-Y-L-C-F-L-T-T-G-P-R-S-S-R-E-N-T-Q-K
M 1	2818.360	N-T-Y-L-C-F-L-T-T-G-P-R-S-S-R-E-N-T-Q-K-S-F-P-A-T
M 2	2790.394	F-L-T-T-G-P-R-S-S-R-E-N-T-Q-K-S-F-P-A-T-S-P-R-E-P
M 3	2827.458	P-R-S-S-R-E-N-T-Q-K-S-F-P-A-T-S-P-R-E-P-V-T-S-R-L

M 4	2753.446	E-N-T-Q-K-S-F-P-A-T-S-P-R-E-P-V-T-S-R-L-R-G-K-A-P
M 5	2608.397	S-F-P-A-T-S-P-R-E-P-V-T-S-R-L-R-G-K-A-P-A-L-S-P-S
M 6	2737.488	S-P-R-E-P-V-T-S-R-L-R-G-K-A-P-A-L-S-P-S-R-E-L-S-F
M 7	2674.444	V-T-S-R-L-R-G-K-A-P-A-L-S-P-S-R-E-L-S-F-T-S-A-P-F

Supplementary table 2: Human GDF5OS peptide spots. 25 Amino acids with 5 AA-Shift.

Seahorse XF24 extracellular flux analyzer automated protocol

Time	Event	Parameter
12:03:59	Start	
12:04:28	Loading Cartridge	
12:04:53	Waiting after lowering cartridge in calibrant	
12:15:00	Mixing Calibrant	
12:16:07	Waiting after mixing	
12:18:13	Calibrating Cartridge	
12:19:32	Final Calibration Measure	
12:22:31	Mixing	
12:27:40	Waiting	
12:29:50	Measuring	
12:35:08	Mixing	
12:40:17	Waiting	
12:42:28	Measuring	
12:47:45	Mixing	
12:52:55	Waiting	
12:55:06	Measuring	
13:00:22	Injecting	oligomycin
13:00:35	Mixing	
13:03:44	Waiting	
13:05:54	Measuring	
13:11:10	Mixing	
13:11:22	Waiting	
13:15:31	Measuring	
13:17:41	Mixing	
13:21:58	Waiting	
13:26:08	Measuring	
13:28:18	Injecting	FCCP
13:32:35	Mixing	
13:36:44	Waiting	
13:38:54	Measuring	
13:43:09	Mixing	
13:43:22	Waiting	
13:47:31	Measuring	
13:49:42	Mixing	
13:53:57	Waiting	
13:58:07	Measuring	
14:30:21	Injecting	Rotenone+AntimycinA
14:34:37	Mixing	
14:37:46	Waiting	
14:39:56	Measuring	
14:25:00	Mixing	
14:28:10	Waiting	

14:30:21	Measuring	
14:34:37	Mixing	
14:37:46	Waiting	
14:39:56	Measuring	

Supplementary table 3: Seahorse XF24 automated protocol.

s